1-23-2013 12:00 AM

Self-cleaning Polyurethane and Polyester Coatings

Yixing Tang
The University of Western Ontario

Supervisor
Paul Charpentier
The University of Western Ontario

Graduate Program in Chemical and Biochemical Engineering
A thesis submitted in partial fulfillment of the requirements for the degree in Master of Engineering Science

SELF-CLEANING POLYURETHANE AND POLYESTER COATINGS

(Thesis format: Monograph)

by

Yixing Tang

Graduate Program in Chemical and Biochemical Engineering

A thesis submitted in partial fulfillment
of the requirements for the degree of
Master of Engineering Science

The School of Graduate and Postdoctoral Studies
The University of Western Ontario
London, Ontario, Canada

THE UNIVERSITY OF WESTERN ONTARIO
School of Graduate and Postdoctoral Studies

CERTIFICATE OF EXAMINATION

Supervisor

Dr. Paul Charpentier

Supervisory Committee

Dr. Lars Rehmann

Examiners

Dr. Mita Ray

Dr. Jin Zhang

Dr. Jun Yang

The thesis by

Yixing Tang

entitled:

Self-cleaning Polyurethane and Polyester Coatings

is accepted in partial fulfillment of the
requirements for the degree of
Master of Engineering Science

Date

Chair of the Thesis Examination Board

Abstract

Self-cleaning titanium dioxide (TiO_2) based polyurethane and polyester nanocomposites were synthesized, characterized and tested in this thesis. A monomer functionalization method ("grafting from" polymerization) was used for synthesizing both novel nano-TiO_2 coordinated polyurethanes (nano-TiO_2-PU) and nano-TiO_2/polyester nanocomposites. This technique provides the advantage of directly attaching nanoparticles to the polymer backbone.

For polyurethane synthesis, two different methods (one-shot and pre-polymer) were explored. Using several characterization techniques, product from the pre-polymer method showed better mechanical properties; therefore, the pre-polymer method was chosen for subsequent nano-TiO_2-PU synthesis. In the nano-TiO_2-PU synthesis, the first step, monomer functionalization, was confirmed using TGA and FTIR characterization. The self-cleaning properties of nano-TiO_2-PU products were examined and demonstrated. As for polyesters, nano-TiO_2 was mixed with two commercial polyesters to investigate their self-cleaning and mechanical properties. With the addition of nano-TiO_2, nano-TiO_2/polycaprolactone (PCL) showed good self-cleaning properties and nano-TiO_2/poly(ethylene terephthalate) (PET) showed enhancement in the mechanical properties.

Keywords

Self-cleaning, polyurethane, polyester, nano-TiO_2, DMPA, photocatalysis, mechanical behavior.

Acknowledgments

There are a great number of people that I would like to acknowledge for their help in the past two years.

First, I would like to express my sincerest gratitude to my supervisor, Dr. Paul A. Charpentier, who has supported me throughout my study with his patience and guidance. Without him, none of this would have been possible.

I would also like to extend acknowledgement to my fellow group members for their help and suggestions, especially Qasem, Renpeng, Adria, Lin, Jenna, Lijuan for their help with all kinds of experiments and instruments.

In addition, I wish to thank all other person who helped me during my research, Harvey, Erden, Ying etc.

Last but not the least; I want to thank all my friends for their encouragement and support.

Table of Contents

List of Tables

List of Figures

Chapter 1

1 Introduction

Recently, self-cleaning coatings have received significant attention, both in academic research[1-5] and for potential commercial applications.[6] Because of their extensive range of possible applications, from self-cleaning window glass and cement to textiles, the technology of self-cleaning coatings has the potential to develop numerous labor-saving devices for our daily lives.[7] In addition to the wide range of promising applications, self-cleaning coatings also offer various advantages, including a reduction in maintenance costs, protection from environmental pollution, elimination of tedious manual effort and a reduction in the time spent on cleaning surfaces.[8,9]

As one of the two major categories in self-cleaning coatings, hydrophilic coatings are examined in this work. This class of coatings is generally produced using titanium dioxide (TiO_2) as the photocatalyst. By absorbing ultraviolet (UV) irradiation, TiO_2 can induce photocatalysis. Photoexcited TiO_2 has strong oxidation power, which can lead to oxidation of organic species and bacteria deposited on the coated surface.[10] Additionally, when TiO_2 is photoexcited, it becomes super-hydrophilic as a result of the creation of hydroxyl groups.[11]

With its photocatalytic and super-hydrophilic properties, TiO_2 based self-cleaning exterior surfaces can be kept clean by sunlight and the action of rainwater. This self-cleaning process usually contains two stages: the absorbed contaminants on the surface are decomposed by photocatalysis in the first stage, followed by the water sheeting action due to the super-hydrophilic surface in the second stage.[9]

In addition to TiO_2, for the formation of polymer nanocomposites, polyurethanes and polyesters were studied in this work. Both polymers are used worldwide for indoor and outdoor applications. Polyurethanes were first discovered by Otto Bayer and his coworkers in 1937.[12] With a hard crystalline segment and a soft amorphous segment, the segmented polyurethanes have unique physical and mechanical properties.[13,14] Therefore,

they are now widely used in surface coatings, high performance adhesives, and synthetic fibers.[15]

Linear polyesters were first synthesized by Carothers and coworkers at DuPont,[16] however, these materials had a low melting point and poor hydrolytic stability. Poly(ethylene terephthalate) (PET), which has a high melting point and good hydrolytic stability, was later discovered by Whinfield and Dickson.[16] After that, polyesters were widely used in our daily life, including synthetic fibers, films, beverage bottles, and molded plastic parts.[16]

Chapter 2

2 Objectives

The objectives of this work were to:

1) Introduce nano-TiO_2 into polyurethane and polyester polymer backbones by direct coordination to the polymer chains;
2) Study the self-cleaning properties of these functionalized polymers;
3) Investigate different model compounds for 'dirt' when conducting the self-cleaning tests; and
4) Investigate the effects of TiO_2 on mechanical and thermal performance of the synthesized polymers.

Chapter 3

3 Literature Review

3.1 Self-cleaning Coatings

The technology of self-cleaning coatings is gaining increasing attention in recent years due to their extensive range of potential applications, i.e. from window glass to cements and textiles.[7-9] Besides these widespread applications, this technology also offers various other advantages[9] including a reduction in maintenance costs, prevention of snow and ice build-up and protection from environmental pollution.

The field of self-cleaning coatings is usually divided into two major categories: hydrophilic and hydrophobic coatings.[7] These two types of coatings both clean themselves through the action of water. In a hydrophilic coating,[8] water spreads over the surface by sheeting, which carries away any dirt and other impurities. These hydrophilic coatings provide an additional property of chemically breaking down the complex dirt deposits in sunlight when using suitable metal oxides.[7] In the hydrophobic technique,[8] water droplets slide and roll over the surface, thereby cleaning the surface.

Despite all the advantages that self-cleaning coatings have shown, each type of coating has certain limitations. The main challenges for super-hydrophobic surfaces are to improve their stability and durability.[9] Erosion during service would result in premature deterioration of the surface roughness and a reduction or complete loss of the super-hydrophobic properties.[9] For the super-hydrophilic surfaces, the limitation of the titanium dioxide light absorption range (only use sub-390 nm light) is a major problem.[7]

3.2 Surfaces and Interfaces

3.2.1 Definition of contact angle

When a drop of liquid is placed on a solid surface, the triple interface formed between solid, liquid and gas will move in response to the forces arising from the three interfacial tensions until an equilibrium position is established.[17] Figure 3.1 shows this situation

where a drop of liquid on a flat solid surface exists with air as the third phase. The angle, θ, between the solid surface and the tangent to the liquid surface at the line of contact with the solid is known as the contact angle.[18]

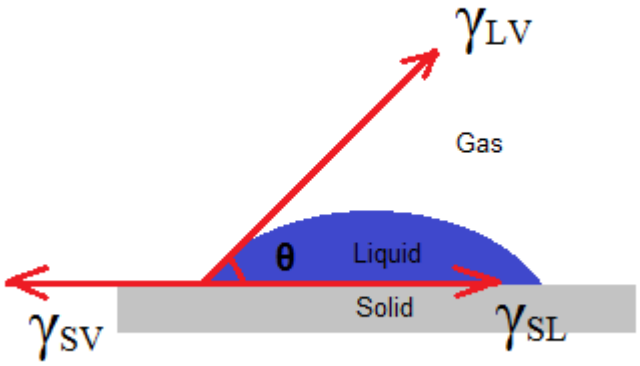

Figure 3.1 Contact angle between the triple interfaces of solid, liquid and gas.[17]

In an ideal surface, the wettability of the solid surface is commonly evaluated by the contact angle given by Young's equation (3.1):[19]

$$\gamma_{SV} = \gamma_{SL} + \gamma_{LV} \cos\theta \qquad 3.1$$

where γ_{SV}, γ_{SL} and γ_{LV} are the interfacial free energies per unit area of the solid-gas, solid-liquid and liquid-gas interfaces, respectively.

The self-cleaning effect is related to the contact angle. In general, if the contact angle is < 90° the solid surface is considered hydrophilic (Figure 3.2b); when the contact angle is > 90° the surface is defined as hydrophobic (Figure 3.2c). Similarly, a surface having a water contact angle approaching zero (<30°) is classified as super-hydrophilic (Figure 3.2a), and a surface with a contact angle > 150° is usually categorized as super-hydrophobic (Figure 3.2d).[8,9]

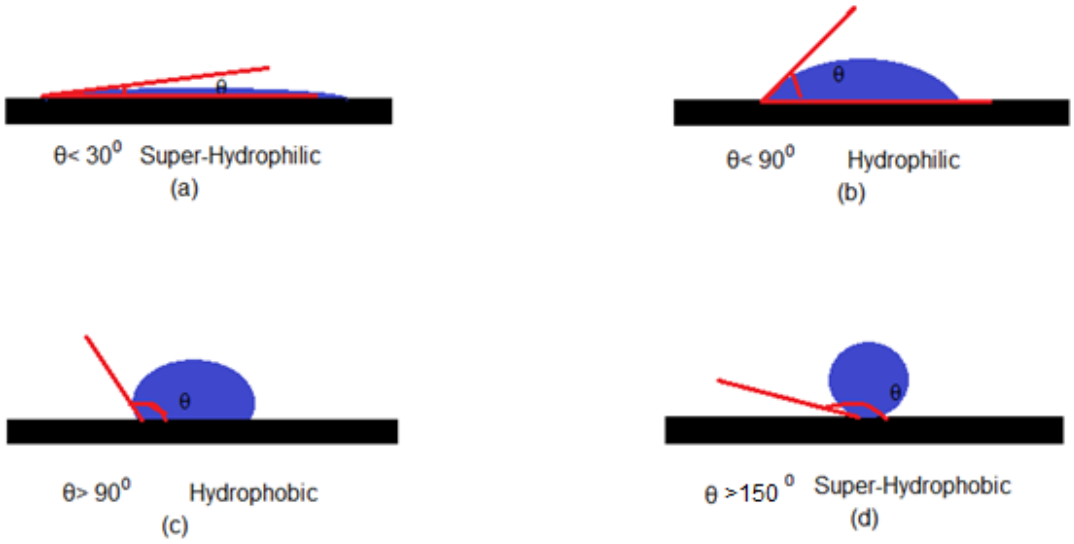

Figure 3.2 Schematic representations: of (a) super-hydrophilic, (b) hydrophilic, (c) hydrophobic and (d) super-hydrophobic surfaces.[8]

3.2.2 Sessile Drop Measurement Methods

The sessile drop technique, which was developed by Neumann et al.,[18] is the most common method for contact angle testing. Because of its accuracy and simplicity,[20] the sessile drop method is now a standard method for contact angle measurement. Other available methods to measure the contact angle include the tilting plate method, the wiching method and the atomic force microscopy method.[20]

The setup for the sessile drop technique is relatively simple, including a light source, a test cell and a microscope.[20] First, the coating surface is placed and leveled on the test cell between the light source and the microscope. Then, a liquid drop, typically water, is deposited onto the coating surface through a syringe. After the liquid drop reaches its equilibrium state, the contact angle can either be read directly from a goniometer or its digital image can be recorded and the contour fitted by a computer.[20]

3.3 Hydrophobic Surfaces

Like many current technologies, self-cleaning technology is bio-mimetic, i.e. inspired

from nature. The lotus leaf is the source of inspiration for this technology in the case of super-hydrophobic materials. Even when rising from muddy water, the lotus leaves stay clean from mud or dirt. This self-cleaning characteristic is commonly referred to as the 'lotus effect', a term first described by biologists Barthlott and Neinhaus.[21]

Since the 21st century, super-hydrophobic surfaces with water contact angles higher than 150^{o} are gaining significant interest for applications both in daily life and in industrial processes.[22] Conventionally, there are mainly two different ways to produce super-hydrophobic surfaces. One strategy is to create a rough structure on a hydrophobic surface, and the other one is to modify a rough surface by materials with low surface energy.[23]

However, the stability and durability of the super-hydrophobic surfaces are main challenges in this technology.[9] Unlike lotus leafs, artificial surfaces can not regenerate the surface constantly and re-grow the damaged surface.[9]

3.4 Hydrophilic Surfaces

Hydrophilic surfaces for self-cleaning applications are generally produced using titanium dioxide (TiO_2),[9] which is the main focus of this study. The photocatalytic oxidation-reduction reactions of TiO_2 irradiated with UV light can decompose organic compounds and bacteria deposited on the surface.[24-26] This photocatalytic reaction originated from the discovery of water-splitting on TiO_2 semiconductor electrodes irradiated with UV light, known as the Honda-Fujishima effect.[11]

Initial studies based on the Honda-Fujishima effect were on systems that could utilize solar energy to produce hydrogen. However, most scientific studies involving this effect have been redirected towards a new line of research-i.e. environmental cleaning.[11]

Academically, the photo-generated super-hydrophilic surface of titanium dioxide was first reported by Wang et al. in Nature in 1997.[27] Water droplets spread out on the titanium dioxide film surface after UV irradiation, resulting in a contact angle of $0^{o}\pm1^{o}$, much lower than that before irradiation($72^{o}\pm1^{o}$). Because of this change in wettability, the coated glass shows remarkable anti-fogging and self-cleaning effects.[28-30]

While commercially, it was until 2001 that Pilkington Glass announced the development of the first self-cleaning windows, Pilkington Activ™.[7] In these self-cleaning windows, there is a unique dual-action self-cleaning coating layer located on the external glass pane. It has both photocatalytic and hydrophilic properties, and works in two stages:[6] first, the coating reacts with natural daylight to break down and loosen organic dirt; then rain or water can spread evenly over the surface of the glass, forming a thin film instead of droplets and helping to wash away any dirt while reducing streaks.

Recent research has found that the photogenerated holes, not the electrons, are responsible for the super-hydrophilic conversion.[31] The mechanism[11] for the highly hydrophilic conversion under UV light irradiation is proposed as shown in Figure 3.3.

First, the photogenerated holes diffuse to the surface and become trapped at oxygen sites of the TiO_2 lattice, producing OH radicals or oxidizing the adsorbed organics directly. The binding length between the titanium cation and the lattice oxygen then expands. Then, H_2O molecules simultaneously release a proton for charge compensation as the expanded Ti-O bond induces H_2O molecule adsorption. This results in an increase in the amount of OH groups at the TiO_2 surface due to the newly formed OH groups. This increase then helps convert one OH group doubly coordinated to Ti atoms at an oxygen defect site into two OH groups, singularly coordinated to each Ti atom.[11]

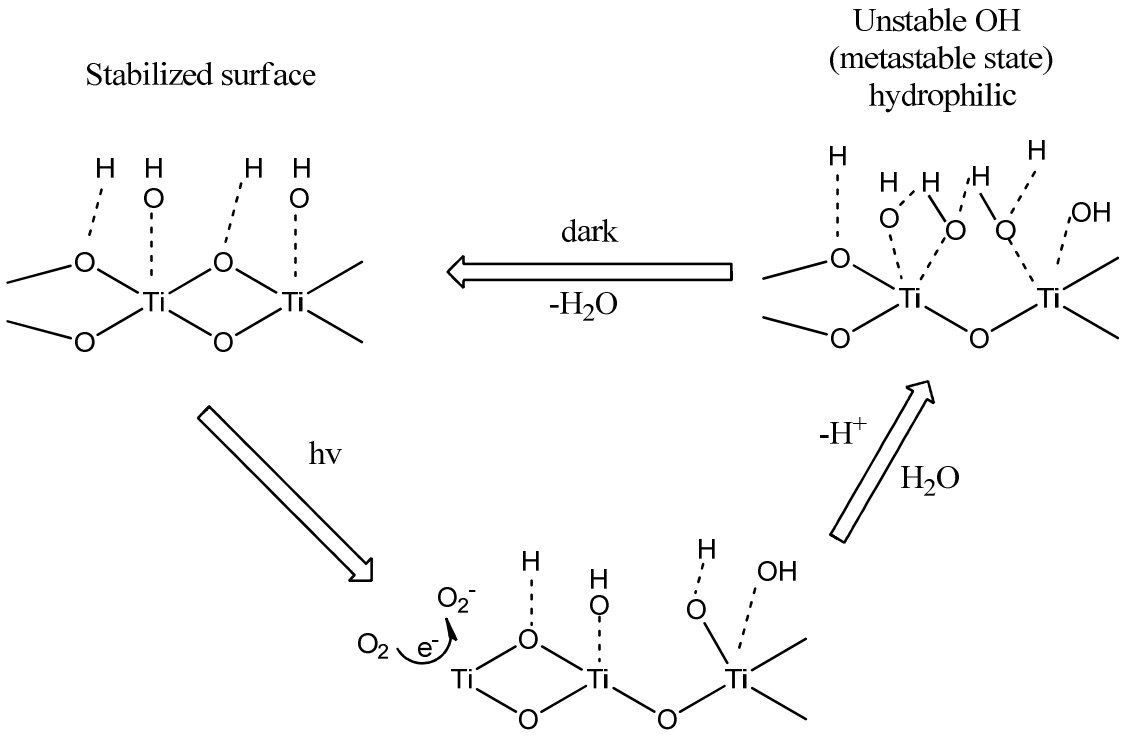

Figure 3.3 Schematic of reversible changes in the amount of hydroxyl groups under UV-light irradiation and in the dark.[11]

The new coordinated OH groups produced by UV light irradiation are considered to be less stable thermodynamically, compared to the initial doubly coordinated OH groups. Therefore, the surface energy increases after UV light irradiation; as the TiO_2 surface covered with the thermodynamically less stable OH groups has a higher surface energy than the initial TiO_2 surface covered with the OH groups.[11]

Also, from Young's equation, we know that when dropping the water droplet onto a surface with a higher surface energy, the droplet spreads more, i.e. the water contact angle is lower.[19] So, the contact angle of the surface decreases after UV light irradiation, forming a super-hydrophilic surface.

3.5 Titanium Dioxide

Titanium dioxide (TiO_2), also known as titania, is one of the most basic materials in our daily lives. Because of its low-cost, nontoxicity, high photocatalytic activity, and chemical inerteness,[32-34] TiO_2 is now the most preferred semiconductor metal oxide

(including ZnO, Fe_2O_3, WO_3, ZrO_2 and CeO_2) and has emerged as an excellent photocatalyst material for environmental purification.[10]

Titanium dioxide exists at room temperature in three forms: rutile, anatase and brookite, each of which occurs naturally. Rutile is the most common and stable form; anatase and brookite are both metastable and can transform into rutile upon heating.[35]

Rutile and anatase are the most widely used crystal forms, both of these phases show photocatalytic activity, while the brookite phase does not. Even though rutile is the most thermodynamically stable phase, anatase is the preferred form for photocatalysis because it has a smaller electron effective mass, a higher Fermi level, and a higher mobility of charge carriers.[36,37]

Titanium dioxide has a wide range of applications, from paint, food coloring to sunscreen.[38] It is the most widely used white pigment because of its brightness and very high refractive index.[5] Approximately 4 million tons of pigmentary TiO_2 are consumed annually worldwide.[38] Also, titanium dioxide is found in almost every sunscreen because of its strong UV light absorbing capabilities and its resistance to discoloration under ultraviolet light.[39] This advantage enhances its stability and ability to protect the skin from ultraviolet light. Moreover, titanium dioxide can also be used for self-cleaning and anti-fogging products, disinfection, air and water purification, when in the anatase crystal form.[39]

However, there is a major drawback of titanium dioxide which limits its application. The band gap of bulk anatase TiO_2 is 3.2 eV, corresponding to a wavelength of 390 nm- near-UV light.[7] Numerous efforts have been made to solve this problem, with TiO_2 doping commonly used to extend the range of light into the visible region.[40,41]

3.6 Photocatalysis

The term photocatalysis consists of the combination of photochemistry and catalysis and implies that light and a catalyst are required to bring about or to accelerate a chemical transformation.[42] In photocatalysis, the photocatalytic activity depends on the ability of

the catalyst to create electron-hole pairs, which therefore generate free radicals (e.g. hydroxyl radicals: •OH) that are able to undergo secondary reactions.[43]

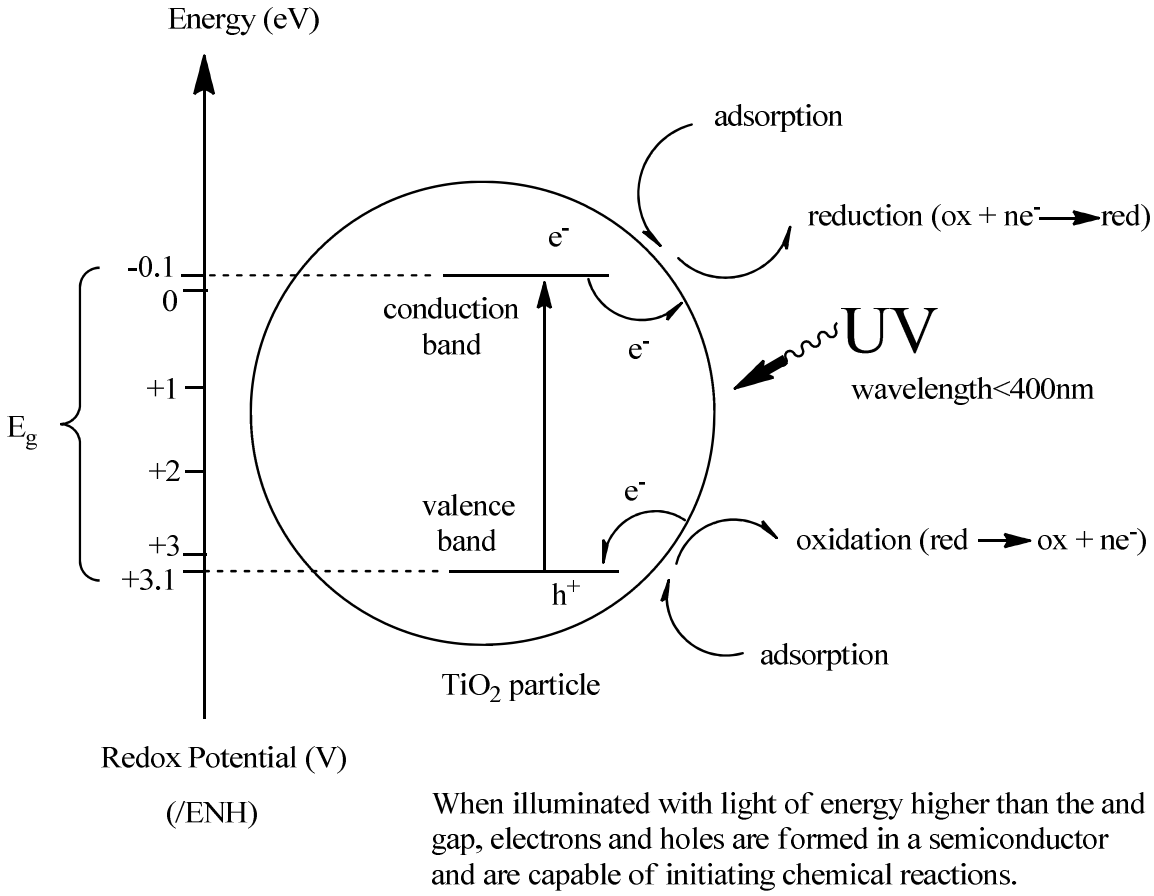

Figure 3.4 Energy band diagram of a spherical titania particle.[44]

When a semiconductor catalyst is exposed to a light source with a higher energy than its band gap energy, it generates excited states in the catalyst that are able to initiate oxidation and reduction reactions, thereby forming molecular transformations. Figure 3.4 shows the scheme of the photocatalytic process over TiO_2.[44]

Typically, the titanium dioxide photocatalysis mechanism is described as follows:[45] the first step, photoexcitation of titania with wavelengths ≤ 380 nm generates an electron-hole pair (Equation 3.2), creating the potential for reduction and oxidation processes to occur at the semiconductor surface.

$$TiO_2 \xrightarrow{light} h_{vb}^{+} + e_{cb}^{-} \qquad \textbf{3.2}$$

The direct reaction between a substrate adsorbed on the surface of the semiconductor and the h_{vb}^{+} or e_{cb}^{-} via electron transfer is typically not considered to be a significant reaction pathway in dilute oxygenated aqueous media.

Oxygen is generally used to scavenge the electron-forming superoxide anion radical (Equation 3.3):

$$O_2 + e_{cb}^{-} \longrightarrow O_2^{\bullet -} \qquad \textbf{3.3}$$

This prolongs the lifetime of the hole thus increasing the probability to oxidize surface hydroxyl groups or adsorbed water to yield a hydroxyl radical (Equation 3.4):

$$OH_{ads}\ (\text{or } H_2O) + h_{vb}^{+} \longrightarrow \bullet OH\ (H^{+}) \qquad \textbf{3.4}$$

The reactive oxidizing species (hydroxyl radical) is likely associated with or bound to the surface of the titania and is often defined as a trapped hole.

The superoxide anion radical formed during photocatalysis can yield hydrogen peroxide in aqueous solution.[46,47] The hydrogen peroxide can then undergo reduction by e_{cb}^{-}, also producing a hydroxyl radical but in relatively low yields[48] (Equation 3.5):

$$H_2O_2 + e_{cb}^{-} \longrightarrow \bullet OH + {}^{-}OH \qquad \textbf{3.5}$$

The hydroxyl radical, once formed, is a very powerful oxidant; that can react with a variety of substrates, especially organic compounds.[49] Addition, hydrogen and electron abstraction, represented in Figure 3.5, are the most common pathways. The reaction pathway depends on the functionality and electronic characteristics of the organic compound. In general, these pathways first lead to radical species. Continued photocatalysis in most cases leads to complete degradation, producing the corresponding mineral acids, water and carbon dioxide.[45]

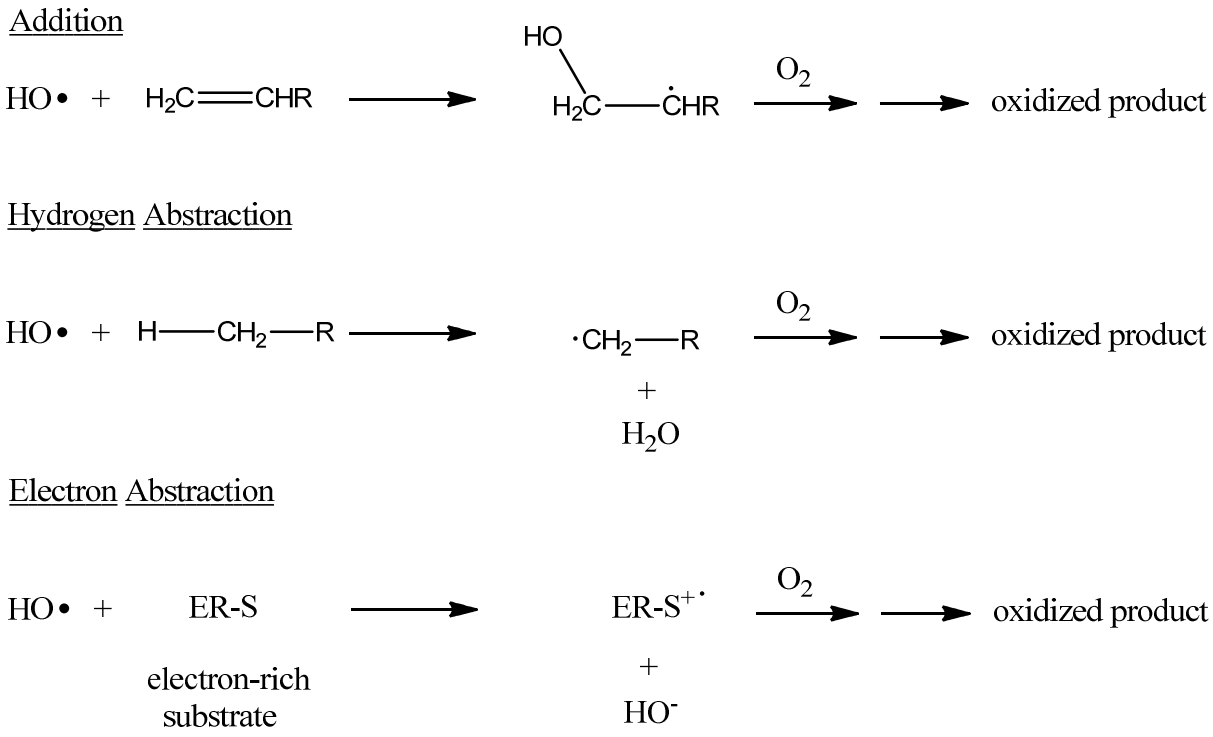

Figure 3.5 Common reaction pathways of hydroxyl radicals with organic compounds.[45]

Although tremendous interest exists for self-cleaning glass, self-cleaning polymers using nano-TiO_2 have been relatively unexplored. Recent discoveries[1,2,5] in the Charpentier lab have shown that TiO_2 can be attached chemically onto carboxylic groups creating unique functional monomers, which are subsequently polymerized. Therefore, various polymer types, particularly those produced by step-growth polymerization, become of interest, which provide tremendous opportunity for attaching the nano-TiO_2 directly to the polymer backbone.

3.7 Step-growth Polymerization

Step-growth polymerization is a type of polymerization class based on the mechanism of polymer growth.[50-52] A great numbers of different chemical reactions can be used to synthesize polymers by step polymerization, including esterification, amidation, the formation of urethanes and aromatic substitution. Polymerizations usually proceed by the

reactions between two different functional groups, for instance, hydroxyl and carboxyl groups, or isocyanate and hydroxyl groups.[53]

Depending on the type of monomer employed, all step-growth polymerizations fall into two groups. The first group involves two different bi-functional and/or poly-functional monomers in which each monomer possesses one type of functional group. The other one involves only one monomer containing both types of functional groups.[53] Figure 3.6 represents these two groups of reactions in a general manner, where A and B stand for the two different types of functional groups.[53]

(1)

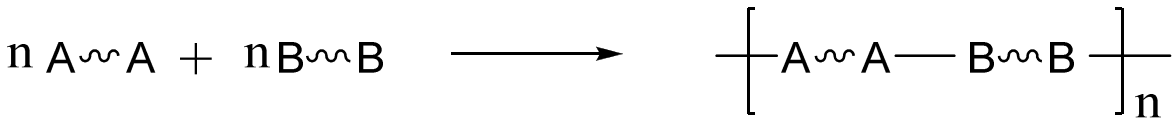

(2)

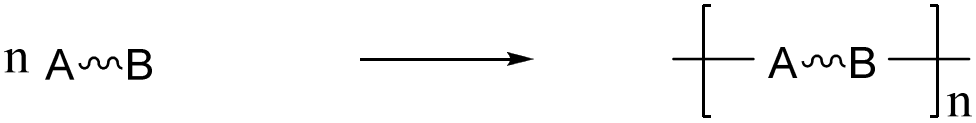

Figure 3.6 Schemes for the two groups of step-growth polymerization reactions.[53]

3.7.1 Kinetics of step-growth polymerization

The polyesterification reaction of a diacid and a diol can be considered as the general form of the kinetics of step-growth polymerization, and is one of the reactions investigated in this thesis. The reaction involves protonation of the carboxylic acid (Figure 3.7),[53]

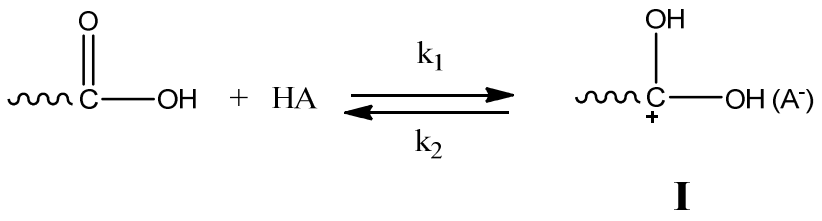

Figure 3.7 Protonation of carboxylic acid during step-growth polymerization.[53]

followed by reaction of the protonated species **I** with the alcohol to yield the ester (Figure 3.8).[53]

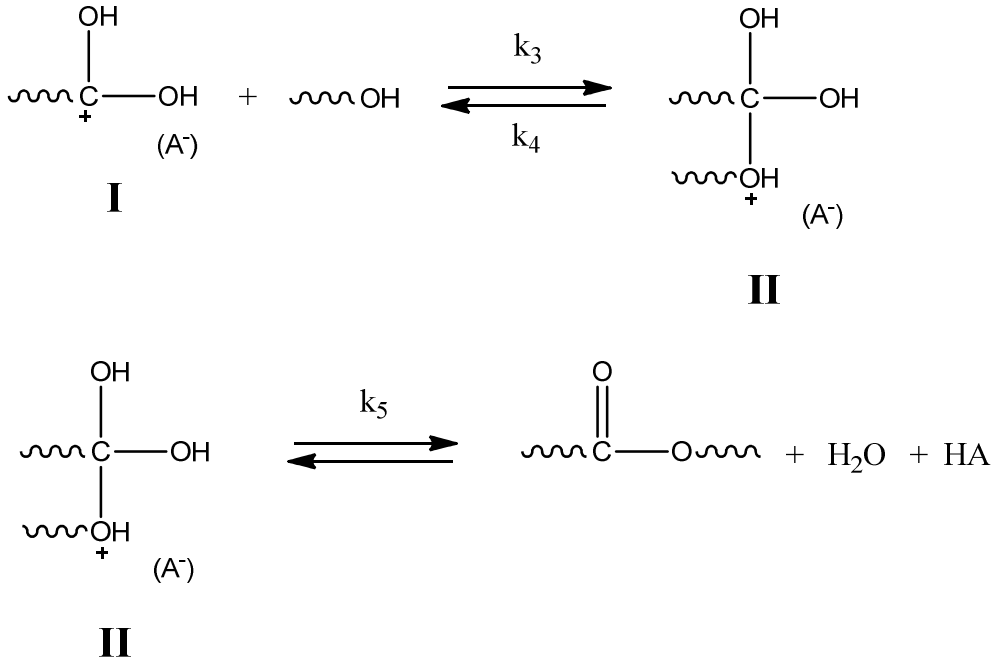

Figure 3.8 Reaction of the protonated species I with the alcohol during step-growth-polymerization.[53]

The rate of a step polymerization is usually expressed in terms of the concentration of the reacting functional groups, which is given by:

$$\mathbf{R} = \frac{\mathbf{-d[COOH]}}{\mathbf{dt}} = \mathbf{k_3[C^+(OH)_2][OH]} \qquad \mathbf{3.6}$$

where [COOH], [OH], $[C^+(OH)_2]$ represent the concentrations of carboxyl, hydroxyl, and protonated carboxyl (I) groups, respectively. Also, there is an equilibrium expression

for the protonation of carboxylic acid,

$$\mathbf{K = \frac{k_1}{k_2} = \frac{[C^+(OH)_2]}{[COOH][HA]}} \quad \textbf{3.7}$$

combining Equation 3.6 and Equation 3.7,

$$\mathbf{\frac{-d[COOH]}{dt} = k_3 K[COOH][OH][HA]} \quad \textbf{3.8}$$

For external catalysis of polymerization, Equation 3.8 can be written as:

$$\mathbf{\frac{-d[M]}{dt} = k'[M]^2} \quad \textbf{3.9}$$

where the various constants have been collected into k′, and integrated to form:

$$\mathbf{k't = \frac{1}{[M]} - \frac{1}{[M]_0}} \quad \textbf{3.10}$$

Introducing *p* (fracture of conversion) yields:

$$\mathbf{[M]_0 k't = \frac{1}{(1-p)} - 1} \quad \textbf{3.11}$$

and the number-average degree of polymerization, $\mathbf{\overline{X_n}}$, is defined as the average number of structural units per polymer chain, which can simply be given as the total number of monomer molecules initially present divided by the total number of molecules present at time t,

$$\mathbf{\overline{X_n} = \frac{[M]_0}{[M]} = \frac{1}{1-p}} \quad \textbf{3.12}$$

combining Equation 3.11 and Equation 3.12, one obtains

$$\mathbf{\overline{X_n} = 1 + [M]_0 k't} \quad \textbf{3.13}$$

3.7.2 Molecular weight control in linear polymerization

In polymer synthesis, obtaining a product with a specific molecular weight is very favorable in that the properties of the polymer will be highly dependent on molecular

weight.[51-53] Molecular weights higher or lower than the desired weight are equally undesirable. There are usually two ways to control the molecular weight in polymerization.[53]

The first is quenching the reaction (for example, cooling) at the appropriate time.[53] From the kinetics of the step-growth polymerization (Equation. 3.13), it is clear that the degree of polymerization is a function of the reaction time. Therefore, it is possible to obtain the desired molecular weight product by controlling the reaction time. However, polymer obtained in this manner is unstable since subsequent heating would lead to changes in molecular weight because the ends of the polymer molecules contain functional groups that can further react with one another.[53]

The other technique which can avoid the above situation, is adjusting the concentration of the two monomers so that they are slightly nonstoichiometric.[53] In this case, one of the reactants is added slightly in excess to the other. Polymerization then proceeds to a point at which one reactant (the stochiometric lower one) is completely reacted and all the chains end up with the same functional groups (the excess one). In this case, further polymerization is not possible and the polymer is stable to subsequent molecular weight changes.[53]

3.7.3 Step-growth polymerization mechanism

The proposed mechanism for step-growth polymerization is essentially the same as that proposed in general for reactions of low molecular weight organic compounds containing the same functional groups.[54-56] One example is the synthesis of nylon, which the polyamides are formed via a simple S_N2 type Lewis acid-base reaction (Figure 3.9), involving the attack of Lewis base, for example, a nucleophilic amine on the electron efficient site of electrophile carbonyl group followed by a loss of proton. In the process, elimination of small molecules occurs, e.g. H_2O.[54]

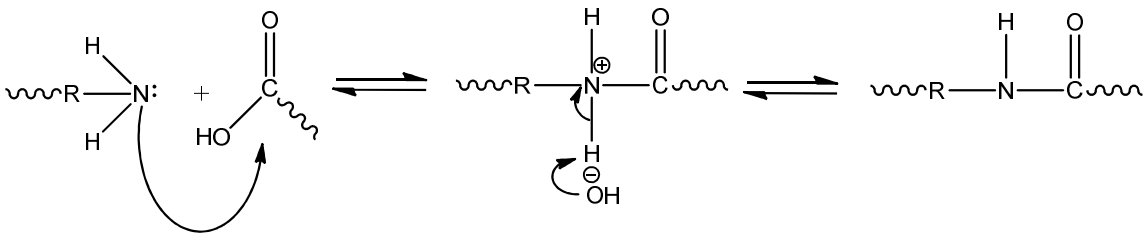

Figure 3.9 Mechanism of Nylon formation.[54]

In this thesis, two types of polymer, polyurethane and polyester, synthesized through step-polymerization are investigated.

3.8 Polyurethane

Polyurethanes will be examined in this thesis for self-cleaning coatings. Polyurethane (PU) is a polymer composed of a chain of organic units joined together by carbamate (urethane) covalent linkages, as shown in Figure 3.10.

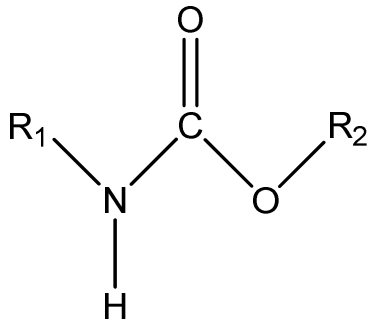

Figure 3.10 Chemical structure of Urethane Linkage.

Polyurethanes are produced by step-growth polymerization of two monomers (one contains two or more isocyanate functional groups while the other contains two or more hydroxyl groups). Because of this unique functional group linkage, polyurethanes are used in a surprising diverse array of applications, including coatings, adhesives, elastomers, foams and paints.[13,14]

3.8.1 Polyurethane Chemistry

A urethane linkage is formed in this reaction by reacting an isocyanate group, -N=C=O with a hydroxyl group, -OH. Polyurethanes are produced by the polyaddition reaction of

polyisocyanate and polyol in the presence of a catalyst. In this case, a polyisocyanate is a molecule with two or more isocyanate functional groups, R-(N=C=O)$_{n\geq 2}$ and a polyol is a molecule with two or more hydroxyl functional groups, R'-(OH)$_{n\geq 2}$. The reaction product is a polymer containing the urethane linkage, -RNHCOOR'-. Figure 3.11 shows a typical reaction for linear polyurethane synthesis in which a diisocyanate is reacted with a diol to produce a linear PU network.

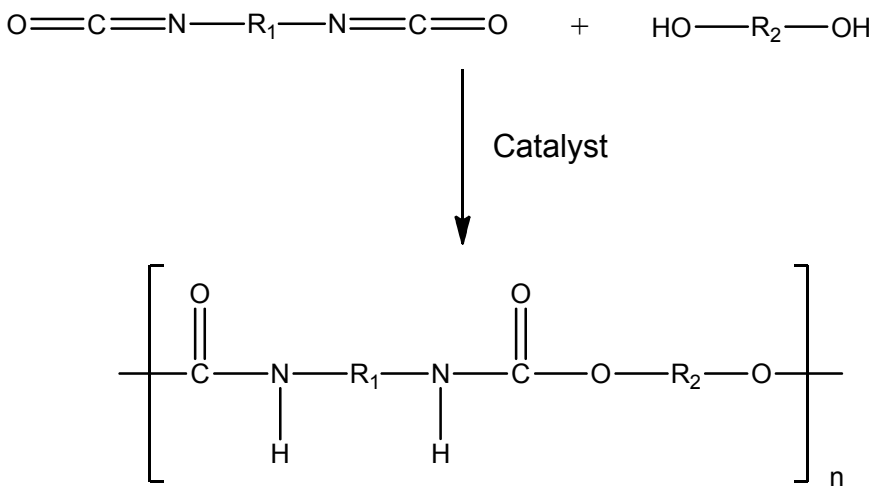

Figure 3.11 Linear polyurethane synthesis.

3.8.2 Starting Materials for Polyurethanes

The first essential component of a polyurethane polymer is the isocyanate monomer. Isocyanates are highly reactive chemicals and will react with any molecule that contains active hydrogen, for example, they can react with water to form a urea linkage.[57]

Commercially available organic isocyanates include aliphatic, cycloaliphatic, araliphatic, aromatic and heterocyclic polyisocyanates.[14,58] Examples of isocyanates[13,14] are ethylene diisocynate; 1,4-tetramethylene diisocyanate; 1,6-hexamethylene diisocyanate; 1,12-dodecane diisocyanate; cyclobutane-1,3-diisocyanate; clclhexane-1,3- and -1,4-diisocyanate, and mixtures of these isomers; perhydro-2,4'-and/or -4,4'-diphenylmethane diisocyanate (HMDI); diphenylmethane-2,4'- and/or -4,4'- diisocyanate (MDI).[13] Figure 3.12 shows the chemicalstructure of 4,4'-dicyclohexylmethane diisocyanate (HMDI), which was used in this study.

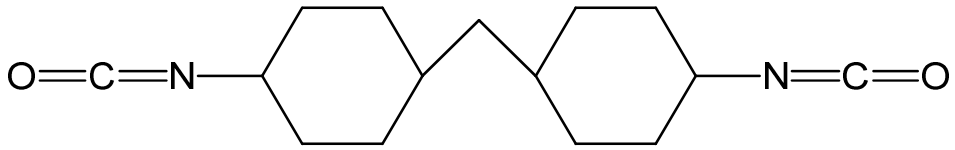

Figure 3.12 Chemical structure of 4,4'-dicyclohexylmethane diisocyanate(HMDI).

The second essential component of the polyurethane polymer is the polyol monomer. The polyol monomer has a profound effect on the properties of the finished polyurethane. There are typically four classes of polyols[14,58]: polyether polyols, amine-terminated polyethers, polyester polyols and polycarbonates. Polyether-based polyols produce very high quality polyurethane foams and elastomers. Among the most important polyether polyols are the polyBD, polytetramethylene etherglycol (PTMEG), polypropylene oxide glycol (PPO) and polybutylene oxide glycol (PBO). PTMEG, also known as PTHF, deserves special comment as a reactant in the production of hydrolysis-resistant polyurethane elastomers.[13] Its chemical structure is shown in Figure 3.13. PTHF (or PTMEG) is the polyol component used predominantly in this thesis.

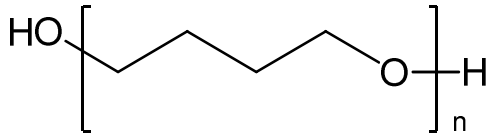

Figure 3.13 Chemical structure of polytetramethyleneetherglycol (PTMEG or PTHF).

In some cases, a chain extender is added to the polyurethane synthesis formulation. These are low molecular weight reactants that produce the familiar elastomeric properties of polyurethanes. The chain extenders provide the hard segment to the segmented polyurethane elastomers. The hard-segment content in the polyurethane backbone is important in the final properties and performance of the polymer.[13] 2,2-bis(hydroxymethyl)propionic acid (DMPA) was used as the bifunctional chain extender in this study, with its chemical structure shown in Figure 3.14.

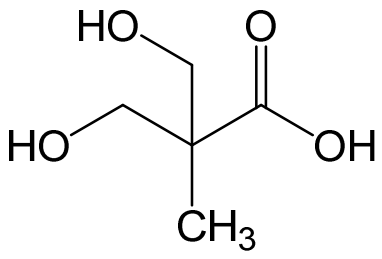

Figure 3.14 Chemical structure of 2,2-Bis(hydroxymethyl)propionic acid (DMPA).

Normally, one or more catalysts is required for PU synthesis in order to achieve a sufficiently fast reaction. Chain extenders containing hydroxyl groups are frequently rather slow. Such catalysts used for PU synthesis are typically organometallics such as dibutyl tin dilaurate (DBTDL); its chemical structure is shown in Figure 3.15. Another potential difficulty with hydroxyl-containing chain extenders is that some of these have a limited solubility in the polyol, thus limiting the amount of chain extender which can be used in the formulation.[13]

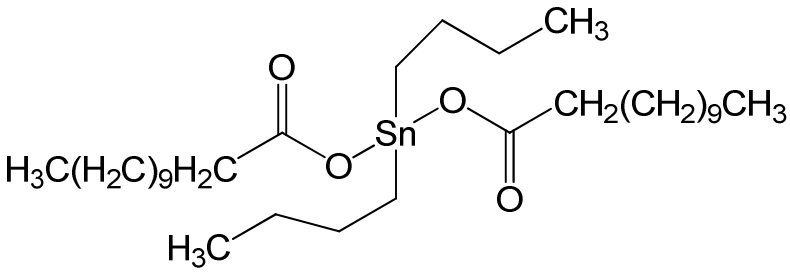

Figure 3.15 Chemical structure of dibutyl tin dilaurate (DBTDL).

3.8.3 Synthesis Processes

Polyurethanes can be prepared by two basic processes.[13] The first method is to mix a liquid diol, a polyol and diisocyanate, which polymerize simultaneously yielding the polyurethane product. To obtain thermoplastic polyurethane, the reactants should be chosen such that they produce a linear structure. This is called the one-shot process as shown in Figure 3.16.

The second method involves the reaction of a linear hydroxyl-terminated polymer with an excess of diisocyanate to form an isocyanate-terminated polymer, called a pre-polymer.

A pre-polymer is either a viscous liquid or a low-melting solid. The next step is chain extension and network formation with a small molecular weight polyol called a chain extender. Figure 3.16 gives the schematic steps of these two processes.

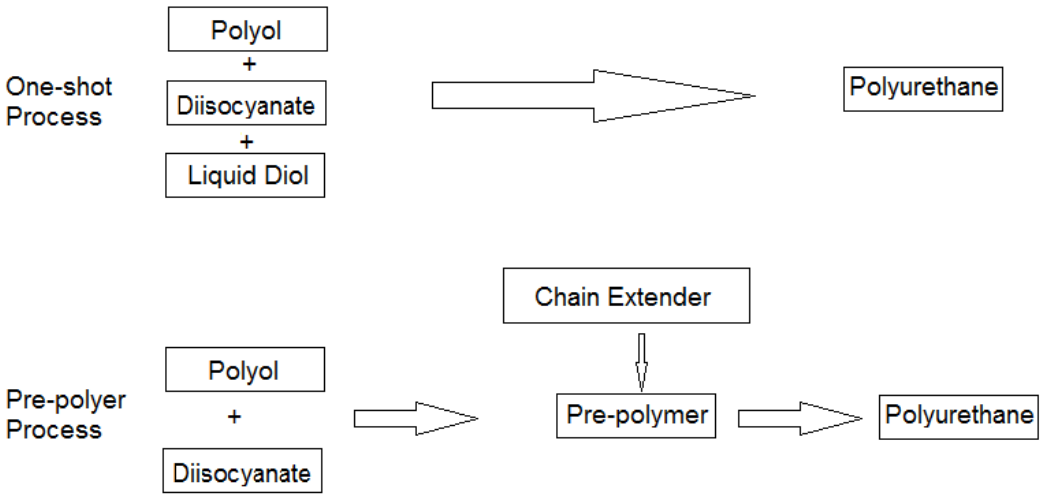

Figure 3.16 Schematic steps of two common polyurethane synthesis processes.[13]

3.8.4 Structure-Property Relations

Polyurethane physical and mechanical properties are controlled by their molecular structure. [13] Segmented polyurethanes are preferred to obtain superior properties.[14] These are block copolymers of the $(AB)_n$ type, consisting of alternating hard and soft segments. Figure 3.17 shows a schematic representation of an ideal segmented polyurethane, where the long chain diol is the soft segment while the diisocyanate and chain extender constitute the hard segment. The soft segments, long chain diol, are mobile and amorphous, while the hard segments are immobile and stiff.[13,14] Because of this phase segregation between the hard crystalline segment and the soft amorphous segment, polyurethanes have unique physical and mechanical properties.[13] Polyurethanes with both the aromatic and aliphatic hard segments have been investigated by many researchers.[14,58-60]

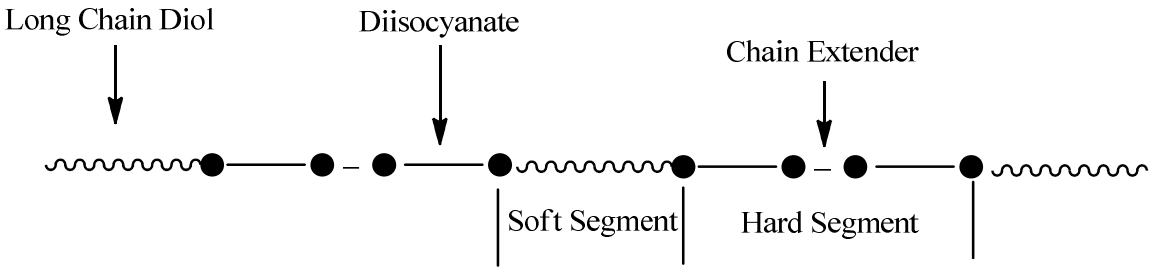

Figure 3.17 Representation of the ideal primary structure of a segmented PU.[61]

The composition and arrangement of the hard and soft segments have a great impact on the resulting physical and mechanical properties of the polyurethane.[13,61,62] The hard segment provides superior tensile strength and hardness; while the soft segment gives the polyurethane elasticity and flexibility.[13] By controlling the synthesis process, the polyurethane product can achieve very good elasticity while maintaining reasonably high tensile strength.[13] Hence, the formulation chemistry of polyurethanes provides an almost infinite number of possibilities for changing the structure of this class of polymer, leading to a rich diversity of physical and mechanical properties.

The chemical composition of soft segments also plays a significant role in polyurethane wettability.[61] Polyurethanes based on the incorporation of a poly(ethylene oxide) (PEO) soft segment exhibit substantial water uptake and, therefore, high moisture vapor transmission rates. Hydrophilic polyurethanes were prepared by Tobolsky and coworkers when PEO was used as the soft segment.[63]

3.9 Polyester

Polyester is another polymer inspected in this study. Polyester is a category of step-growth polymer which contains the ester functional group in the main backbone chain (Figure 3.18).

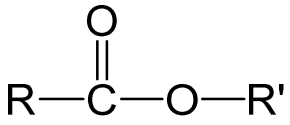

Figure 3.18 Chemical structure of ester functional group.

Polyesters are produced by step-growth polymerization of two monomers (one monomer contains two or more carboxyl functional groups while the other monomer contains two or more hydroxyl groups). Polyesters are used worldwide and have a wide variety of applications, including synthetic fibers, films, beverage bottles, and molded plastic parts.[16]

3.9.1 Linear aliphatic polyester

Linear aliphatic polyesters were first synthesized by Carothers and coworkers at DuPont,[64] which are nowadays among the most used biodegradable polymers.[65] Because of it has similar linkages and structure as frequently encountered materials, such as shellac, a naturally occurring aliphatic polyester, it is environmentally degradable.[65] Numerous biodegradable polyesters had been developed in the 20th century.

There are two major applications that biodegradable polyesters currently have: the first is as biomedical polymers that contribute to the medical care of patients and the other one is for ecological applications.[66] Most of the currently available polyesters are used only for either one of the two purposes, but some can be used for both applications,[66] as shown below.

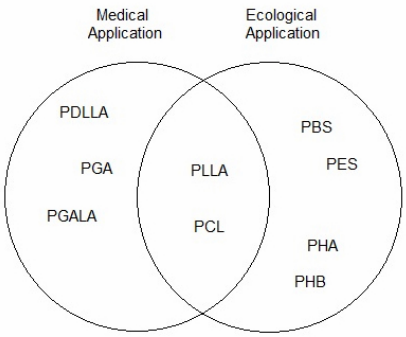

Figure 3.19 Application of biodegradable polyesters.[66] PDLLA: poly(DL-lactide); PGA: poly(glycolide), poly(glycolic acid); PGALA: poly(glycolide-co-lactide); PLLA: poly(L-lactide), poly(L-lactic acid); PCL: poly(ε-caprolactone); PBS: poly(butylene succinate); PES: poly(ethylene succinate); PHA: poly(hydroxyalkanoate); PHB: poly(3-hydroxybutyrate).

Polycaprolactone (PCL) was chosen as one of the aliphatic polyesters investigated in this study. Synthesis of PCL usually involves the ring-opening polymerization of its monomer, ε-carprolactone (shown in Figure 3.20). It is a semicrystalline polymer with a degree of crystallinity of 50%, a low Tg of about -60^{o}C.[65] The processing of this materials are usually injection molding, film blowing and extrusion.[65]

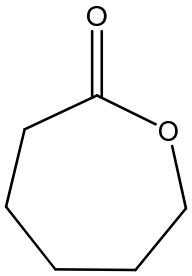

Figure 3.20 Chemcial Structure of ε-carprolactone.

PCL are widely used in several fields ranging from agricultural implements to biomedical applications. It has been used as a soil-degraded container material and as thin-walled tree seedling container.[65] Carpronor^{TM}, a one year implantable contraceptive device, was made of PCL.[67] Also, by blending with starch and its derivatives, it has been used in shopping bags.[68]

Because of its biocompatibility, low glass-transition temperature (T_g) and high permeability[69], PCL is one of the most commonly used materials in biodegradable drug delivery systems.[65] Various drug-delivery devices made of PCL can be easily degraded by hydrolysis in physiological conditions (such as in the human body).[70,71]

3.9.2 Poly(ethylene terephthalate) (PET)

Unlike linear aliphatic polyesters, poly(ethylene terephthalate) (PET), discovered by Whinfield and Dickson,[64] has a high melting point and good hydrolytic stability. Because of its good physical properties, PET is the most used polyester and third most produced polymer worldwide. The main applications of PET are fibers for textiles, films and bottles because of its excellent properties as tensile impact strength, chemical resistance, processability, clarity and thermal stability.[16,72,73]

Conventionally, PET has been manufactured via condensation polymerization.[16] The polymerization normally proceeded in two steps,[74] i.e. the esterification and condensation steps, with the latter step occurring under higher temperatures and vacuums, helping to drive the polymer to higher molecular weights. Figure 3.21 shows the schemes for PET polymerization process.

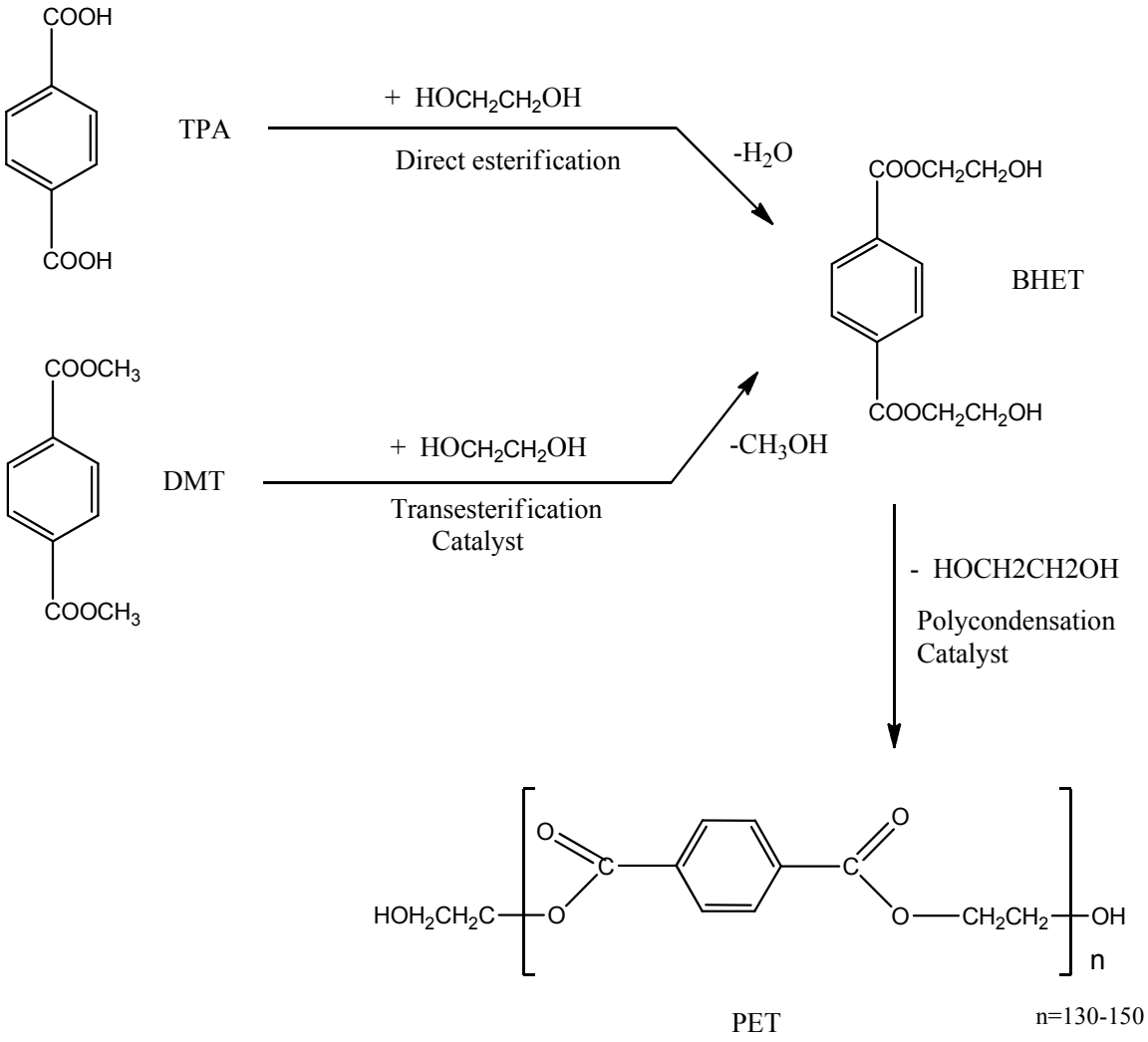

Figure 3.21 Schemes for PET polymerization process.[16]

In the first step, there are typically two different routes were used: transesterification of dimethylester with diol[74-76] or direct esterification of a diacid with adiol.[74,77]

Dimethyl terephthalate (DMT) and ethylene glycol (EG) are the monomers used for the transesterification reaction. DMT and EG with catalysts are charged into a reactor

equipped with a slow stream of nitrogen gas at 170-210 ^{o}C. Methanol is collected into a graduated receiver as a by-product to estimate the extent of conversion during this process. The reaction is completed when the distillation of methanol is ceased and bis-(2-hydroxyetheyl) terephthalate (BHET) is synthesized in the first step.[16]

After the development of a new purification process for terephthalic acid (TPA), it became the preferred raw material for pre-polymerization. Reaction temperature in this process is generally between 240-260 ^{o}C. Catalysts are not typically used in this reaction in that the acid functional groups of TPA can catalyze the reaction. Similarly to transesterification, the condensate, in this case water, should also be collected to estimate the conversion.[16]

In the second step, BHET synthesized from the first step is steadily heated to 280 ^{o}C and then evacuated to low pressure while maintaining the temperature. In this step, EG is the by-product and should be collected for conversion estimation.[16]

Recently, several papers[72,78-81] have reported a novel synthesis method using the ring-opening polymerization of various cyclic oligomers. The ring-opening polymerization has several advantages over conventional polymerization. For one, there is no by-product produced from the ring-opening polymerization.[79,80] By-product removal requires both high temperature and high vacuum using the conventional synthetic method.[74] Second, the reaction is rapid for the ring-opening polymerization.[72] Also, higher molecular weights can be more easily achieved. Molecular weights as high as 100,000-300,000 g/mol were reported for ring-opening polymerizations, while the highest molecular weights achieved by polycondensation are 40,000-60,000 g/mol.[16]

Chapter 4

4 Synthesis and Characterization of TiO_2-Polyurethane Nanocomposites

Nano-titania-polyurethane (nano-TiO_2-PU) composite coatings were synthesized using a "grafting from" polymerization technique, where nano-TiO_2 was chemically attached to the polymer backbone with a bifunctional monomer, 2,2-bis(hydroxymethyl) propionic acid (DMPA). An available–COOH group of this monomer can coordinate to nano-TiO_2, whereas the two available -OH groups can react with diisocyanate groups through step-growth polymerization. TGA and FTIR were performed to confirm coordination and identify the coordination binding mode. Contact angle analysis showed that the resulting polyurethane nanocomposites surface became more hydrophilic when exposed to UV light. Self-cleaning was also confirmed using stearic acid and DMPA as models for 'dirt', with the results showing that higher TiO_2 concentrations in the PU nanocomposites demonstrated superior self-cleaning property.

4.1 Introduction

Self-cleaning coatings using nanostructured titania (nano-TiO_2) have been of significant interest both academically and industrially.[1,82,83] Currently, TiO_2 photocatalysis is actively used in environmental decontamination[84,85] because of its photodegradation of organic compounds. Although most photocatalytic self-cleaning coatings research has focused on self-cleaning glass, self-cleaning polymers for paints and coatings are of significant potential industrial and scientific importance.[1] However, little work has been performed on the chemistry for the integration of nano-TiO_2 into polymers for self-cleaning coatings, in which the nanoparticles are chemically linked to the polymer chains-i.e. forming inorganic/organic hybrids.

Inorganic/organic hybrids are emerging materials for polymer coatings due to their extraordinary and unique combination of properties originating from the synergism between the inorganic nanoparticles and the polymer.[1] However, titania nanoparticles have a strong tendency for aggregation and agglomeration in polymer matrixes due to

their relatively large surface area compared to their particle size and their low interaction forces with the polymer substrate.[5] In order to overcome this problem, various efforts have been made by researchers. One common approach is to de-aggregate the agglomerated nanoparticles using a mechanical method such as ultrasonic. However, this approach is restricted due to the limited interaction between the inorganic fillers and the organic matrix.[5] An improved approach termed 'grafting from' polymerization involves attaching nano-TiO_2 chemically to the polymer chains.[1,2,5]

Polyurethanes (PUs) are polymers composed of organic units containing urethane linkages. With a broad selection of various raw materials and catalysts, different production methods, and a variety of processing methods, PU can be manufactured into products with a diversity of properties.[15] Today, polyurethanes are produced in the form of foams (both flexible and rigid), elastomers, coatings and adhesives. Even with the wide range of raw materials, the principal chemical reaction involved in the synthesis of polyurethanes (PU) is characterized as the reaction between isocyanate functional groups (-N=C=O) and hydroxyl groups (-OH), which leads to the formation of urethane linkages. The scheme of this characteristic reaction is shown in Figure 4.1.

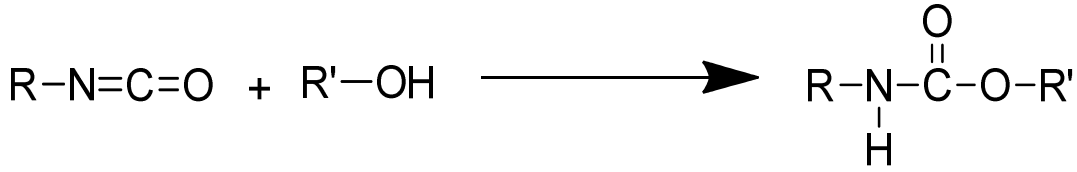

Figure 4.1 Scheme for urethane linkage formation.

There are two synthesis methods commonly used for PU synthesis,[13,14] i.e. the one-shot method and the pre-polymer method. Here, the chemical reaction principles of PU synthesis are the same (i.e. urethane formation as shown in Figure 4.1). However, the addition sequences of monomers applied on these two approaches (shown in Figure 4.2) are different.

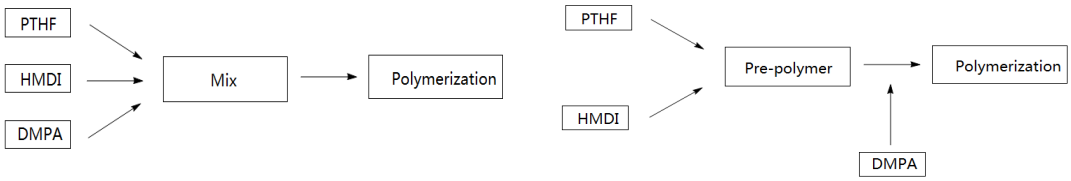

(a) (b)

Figure 4.2 Adding sequences of: (a) One-shot process and (b) Pre-polymer process.

In this chapter, polytetrahydrofuran (PTHF) and 4,4-methylenebis(cyclohexylisocyanate) (HMDI) were chosen as the two raw materials to synthesize PU. DMPA not only can serve as a chain extender because of its two hydroxyl groups, but can also act as the coordination link to TiO_2 owing to its carboxyl group. Several researchers have studied the carboxyl group coordination to titanium dioxide in recent years. Rotzinger et al.[86] proposed three possible structures of carboxylate coordination to a titania surface. (Figure 4.3)

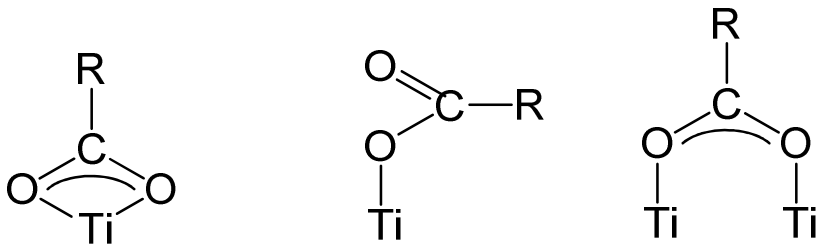

(a) (b) (c)

Figure 4.3 Binding modes of carboxyl group with titania. (a) Chelating bidentate, (b) Monodentate and (c) Bridging bidentate.[86]

In the first structure, carboxylate is bound to one Ti^{IV} center in a chelating bidentate mode (Figure 4.3a). The carboxylate functionality can also be bound to one Ti^{IV} in a monodentate ('ester type') mode (Figure 4.3b). Finally, the carboxyl group can bind with each of its oxygen atoms to a Ti^{IV} center of the surface yielding the bridging bidentate mode (Figure 4.3c).[86]

In this study, the 'grafting from' polymerization method was applied to synthesize the titanium dioxide functionalized polyurethane (nano-TiO_2-PU). Using this method, the

final polymer was functionalized by going through the standard polymerization process using the functionalized monomer. TGA and FTIR were performed to confirm and identify the coordination GPC was performed to characterize the polymer molecular weights while tensile testing results showed that the product from the pre-polymer method had superior mechanical properties than the one from the one-shot method. Contact angle tests were performed to study the surface hydrophilicity while the self-cleaning was evaluated using stearic acid and DMPA as models for 'dirt'.

4.2 Experimental

4.2.1 Materials

All chemicals were either purchased from Sigma-Aldrich (Mississauga, ON) or Caledon Labs (Georgetown,ON). Poly(tetrahydrofuran) (PTHF) with an average molecular weight of 1000 Daltons was preserved in a vacuum oven at 30 ºC to remove all moisture and maintain in the liquid form before use. Titanium dioxide (anatase nanopowder, <25nm particle size; rutile nanopowder, < 100nm particle size) was calcined at 400^{o}C before use. 4,4′-methylenebis(cyclohexylisocyanate) (HMDI), 90%, mixture of isomers,2,2-Bis(hydroxymethyl)-propionic acid (DMPA), 98%, stearic acid, reagent grade, 95%, dibutyltindilaurate (DBTDL), 95%, 2-propanol, anhydrous, 99.5%, tetrahydrofuran (THF), andydrous, inhibitor free were used as prepared by Sigma-Aldrich. Methanol, reagent, 99.8%, tetrahydrofuran (THF), HPCL grade, ≥99.9% were used as prepared by Caledon Labs.

4.2.2 Experimental Setup

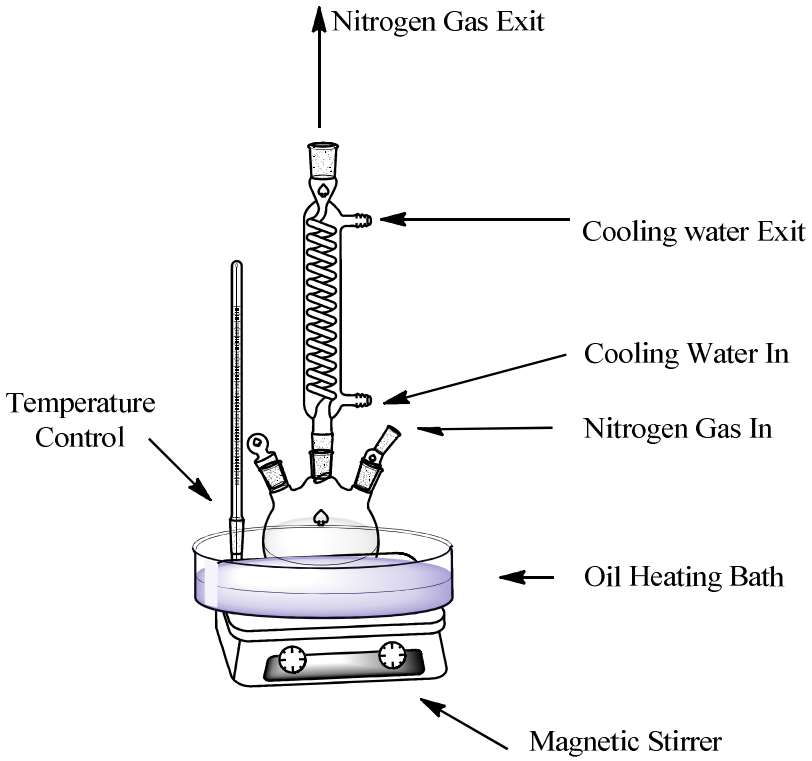

Figure 4.4 Polyurethane Synthesis Setup.

The synthesis experimental setup, as illustrated in Figure 4.4, consists of an oil bath for reaction temperature control and a three-neck round-bottomed flask equipped with a mechanical stirrer, a nitrogen inlet and a condenser for: a) mixing solvents, reactants and catalyst during polymerization, b) providing a purge stream of nitrogen gas to avoid any inhibitor (moisture, oxygen) in the air that could inhibit the reaction, c) cooling hot vapors into liquid back to the flask.

A VWR®ceramic top hot plate stirrer with temperature control was used to provide mechanical stirring and heating. All glassware was dried in an oven at 80 ºC and cooled in a desiccator overnight to avoid moisture.

4.2.3 Polyurethane Synthesis using Pre-polymer Method

For the pre-polymer method, HMDI and PTHF mixture at a molar ratio 2:1 was dissolved in THF solvent with DBTDL (0.1%wt) as catalyst. The reaction was kept at 60 ºC under

nitrogen gas flow and constantly mixed by magnetic stirring. After 2 h reaction, the said pre-polymer was then polymerized at a 1:1 molar ratio with a chain extender, DMPA. The whole process was under nitrogen with the polymerization carried out for 24-48 h. At the end of the reaction, the mixture solution would reach a high viscosity level to cause the stopping of the stirring bar. The reaction was then stopped and the product was transferred into methanol solvent to quench the reaction. The methanol solution of PU contained in a Teflon plate was then placed into a vacuum oven at room temperature to obtain a dry polyurethane coating.

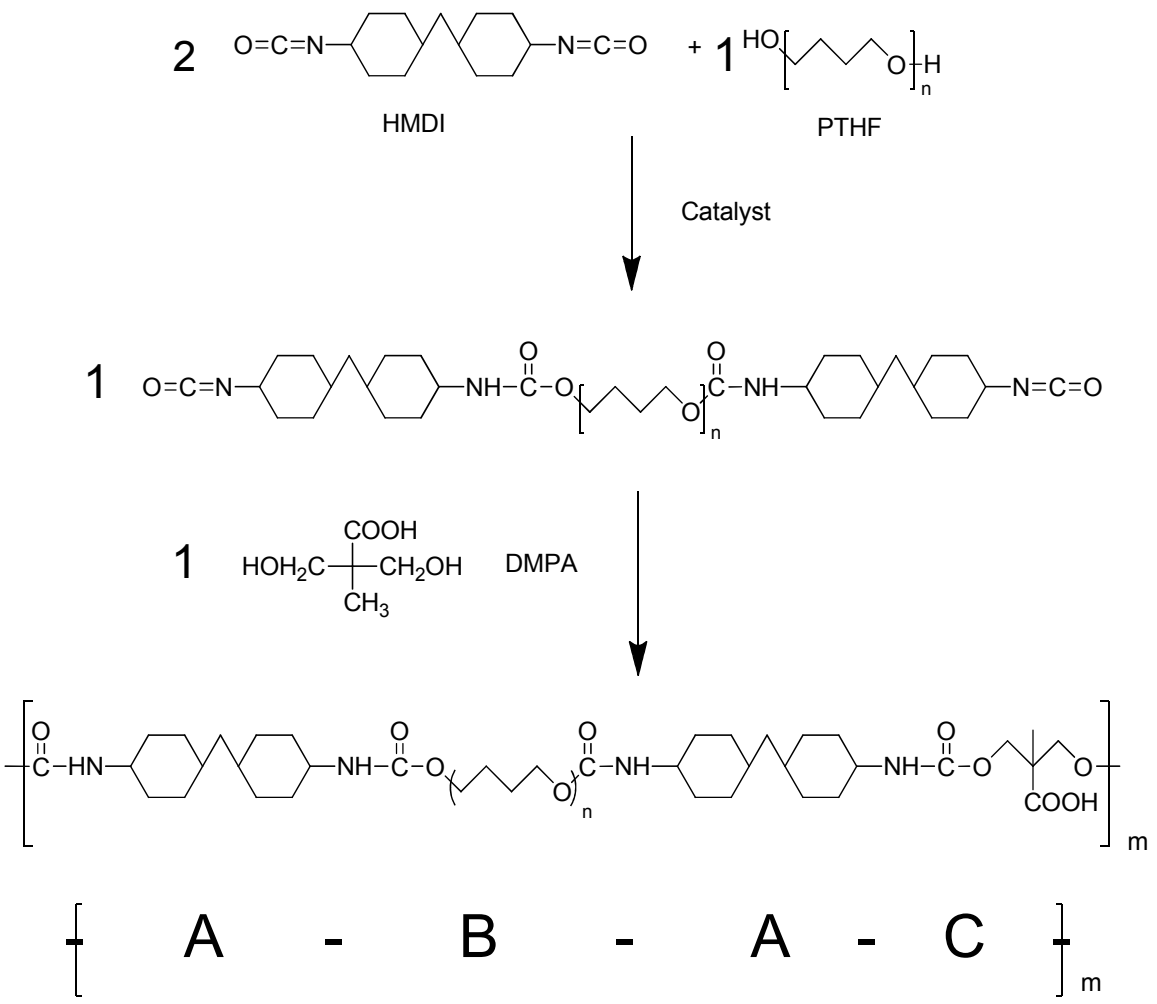

Figure 4.5 Schemes for Pre-polymer Method Polymerization Chemistry.

In this method, HMDI (A) and PTHF (B) are introduced into the reactor firstly at a molar ratio of 2:1, followed by addition of DMPA (C)(as shown in Figure 4.2 b) to function as a

chain extender. Therefore, pre-polymer would first be formed with a structure of –A-B-A- and only isocyanate functional groups would remain in the matrix after two hours reaction. By then adding DMPA into the reaction, the DMPA reacts with pre-polymer forming an alternative copolymer with a –A-B-A-C- repeating unit. Figure 4.5 shows the chemistry schemes for this polymerization process.

4.2.4 Polyurethane Synthesis Using One-shot Method

For the one-shot process, HMDI (A), PTHF (B) and DMPA (C) mixtures at a molar ratio 2:1:1 were dissolved in THF solvent with DBTDL (0.1%wt) as catalyst. The reaction was carried out under constant mixing via a magnetic stirrer at 60 ºC. The whole process was under nitrogen with the polymerization carried out for 24-48 h. At the end of the reaction, the mixture solution would reach a high viscosity level to cause the stopping of the stirring bar. The reaction was then stopped and the solution transferred into methanol to quench the reaction. The methanol solution of PU contained in a Teflon plate was then placed into a vacuum oven at room temperature to obtain dry polyurethane coating.

As shown in Figure 4.2 a, for one-shot method, three ingredients including HMDI (A), PTHF (B) and DMPA (C) were all added into the reactor at the beginning of the reaction, and the reactions among the three monomers happen simultaneously and randomly. As a result, the copolymer chain would be randomly arranged, as shown in the following Figure 4.6.

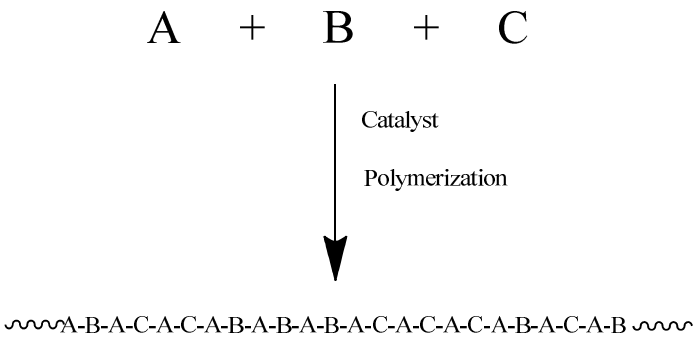

Figure 4.6 Random Copolymer Chain Structure.

4.2.5 Monomer functionalization

As mentioned before, the carboxyl group in DMPA was used to coordinate with titanium dioxide as shown in Figure 4.7. After the monomer functionalization of DMPA with nano-TiO_2(anatase nanopowder, <25nm particle size), a new functionalized monomer, termed nano-TiO_2-DMPA, was synthesized. All functional nano-TiO_2-DMPA used anatase nano-powder for reaction in that previous research showed rutile nano-powder had poor coordination to DMPA.[5]

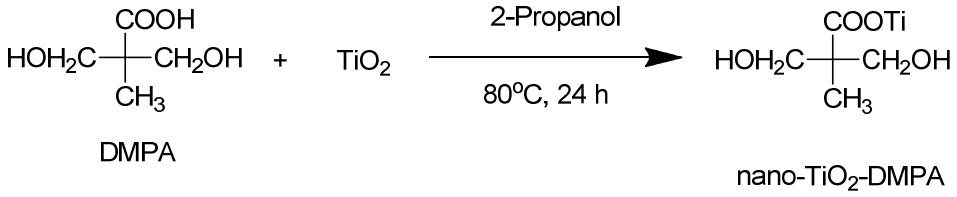

Figure 4.7 Scheme for Monomer Functionalization.

The procedure is described as follows: 1g nano-TiO_2 and 4g DMPA powers were dispersed into 40mL iso-propanol solvent, which was heated at 80ºC under nitrogen gas flow for 24h after 1 h ultrasonication. The mixture was then centrifuged at 5000 rpm for 10 min so as to separate into a solid from solution. The solids recovered were then re-dispersed into methanol solvent and re-precipitated by centrifugation for several times until the solution became clear. The resulting solid products were then dried overnight in vacuum oven at 80ºC.

4.2.6 Synthesis of nano-TiO_2-PU using Pre-polymer Method

Because of its product having superior mechanical properties, the pre-polymer method was chosen as the method for functional polyurethane synthesis. The polymerization step is similar as mentioned previously with the exception of using nano-TiO_2-DMPA instead of DMPA for the reaction. Figure 4.8 shows the chemical scheme for this process.

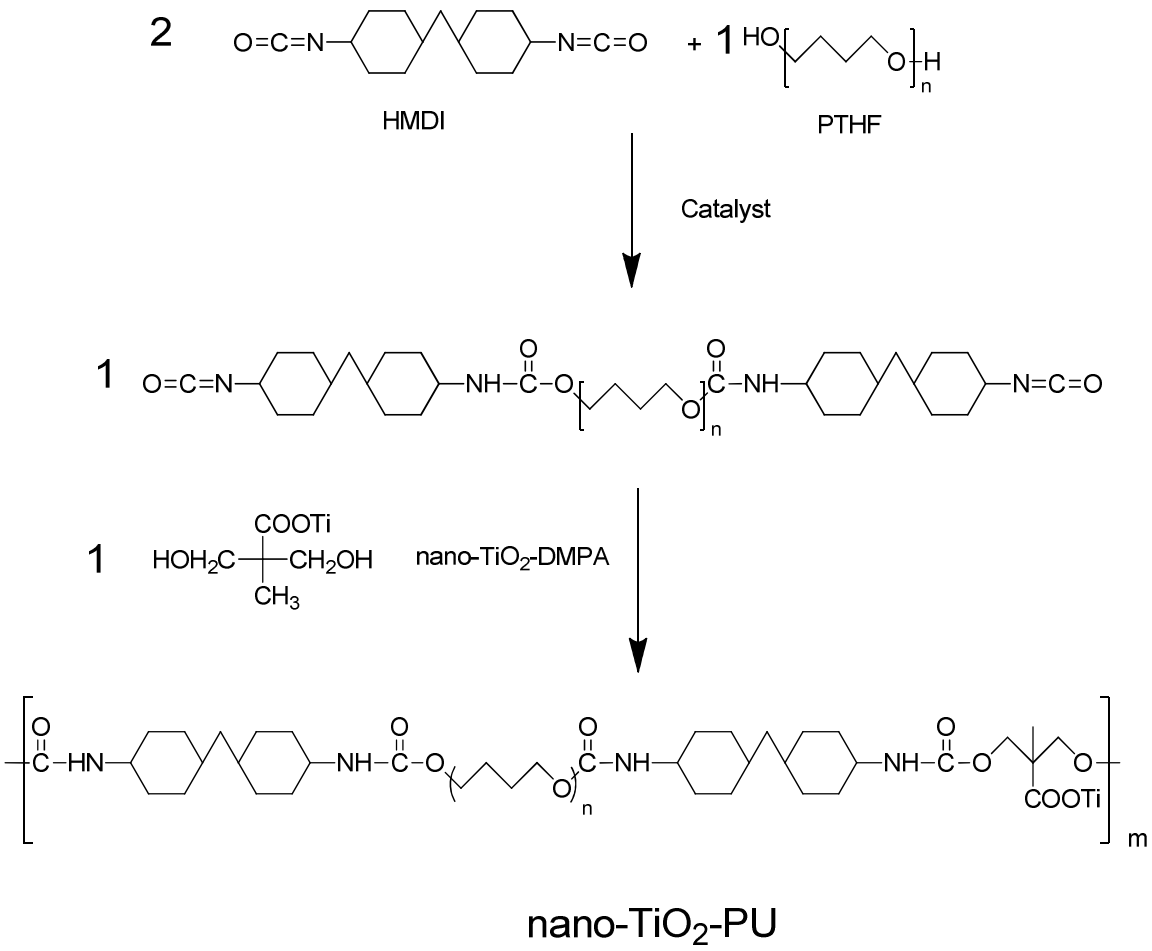

Figure 4.8 Scheme for nano-TiO_2-PU synthesis.

4.2.7 Commercial PU and TiO_2/PU mixture preparation

Samples were prepared in two different ways. First, simply blend the same amount of two raw materials, and place the resulting blends into a Teflon mold (length:110mm, width: 50mm, depth: 10mm) . This is the commercial way to apply polyurethane coating onto the uncoated surface.

For TiO_2/PU sample, because of the high viscosity of the polyurethane raw materials, TiO_2 was not able to sufficiently disperse throughout the polyurethane matrix. Therefore, TiO_2 (1wt% or 2wt% of the polyurethane) was dispersed in 5mL acetone solvent with the aid of ultrasonication. The same amounts of two raw materials (usually 3mL of each) were then added into the solution which was subsequently placed into Teflon molds(length:200mm, width: 50mm, depth: 10mm). To avoid experimental bias, the

preparation process of pure PU samples used for tensile test also involves the 5mL aceton solvent. Samples prepared were then performed under tensile tension testing according to the ASTM D882-10 standard.

4.3 Characterization

4.3.1 Fourier Transform Infrared Spectroscopy

FTIR analysis was performed using an ATR-FTIR spectroscope (Nicolet 6700 FT-IR Spectrometer, Thermo Scientific, USA) in the range of 500-4000 cm^{-1} with 32 scans for each sample to measure and identify the variations of the functional groups and characteristic peaks.

4.3.2 Gel Permeation Chromatography

Gel Permeation Chromatography (GPC) was used to determine the molecular weight of polyurethane. 30 mg of polyurethane sample was first dissolved in 10 mL THF solvent. The solution was then filtered by syringe filter featuring 0.2 μm pore size. 100 μL of filtered solution was taken from the vial each time for the gel column (GPCmax VE-2001,Viscotek, USA) with a flow rate of 1mL/min THF solvent at room temperature. Signals are collected by detector (TDA 302 triple detector array, Viscotek, USA) during a 45 minute run. Polystyrene standards with known molecular weights were used to calibrate the system.

4.3.3 Thermo-Gravimetric Analysis

Thermo-gravimetric Analysis (TGA) was used to measure the thermal stability of the polyurethane coatings. TGA analysis was performed using a TGA analyzer (SDT Q600, TA Instruments, USA) and the spectra were analyzed using Universal Analysis 2000 software. Experiments were carried out under nitrogen gas atmosphere. Samples weighing about 10-15 mg were kept in a alumina sample pan and heated to 800ºC from room temperature at a heating rate of 10ºC/min. The real time weight loss as function of temperature is recorded during the experiment using Universal Analysis 2000 data acquisition system.

4.3.4 Differential scanning calorimetry

Differential scanning calorimetry (DSC) was performed using a differential scanning calorimeter (SDT Q600, TA Instruments, USA) with the spectra analyzed using the instrument software (Universal Analysis 2000, TA Instruments, USA). Experiments were carried out under nitrogen gas atmosphere. Samples weighing 10-15 mg were kept in a alumina sample pan and heated from room temperature to 200ºC at a heating rate of 10ºC/min. The real time heat flow as function of temperature was recorded during the experiment using Universal Analysis 2000 data acquisition system.

4.3.5 Mechanical Property Test

Tensile tests were performed to determine the mechanical properties using a tension tester (5943 Single Column Tabletop Systems, Instron, USA) according to the ASTM D882-10 standard.

For synthesized pure PU samples, 2 g of PU was first dissolved in 20mL THF solvent. After fully dissolved, the solution was then poured into rectangular Teflon dishes (length:110mm, width: 50mm, depth: 5mm) to form thin films of PU coatings (usually around 0.30mm thickness). The thin PU films were then shaped into rectangular by l00 mm length and 5-10 mm width using scissors. Specimens were loaded between grips with 50 mm gauge length and tested at a constant crosshead speed of 500 mm/min.

For commercial PU samples, preparation process was mentioned in section 4.2.7. These sample films were shaped into rectangular by 200mm length and 5-10mm width using scissors. Specimens were loaded between grips with 100mm gauge length and tested at a constant crosshead speed of 50mm/min.

4.3.6 Contact Angle Characterization

Hydrophilic and hydrophobic behavior was evaluated by measuring the contact angle of a water droplet on the films under ambient conditions using the sessile drop method. The contact angle measurement was performed using a standard contact angle goniometer Model 200,ramé-hart instrument co., USA). The coating surface was placed and leveled on the test cell between the light source and microscope. Then 10μL water droplet was

deposited onto the coating surface through a syringe. After the liquid drop reaches its equilibrium state, its digital image was recorded and the contour fitted by software (DROPimage Standard v2.4, Ramé-Hart instrument co., USA).

4.3.7 Self-cleaning Property Test

Photocatalytic activity that leads to the self-cleaning property of the nano-TiO_2-PU coatings was examined by monitoring the degradation of 'dirt' on the polymer surface. Weight loss of samples was recorded during the degradation process with stearic acid and DMPA being chosen as the model compounds for 'dirt'.

The test process started with dissolving 2g nano-TiO_2-PUwith excess 'dirt' compound (0.2g, 10%wt) into 20mL THF solvent. The solution was then poured into round Teflon dishes (d=70mm) to form thin films of the nanocomposite. The films were then irradiated perpendicular to the light source at a constant distance of 5cm with a high intensity UV lamp (Blak-Ray B100-AP,UVP, USA). The weight changes of samples were recorded during the irradiation using an analytical balance (accuracy 0.1mg). Also, samples (before and after UV irradiation) were analyzed by FTIR, TGA, DSC accordingly.

4.4 Results and Discussion

Pure polyurethanes were synthesized by the two different methods shown in Figure 4.2 using the same raw materials. As shown in Figure 4.9, products in both figures are transparent coatings; no obvious differences were observed between the two products and both coatings were found quite flexible.

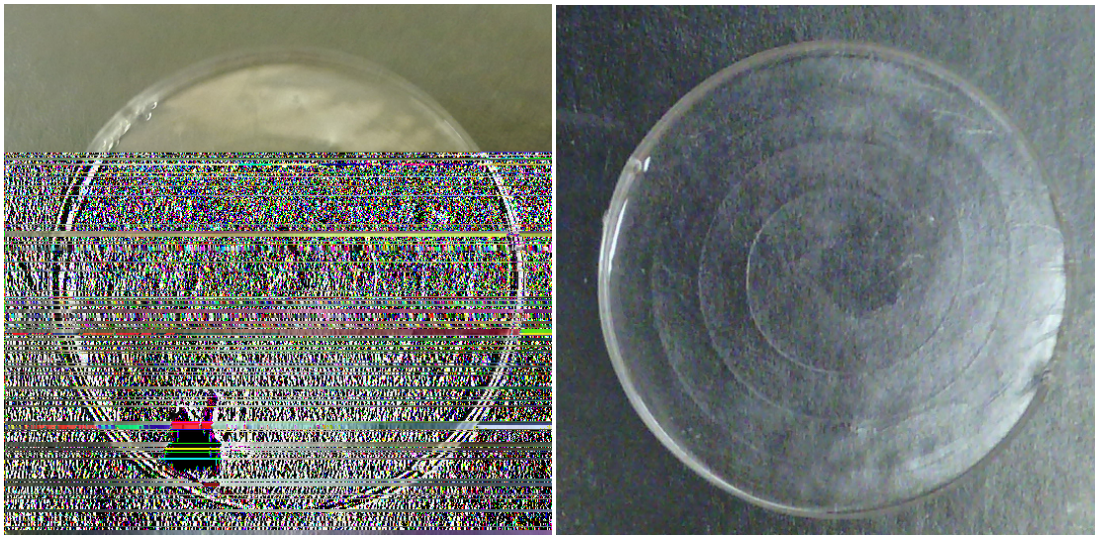

Figure 4.9 Digital pictures of (a) PU from one-shot method (experimental section 4.2.4)and (b) PU from pre-polymer method (experimental section 4.2.3). Raw materials: HMDI, PTHF and DMPA. Reaction taken place at 60^{o}C under nitrogen flow protection.

4.4.1 FTIR analysis of pure PU

The final pure PU products from both synthesis methods were characterized by FTIR analysis in absorbance mode. FTIR spectra of PU from both methods are shown in Figure 4.10, where all anticipated peaks were detected, which prove that polyurethane was formed. The peaks from the N-H stretch at 3320^{-1} and C=O stretch at 1700^{-1} are characteristic urethane linkage peaks, which are similar compared to other literature.[15,87] Also, the absence of isocyanate peak (≈ 2260^{-1}) further confirms polyurethane formation from complete conversion of monomer.

The characteristic IR absorptions using the one-shot method and the pre-polymer method are almost identical, indicating that both techniques gave the polyurethanes with the same chemical composition.

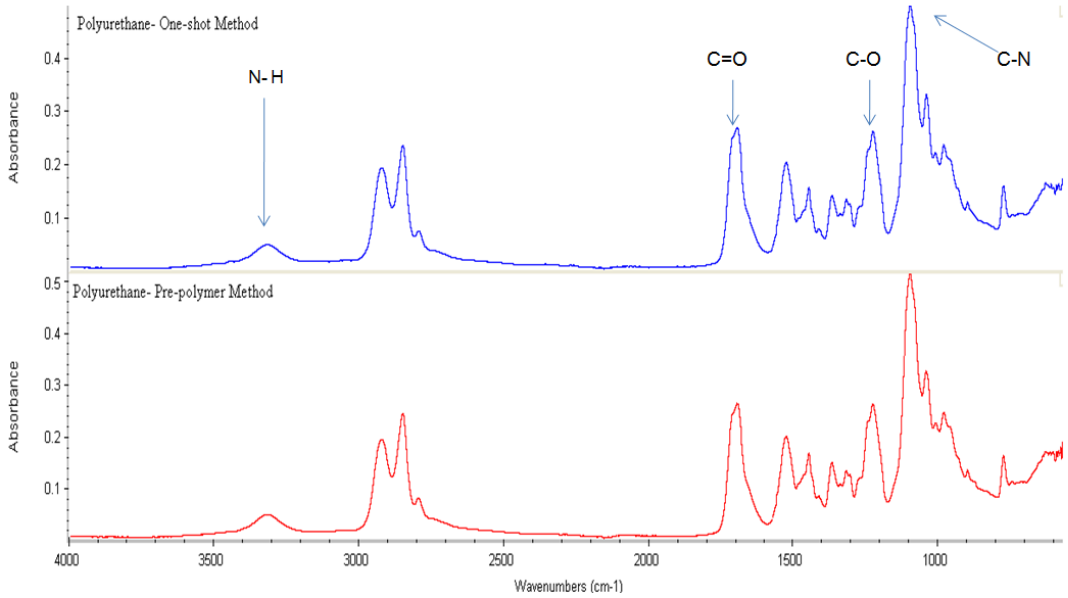

Figure 4.10 FTIR spectra of PU from one-shot method (experimental section 4.2.4)and PU from pre-polymer method (experimental section 4.2.3). Raw materials: HMDI, PTHF and DMPA. Reaction taken place at 60^{o}C under nitrogen flow protection.

A summary of the characteristic IR absorption peaks in the polyurethanes is given below in Table 4.1. All functional group assignments of characteristic peaks are based on the standard IR absorption literature.[88,89]

Table 4.1 Characteristic IR absorption peaks in PU. Raw materials: HMDI, PTHF and DMPA. Reaction taken place at 60^{o}C under nitrogen flow protection.

Frequency, cm^{-1}	Bond	Functional group
3320	N-H stretch	Urethanes
2950,2850	C-H stretch	Alkanes
1700	C=O stretch	Urethanes
1530	C-C stretch in ring	Alkanes
1450	C-H bend	Alkanes
1250	C-O stretch	Urethanes
1100	C-N stretch	Urethanes

4.4.2 Molecular weight of pure PU

GPC analysis was performed to investigate the molecular weight of resulting polymer. Figure 4.11 shows typical GPC chromatograms for polystyrene (a) and polyurethane (b).

For polystyrene (PS) chromatogram, three peaks (Red for RI signal, black and green for low/high angle light scattering) on retention volume 25-29 mL overlap with each other, indicating the presence of macromolecular molecule, or in another word polymer. The molecular weight of this PS standard is 93,355 Da.

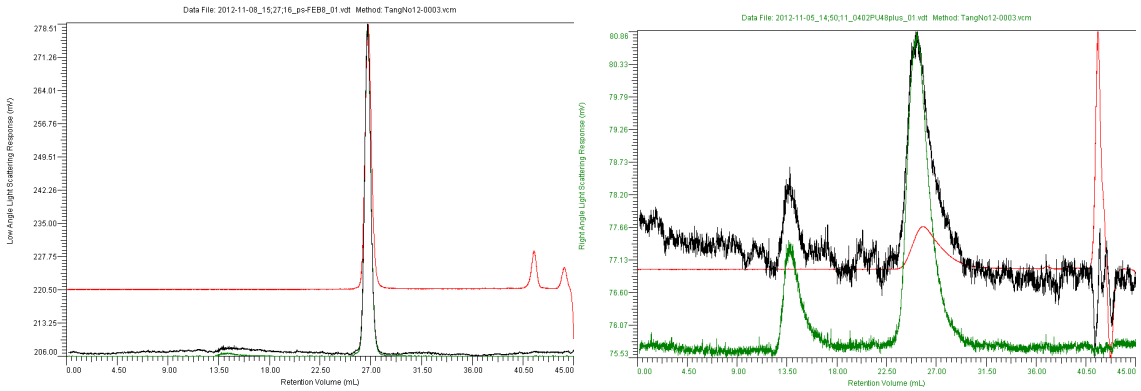

(a) (b)

Figure 4.11 GPC chromatograms for (a)polystyrene standard (M_w=93,355) and (b) synthesized PU (M_w=15,037) from pre-polymer method (experimental section 4.2.3). Raw materials: HMDI, PTHF and DMPA. Reaction taken place at 60^{o}C under nitrogen flow protection.

For the PU chromatogram, three peaks (Red for RI signal, black and green for low/high angle light scattering) on retention volume 22-29 mL overlap with each other, indicating the presence of polymer. At retention volume 11-18mL, the absence of red peaks indicates this is an inorganic particle, which suggests the presence of inorganic catalyst. By comparing to PS standard, PU samples have average molecular weight of 15,037±1046 Da (calculated from GPC software) after 3 runs.

4.4.3 Mechanical property of pure PU samples

As described in the experimental section, the one-shot process and the pre-polymer process would generate different copolymer chain arrangements. It is shown in Figure 4.12 that the tensile strength of the polyurethanes from the pre-polymer method (PU-PP) =16.6 MPa, which is significantly higher (60%) than that of the polyurethanes from the one-shot method (PU-OS) (10.2 MPa). Meanwhile, the Young's Modulus results from

Table 4.2 show that PU-PP (4.44 MPa) has a higher modulus value than PU-OS (3.98 MPa).

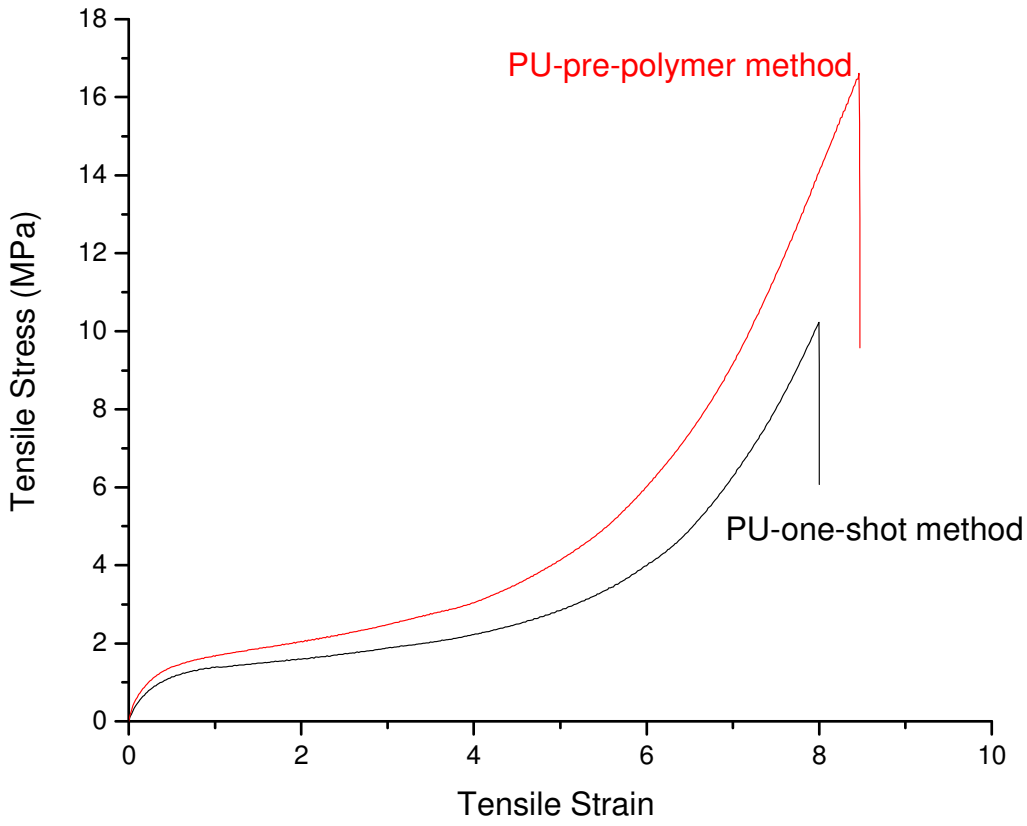

Figure 4.12 Tensile stress-strain plots of PU from one-shot method (experimental section 4.2.4)and PU from pre-polymer method (experimental section 4.2.3). Raw materials: HMDI, PTHF and DMPA. Reaction taken place at 60^{o}C under nitrogen flow protection. Sample(test length: 50mm, width: 5-10mm, thickness: around 0.30mm) was tested at a constant crosshead speed of 500mm/min.

As previously discussed, product from the pre-polymer method would form alternative copolymer with an –A-B-A-C- repeating unit; while product from the one-shot method would be random copolymer. It is widely known that polymer chains with defined arrangements are more favourable in crystallization than randomly arranged polymer

chains. At the same time, crystallization is a very important factor towards enhancing the mechanical properties.[90-92]

Thus, the superior mechanical properties of PU-PP when compared to PU-OS can be explained as polyurethanes from the pre-polymer method are more favorable in crystallization than the ones from the one-shot method; therefore, they have a higher Young's modulus and modulus strength. Because of its superior mechanical property, the pre-polymer method was chosen as the nano-TiO_2-PU synthesis method. Table 4.2 provides the summary of the tensile test results.

Table 4.2 Summary of tensile test results of PU from one-shot method (experimental section 4.2.4)and PU from pre-polymer method (experimental section 4.2.3). Raw materials: HMDI, PTHF and DMPA. Reaction taken place at 60^{o}C under nitrogen flow protection. Sample(test length: 50mm, width: 5-10mm, thickness: around 0.30mm) was tested at a constant crosshead speed of 500mm/min.

Sample Name	Sample No.	Young's Modulus (MPa)	Tensile Strength (MPa)
PU (pre-polymer method)	1	4.44	16.8
	2	4.44	16.0
	3*	4.44	16.6
	Avg. ± S.D.	4.44±0.00	16.47±0.42
PU (one-shot method)	1	4.06	10.8
	2*	3.93	10.2
	3	3.95	9.62
	Avg.± S.D.	3.98±0.07	10.21±0.59

* These two test results were chosen to stand for each sample in Figure 4.12.

4.4.4 Monomer Functionalization

As previously discussed, DMPA is functionalized by coordination to nano-TiO_2 when dispersed in iso-propanol solvent. There are three possible coordination structures: chelating bidentate mode, monodentate mode and bridging bidentate mode.

In order to confirm coordination, nano-TiO_2-DMPA was characterized by TGA. Results of nano-TiO_2-DMPA and nano-TiO_2/DMPA mixture (the same weight percentage) were compared in thermogavimetric (TG) plots and derivative thermogavimetric (DTG) plots.

Figure 4.13 shows the TG plots of the nano-TiO_2-DMPA and nano-TiO_2/DMPA mixture, featuring its weight percentage change versus temperature. Weight percentages of both samples remain at about 50% since 450°C, indicating that both samples contain 50% nano-TiO_2 because TiO_2 cannot be thermally decomposed at 600°C.[35,38]

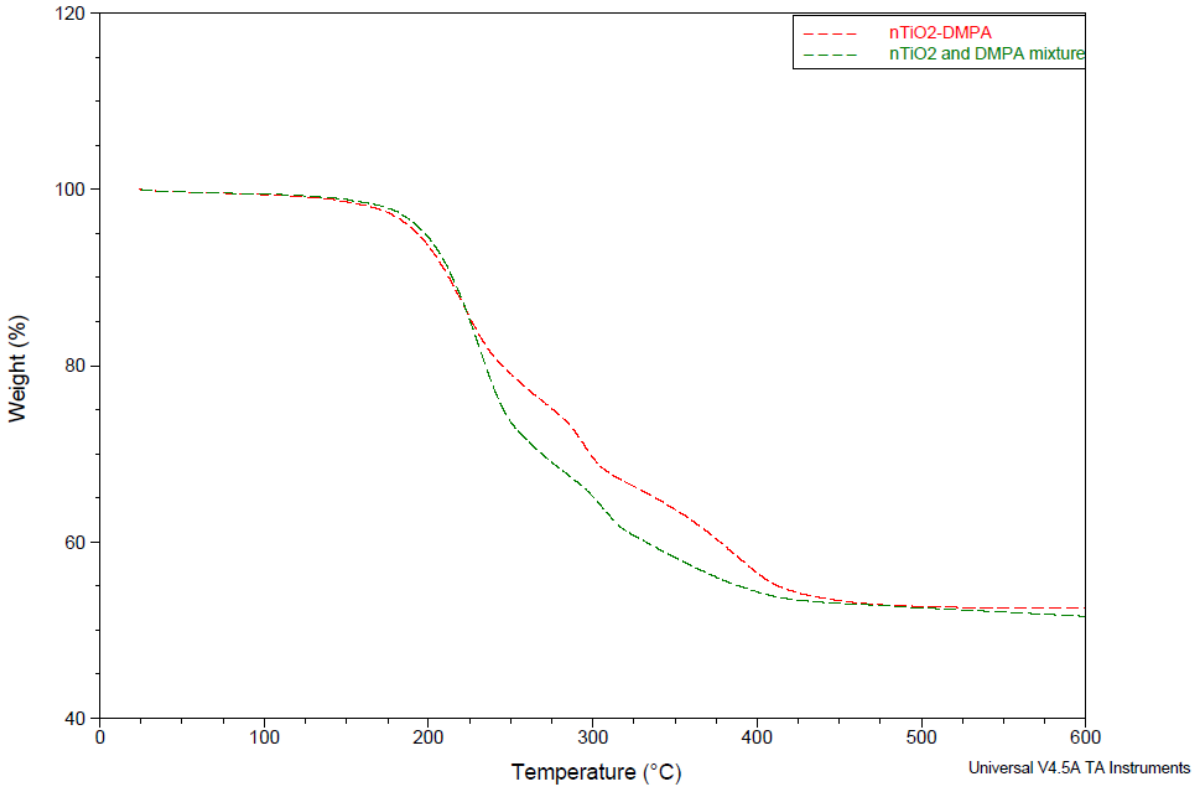

Figure 4.13 TG curves for nano-TiO_2-DMPA functionalized monomer from experimental section 4.2.5 and nano-TiO_2/DMPA physical mixture. nano-TiO_2 used in both samples are anatase nano-powder. Samples are heated at a rate of 10°C/min under nitrogen flow from room temperature to 600°C.

In addition, the organic part (i.e. DMPA) of nano-TiO_2-DMPA decomposed slower than the one in the nano-TiO_2/DMPA mixture, indicating this sample was more stable than DMPA in the nano-TiO_2/DMPA mixture. In the nano-TiO_2/DMPA mixture, DMPA and nano-TiO_2 only have physical interactions. Therefore, for the more thermo stable nano-TiO_2-DMPA sample, DMPA has not only physisorption to nano-TiO_2 but also chemisorptions(chemical coordination) to nano-TiO_2.[93,94]

Figure 4.14 shows the DTG plots of the nano-TiO_2-DMPA and nano-TiO_2/DMPA mixture, featuring its derivative weight percentage change versus temperature. From the nano-TiO_2/DMPA mixture curve, DMPA decomposition can be divided into two parts. The decomposition of alcohols and carboxylic acids usually takes place (180^oC) before the decomposition of the remaining carbon chain (280^oC), which correspond to the two peaks in Figure 4.14.[95,96]

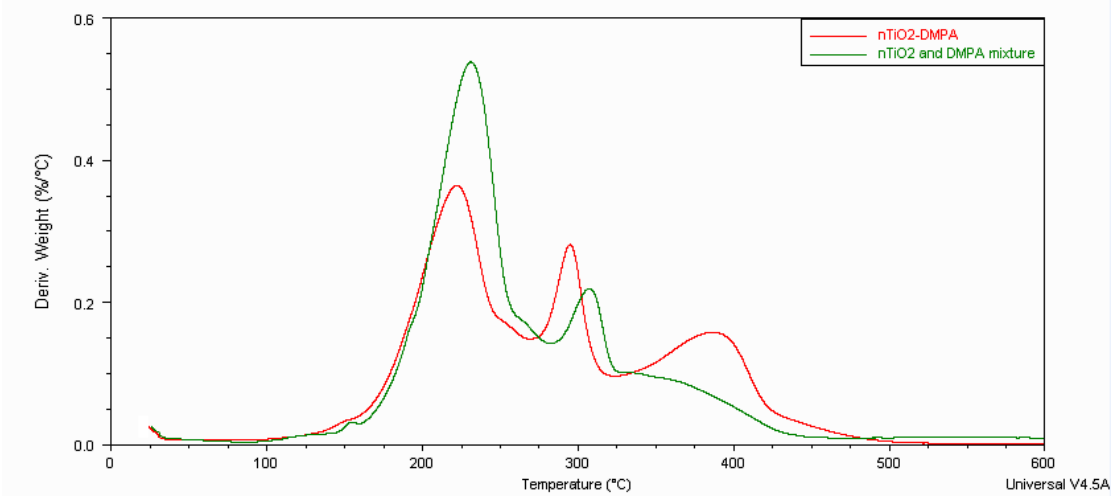

Figure 4.14 DTG curves for nano-TiO_2-DMPA functionalized monomer from experimental section 4.2.5 and nano-TiO_2/DMPA physical mixture. nano-TiO_2 used in both samples are anatase nano-powder. Samples are heated at a rate of 10^oC/min under nitrogen flow from room temperature to 600^oC.

From the nano-TiO_2-DMPA curve, an additional third peak of thermal decomposition that begins at 320^oC is observed. This additional step also proves the functionalization of DMPA and represents the functionalized carboxyl groups coordinated to nano-TiO_2.[2]

Monomer functionalization can be further proven through FTIR characterization. Spectra of nano-TiO_2, DMPA and nano-TiO_2-DMPA were compared and analyzed. FTIR analysis in Figure 4.15 shows the specific characterization peaks for nano-TiO_2-DMPA and TiO_2. TiO_2 has a broad and strong absorption band approximately in the range of

800-500 cm^{-1}.[97,98] Accordingly, both TiO_2 and nano-TiO_2-DMPA show an absorption in the same region in Figure 4.15, proving the TiO_2 existence in nano-TiO_2-DMPA.

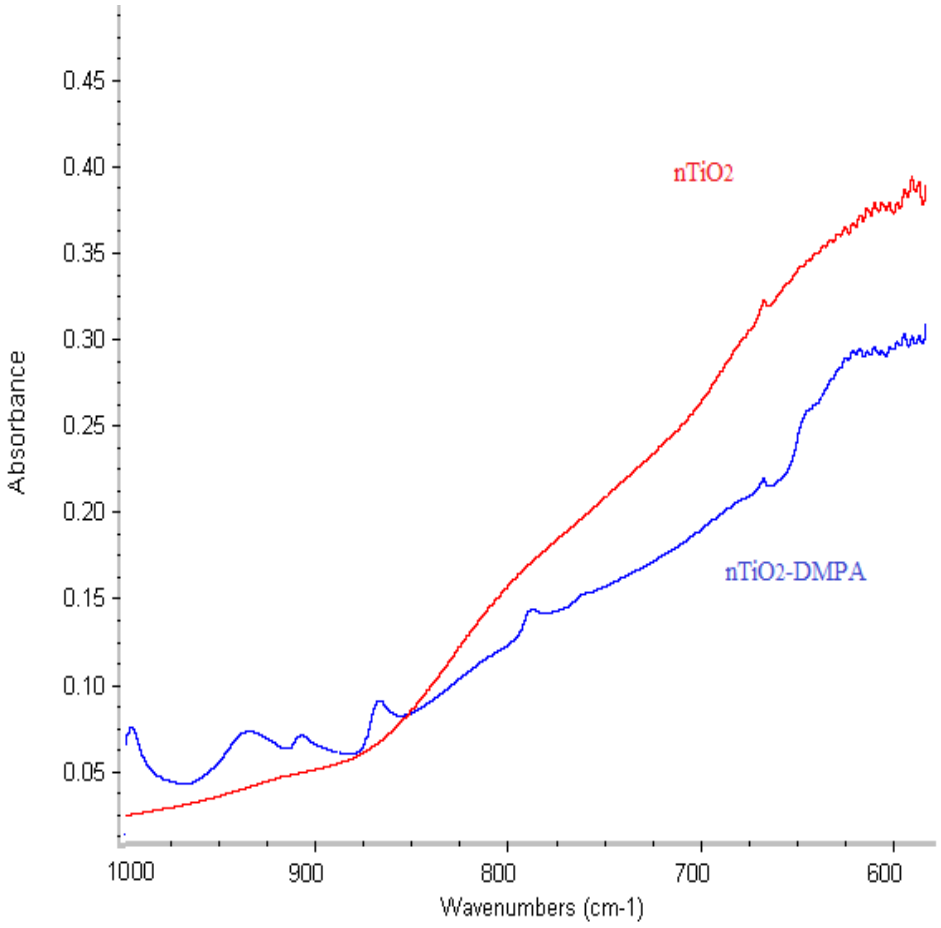

Figure 4.15 FTIR spectra of nano-TiO_2-DMPA and TiO_2 in the region of 1000-600cm^{-1}.

Figure 4.16 shows the FTIR spectra for nano-TiO_2-DMPA and DMPA. It is observed that most peaks in both spectra correspond to each other, indicating the presence of DMPA in nano-TiO_2-DMPA.The carboxylic group characteristic peaks in DMPA spectrum include 1700cm^{-1} (C=O stretch), 1230cm^{-1},1140cm^{-1}, 1050cm^{-1} (all C-O stretch), 3200cm^{-1} and 2600-2500cm^{-1} (all O-H stretch).[88,89] A summary of the DMPA characteristic IR absorption peaks is given below in Table 4.3.

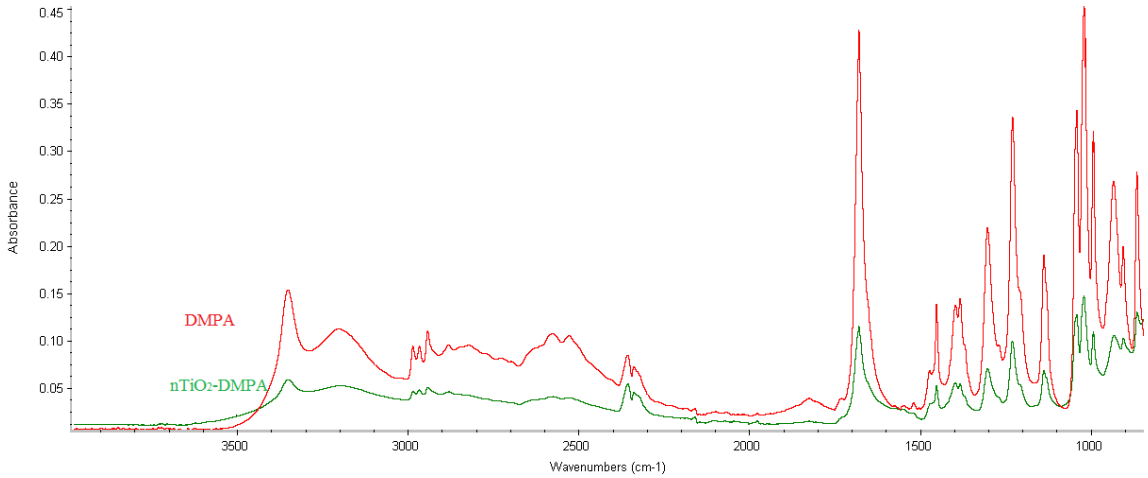

Figure 4.16 FTIR spectra for nano-TiO_2-DMPA and DMPA in the region of 4000-1000cm^{-1}.

Table 4.3 Characteristic IR absorption peaks in DMPA.

Frequency, cm^{-1}	Bond	Functional group
3350	O-H stretch	Alcohols
3200	O-H stretch	Carboxylic acids
3000-2900	C-H stretch	Alkanes
2600-2500	O-H stretch	Carboxylic acids
1700	C=Ostretch	Carboxylic acids
1450	C-H bend	Alkanes
1390,1300	C-H rock	Alkanes
1230,1140,1050	C-O stretch	Alcohols, Carboxlic acids

In Figure 4.17, it is noticed that the absorption peaks at 3200 cm^{-1} and 2600-2500 cm^{-1} on the DMPA spectrum disappeared on the nano-TiO_2-DMPA spectrum. This further confirms the nano-TiO_2 coordination to the carboxylic acid group since both peaks correspond to the carboxylic acid group in DMPA. Moreover, the disappearing peaks represent O-H stretching in the carboxylic group; and peaks represent C=O (1700 cm^{-1}) and C-O (1250-1050 cm^{-1}) stretching in the carboxylic group which still exist in Figure 4.16. Therefore, the coordination type can be identified as the monodentate mode (Figure 4.3b) in which the Ti-O stretch replaces the O-H stretch.

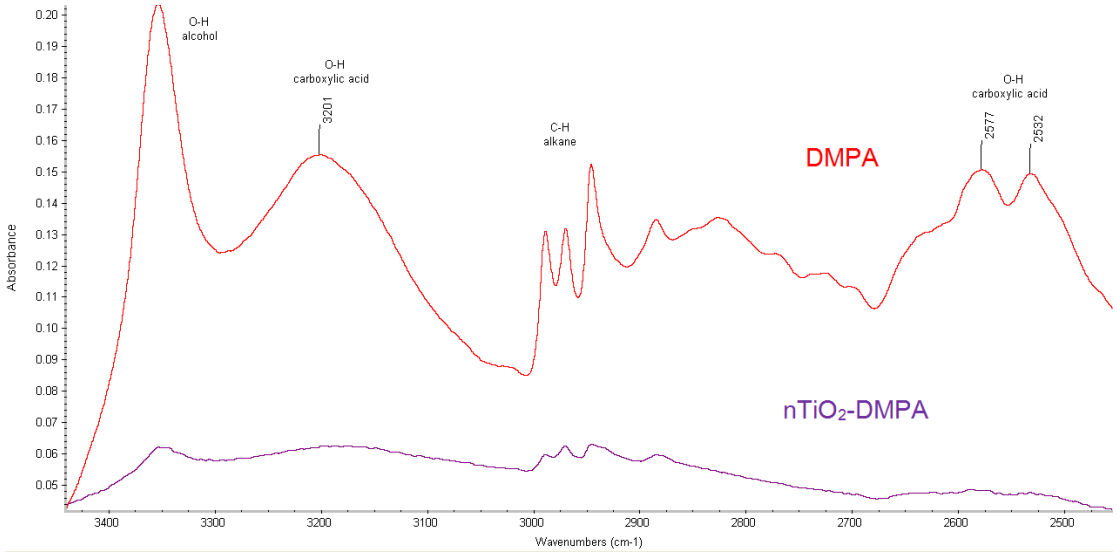

Figure 4.17 FTIR spectra for nano-TiO_2-DMPA and DMPA in the region of 3500-2500cm^{-1}.

4.4.5 nano-TiO_2-PU physical appearance

As mentioned in the experimental section, nano-TiO_2 particle functional polyurethanes (nano-TiO_2-PU) were synthesized by the pre-polymer method. As shown in Figure 4.18, nano-TiO_2-PU appears as a white colour as opposed to PU which is transparent.

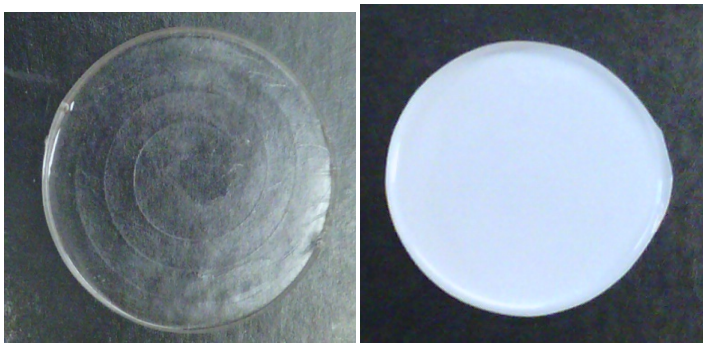

(a) (b)

Figure 4.18 Digital pictures of (a) pure PU (experimental section 4.2.3). Raw materials: HMDI, PTHF and DMPA. Reaction taken place at 60^{o}C under nitrogen flow protection. and (b) 1% nano-TiO_2-PU (experimental section 4.2.6). Raw materials: HMDI, PTHF, DMPA, anatase nano-TiO_2. Reaction taken place at 60^{o}C under nitrogen flow protection.

4.4.6 Surface Hydrophilicity

As mentioned earlier, the self-cleaning effect is related to surface hydrophilicity. Hydrophilic surfaces can clean themselves only by the action of water when they are super-hydrophilic. The characterization of surface hydrophilicity is performed by examining the contact angle, i.e. the angle formed between a liquid droplet deposited on the surface of a solid.

The sessile drop method was chosen as the measurement method for contact angle because of its accuracy and simplicity. In order to form a flat test surface for contact angle measurements, polymer coatings were coated on microscope slides using spin-coating at 500 rpm for 5 min.

Many groups: Guan et al.[99], Wang et al.[27], Sakai et al.[29] have reported that films consisting of only TiO_2 has a water contact angle close to zero ($0^o \pm 1^o$) upon UV irradiation. Photo-generated holes first produce OH radicals which can result in an increase of OH groups, thus increasing the surface energy which therefore leads to the decrease of contact angle, and forming a super-hydrophilic surface as a result.[11] Therefore, with nano-TiO_2 coordination, nano-TiO_2-PU surface should show a decrease in contact angle upon UV irradiation.

Figure 4.19 shows the pictures of the contact angle for pure PU and nano-TiO_2-PU (both before and after 4h UV irradiation). Before UV irradiation, both the pure PU and nano-TiO_2-PU have contact angles near 90°, indicating our synthesized PU is a semi-hydrophobic/ semi-hydrophilic polymer. However, after UV irradiation for 4h, the contact angle of nano-TiO_2-PU dropped to around 60°, while the contact angle of pure PU remains 90°. This indicates that nano-TiO_2-PU surfaces are turning into a hydrophilic surface when exposed to UV light.

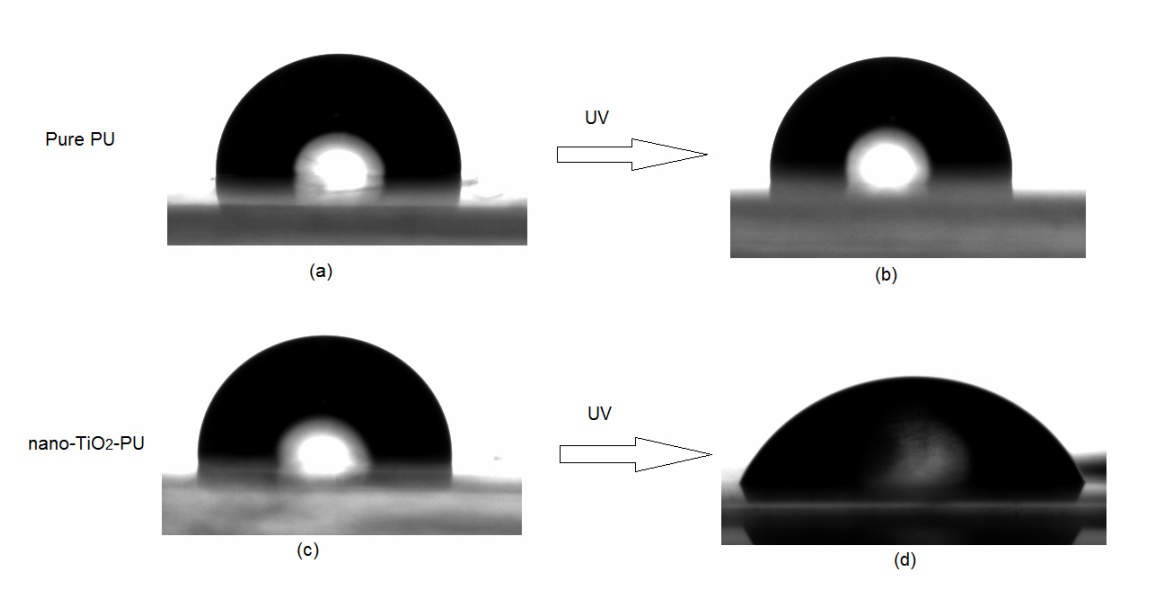

Figure 4.19 Contact Angle Picture of: a) Pure PU before UV irradiation, b) Pure PU after UV irradiation, c) nano-TiO_2-PU before UV irradiation and d) nano-TiO_2-PU after 4h UV irradiation.

A detailed summary of the contact angle test results are given in Table 4.4. The average contact angle of pure PU is 95.2° before UV irradiation and then changed to 93.4° after UV irradiation. The contact angle did not change much for this sample; the change was even in the error region. For nano-TiO_2-PU sample, the contact angle is 90.5° before UV irradiation, and then dropped to 58.1° after 4h UV irradiation.

Table 4.4 Contact angle test results of pure PU and nano-TiO_2-PU (both before and after 4h UV treatment).

Sample Name	Sample No.	Before UV		After UV	
		Contact Angle/°	Average ±S.D./ °	Contact Angle/°	Average ±S.D./ °
Pure PU	1	95.8	95.2 ±1.2	94.8	93.4 ±1.9
	2	93.8		94.2	
	3	96.0		91.2	
nano-TiO2-PU	1	90.0	90.5 ±0.6	56.5	58.1 ±1.7
	2	91.2		58.0	
	3	90.3		59.8	

Moreover, as the UV irradiation time was extended, the contact angle of nano-TiO_2-PU surface did not decrease further. This is because the main composition of the surface is PU which is a semi-hydrophilic polymer. Therefore, with the additional TiO_2, the nano-TiO_2-PU surface becomes more hydrophilic, but not a super-hydrophilic surface.

4.4.7 nano-TiO_2-PU photo-catalysis using stearic acid as 'dirt'

For the self-cleaning study, stearic acid was used as a model compound for 'dirt', which is commonly chosen due to its hydrophobic nature.[3,4,100] Stearic acid is a saturated fatty acid with an 18 carbon atom chain, and its chemical formula is $CH_3(CH_2)_{16}COOH$. It occurs in many animal and vegetable fats and oils, which makes it the perfect model compound for self-cleaning.

In this thesis, self-cleaning was investigated by monitoring the weight change of the sample during UV irradiation. Additionally, DSC was performed to prove the degradation of stearic acid.

Figure 4.20 shows the DSC analysis curves of stearic acid and nano-TiO_2-PU with excess stearic acid, both before and after UV treatment. From the stearic acid curve, a large endothermic peak is observed, which indicates a phase transition of the sample. Also, the melting point of stearic acid has been widely reported as 69.6℃, which corresponds to the endothermic peak shown in Figure 4.20. Therefore, in this case, this endothermic peak represents the melting process of stearic acid.

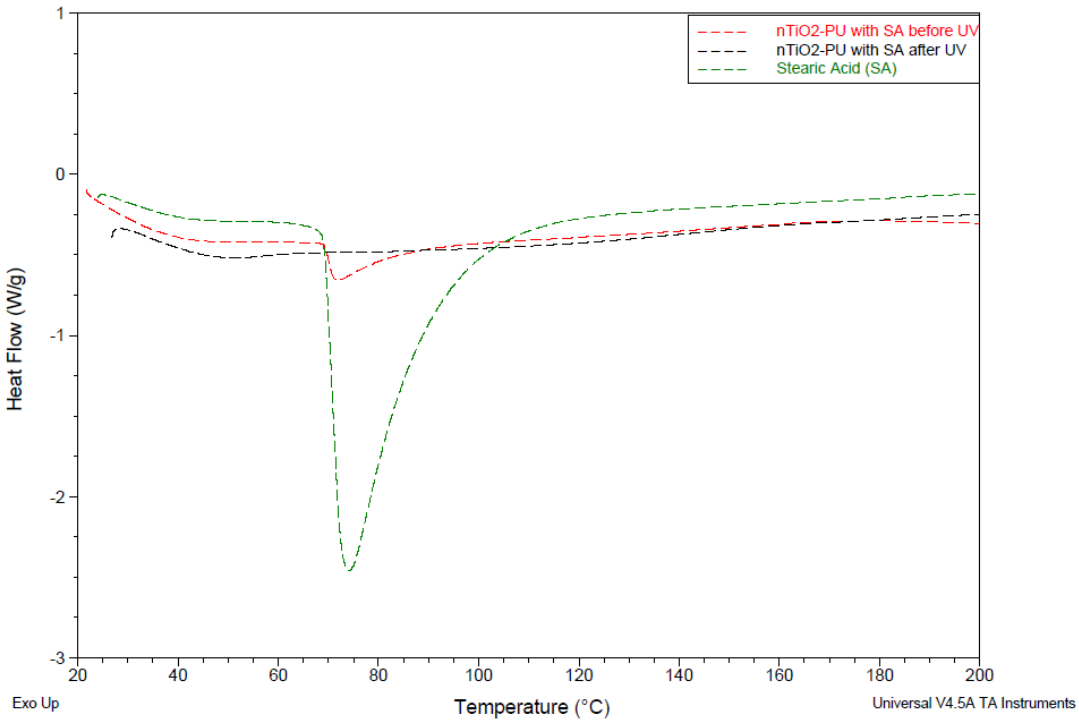

Figure 4.20 DSC analysis curves of stearic acid and nano-TiO_2-PU with excess stearic acid before and after UV treatment.

Also, from the nano-TiO_2-PU with stearic acid before UV curve, the same endothermic peak appears in the same location, with a lower intensity. This proves the existence of stearic acid in this sample. However, there is no endothermic peak in that region or any other region in the curve of nano-TiO_2-PU with stearic acid after UV treatment. All these evidence corroborate that stearic acid is degraded after UV irradiation.

In addition, the weight change of nano-TiO_2-PU with stearic acid was recorded during UV irradiation, with the result shown in Figure 4.21. 10% stearic acid was added into the sample, giving the 110% value at the beginning of the test. TiO_2 concentration of the nano-TiO_2-PU sample is 1% in this graph. The weight of sample continues to drop as the time of UV irradiation increases, with this drop decreasing drastically in the earlier stage, which is attributed to the decreasing concentration of stearic acid.

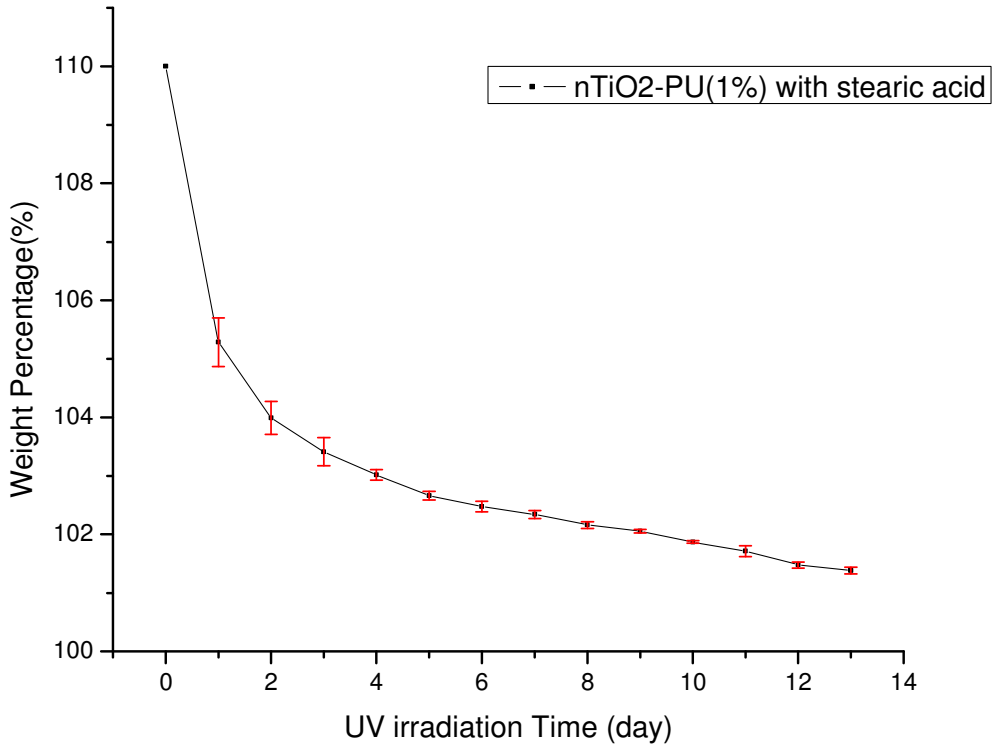

Figure 4.21 Weight change (by percentage) of nano-TiO_2-PU with 10% stearic acid during UV treatment. Error bars show the ± standard deviation of the test results.

Furthermore, the self-cleaning efficiency of nano-TiO_2-PU with different TiO_2 concentrations was also investigated by comparing the weight of sample during the same amount of UV exposure time. Results are shown in the following chart (Figure 4.22).

The weight percentages for all samples begin at 110%, due to the 10% additional stearic acid added. For the pure PU sample, there is about 1% weight loss without TiO_2 presence after 1 day, meaning stearic acid can be degraded only with UV exposure. As the time of UV irradiation increases, the weight continued dropping, but very slowly. After 4 days, there is only a little over 2% weight loss, indicating that UV irradiation alone is not enough to fully degrade stearic acid.

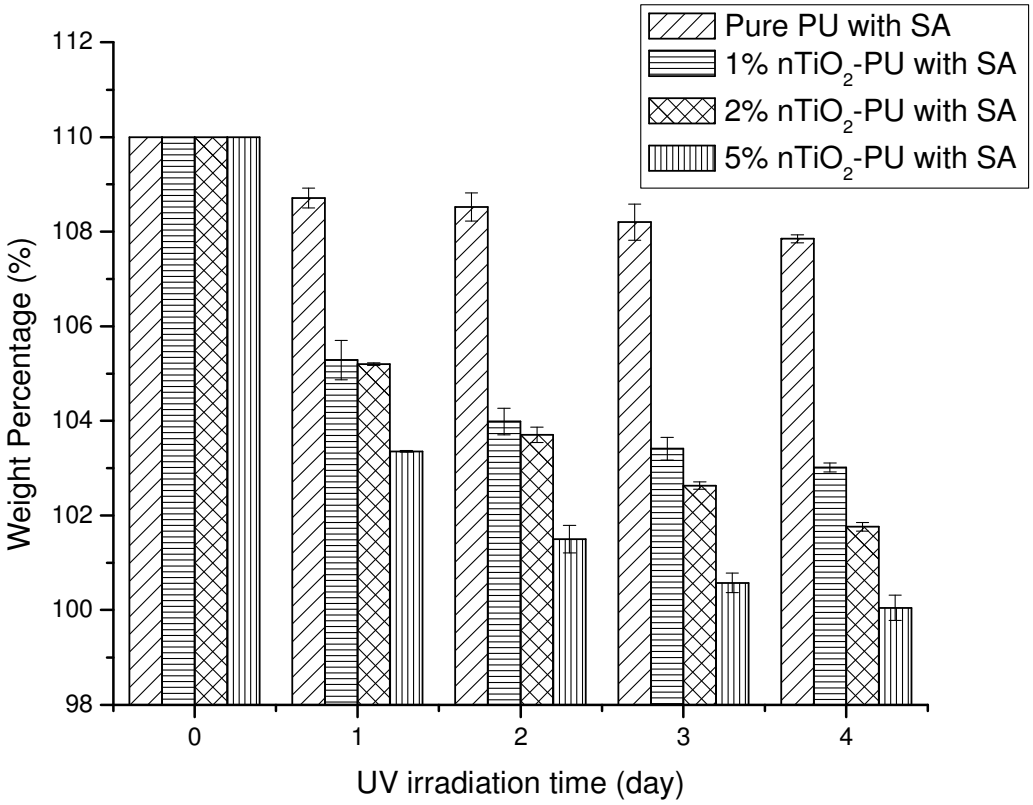

Figure 4.22 Weight changes (by percentage) of pure PU, 1% nano-TiO_2-PU, 2% nano-TiO_2-PU and 5% nano-TiO_2-PU with 10% stearic acid during UV treatment. Error bars show the ± standard deviation of the test results.

For all the nano-TiO_2-PU samples, the weight loss is clearly higher than the pure PU sample. Also, with higher TiO_2 concentrations, the weight loss is higher, indicating the TiO_2 presence is crucial for stearic acid degradation. With higher TiO_2 concentration (i.e. 5%), the self-cleaning property is much better.

Also later during experiment, as the UV irradiation time was extended, it is noticed that the weight percentage is lower than 100% after a week for the 2% and 5% nano-TiO_2-PU samples. This indicates the organic part (PU) of the nano-TiO_2-PU sample itself is becoming degraded during the same time. The degradation process takes place when exposed to high intensity and close exposure of UV light for a very long time. With only

this amount of degradation, we are confident that self-degradation of nano-TiO_2-PU would not be a major issue for daily use since sunlight only contains a limited amount and intensity of UV light.

The TGA results in Figure 4.23 also corroborate this PU self-degradation problem. The decomposition process of sample before and after UV irradiation is still similar to each other.

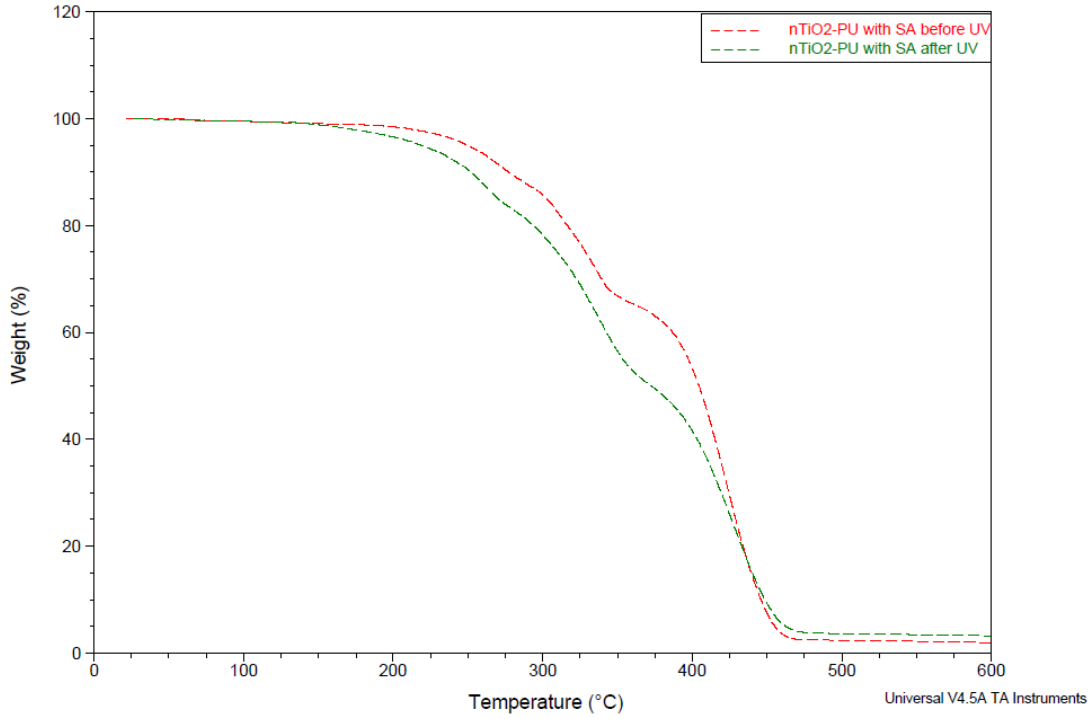

Figure 4.23 TGA curves of nano-TiO_2-PU with stearic acid before and after UV treatment.

Both samples begin decomposition in a similar temperature region (around 200℃) and end decomposition at almost the same temperature (around 500℃). However, the sample after UV treatment decomposes faster than the one before UV treatment. This can be explained as the PU degradation is mostly experienced by a chain scission mechanism,[101] in which a few short chains were formed and then degraded during the UV irradiation process.

In addition to investigate the effect of different concentrations of TiO_2 on self-cleaning, the effect of different forms of TiO_2 was also studied. Figure 4.24 shows the results of self-cleaning experiments of nano-TiO_2-PU samples with 5% of anatase and rutile. Because of the poor coordination between rutile and DMPA,[5] rutile PU samples were simply physical mixture of rutile and pure PU, where as anatase PU sample were functional PU, i.e. nano-TiO_2-PU.

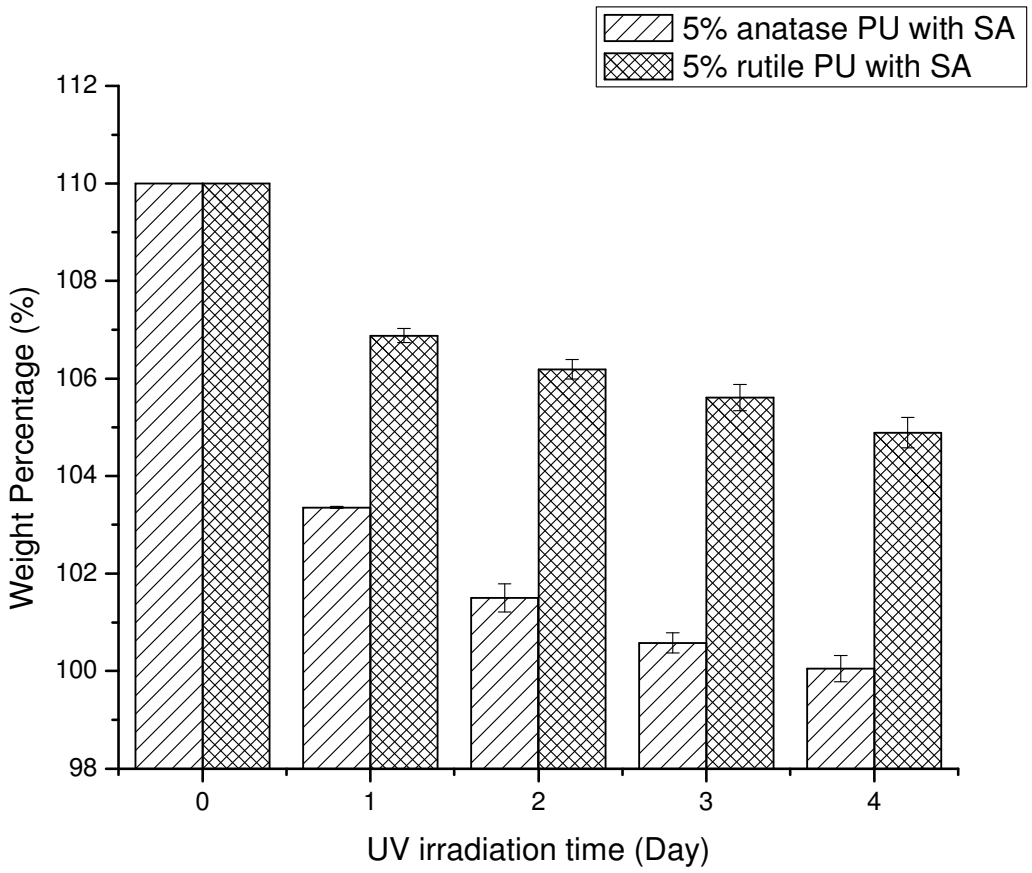

Figure 4.24 Weight Changes (by percentage) of 5% anatase PU, 5% rutile PU with 10% excess stearic acid during UV treatment. Error bars show the ± standard deviation of the test results.

From Figure 4.24 it is clear that anatase PU had more weight loss than rutile PU, indicating a better self-cleaning property. Within 4 days, the anatase PU sample reached

100%, indicating complete degradation of stearic acid. In comparison for the rutile PU sample, only 5% of weight loss was observed, demonstrating that only half of the stearic acid was degraded. This result is consistent with theory as anatase is the preferred form of TiO_2 for photocatalysis due to the smaller electron effective mass, a higher Fermi level and a higher mobility of charge carriers.[36,37] And in this case, self-cleaning property is directly linked to photocatalysis.

4.4.8 nano-TiO_2-PU photocatalysis using DMPA as 'dirt'

In addition to using stearic acid as a model 'dirt' compound for the self-cleaning tests, additional DMPA was also used for comparison. DMPA was chosen in this thesis because of its availability in this study; and it is an organic acid, similar to stearic acid with a shorter carbon chain structure.

Similar as with stearic acid, an additional 10% DMPA was added onto the nano-TiO_2-PU coating as a model 'dirt' compound in order to study the self-cleaning property. In Figure 4.24, three spectra featuring nano-TiO_2-PU, nano-TiO_2-PU with DMPA before and after UV irradiation are shown. It is clear that the IR absorption at 3350 cm^{-1} (hydroxyl stretch absorption from DMPA) only appears on the nano-TiO_2-PU surface with DMPA before UV treatment. After UV irradiation, the hydroxyl absorption disappeared in the spectrum, indicating DMPA was degraded after UV exposure.

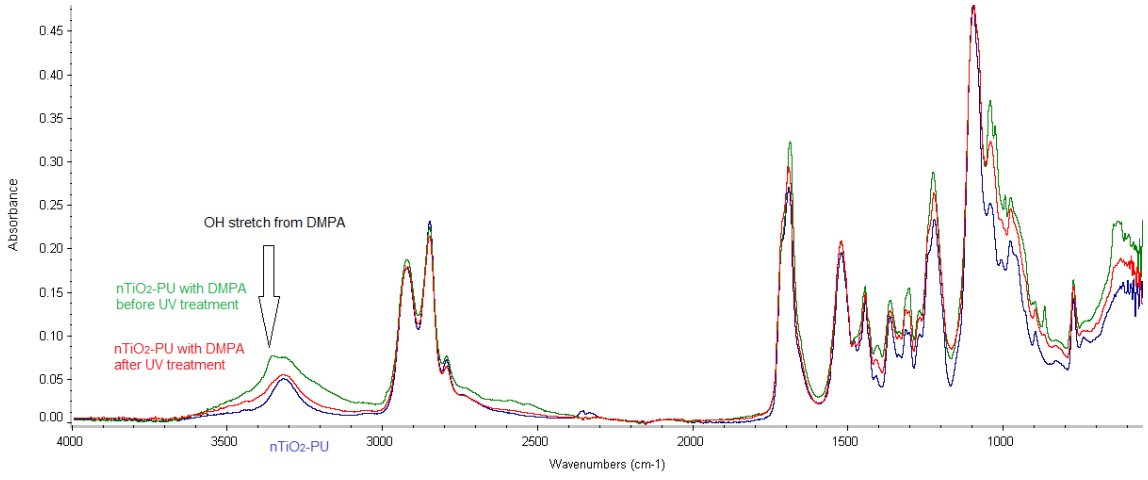

Figure 4.25 FTIR spectra of nano-TiO_2-PU, nano-TiO_2-PU with excess DMPA before and after UV treatment.

In the meantime, the degradation process of this excess DMPA was also monitored by weight change when exposed to UV light. The following Figure 4.25 shows the weight percentage change of the nano-TiO_2-PU sample when treated with UV irradiation for various lengths of time. The weight percentage begins with 110% because of the 10% additional DMPA. The concentration of TiO_2 in nano-TiO_2-PU is also 1%.

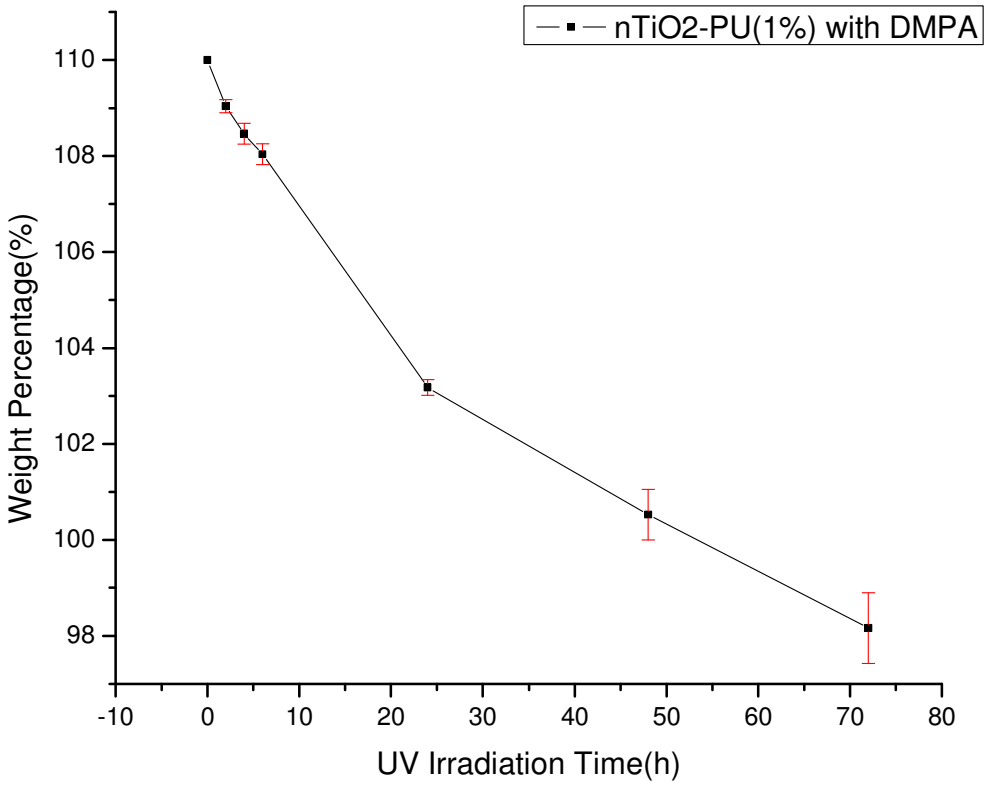

Figure 4.26 Weight change (by percentage) of nano-TiO_2-PU with additional 10% DMPA during UV treatment. Error bars show the ± standard deviation of the test results.

It is clear that the weight of sample continues to drop as the time of UV irradiation increases. The rate of the degradation also decreased as the UV irradiation time increased. This situation is similar as with stearic acid; and can also be explained as the amount of DMPA decreases, the apparent degradation rate of DMPA decreases.

After about 55h, the weight of sample dropped to 100%, indicating the degradation of DMPA is complete. When the length of UV exposure time was extended after DMPA degradation, we find that the weight was still dropping. This means the nano-TiO_2-PU was degrading itself when exposed to UV light, which corresponds to the result for self-cleaning study using stearic acid as 'dirt'.

Moreover, the self-cleaning efficiency of nano-TiO_2-PU with different TiO_2 concentrations was also studied by the weighting sample during UV exposure. The following chart (Figure 4.26) shows the result of this study in which 10% DMPA was added into pure PU, 0.5% nano-TiO_2-PUand 1% nano-TiO_2-PU samples, giving all samples 110% weight percentage at the beginning of the test.

From the weight change of the pure PU sample, about 3.3% of weight was lost from degradation after 24 h of UV exposure, even without the presence of nano-TiO_2. But the weight of pure PU sample decreased very slowly after 24 h, meaning that UV exposure gives partial DMPA degradation, however, not complete degradation.

Also from this figure, PU with a higher TiO_2 concentration has more weight loss at the same UV exposure time. After 48 h, DMPA was mostly degraded in the 1% nano-TiO_2-PU sample whereas it took 72 h for the 0.5% nano-TiO_2-PU sample.

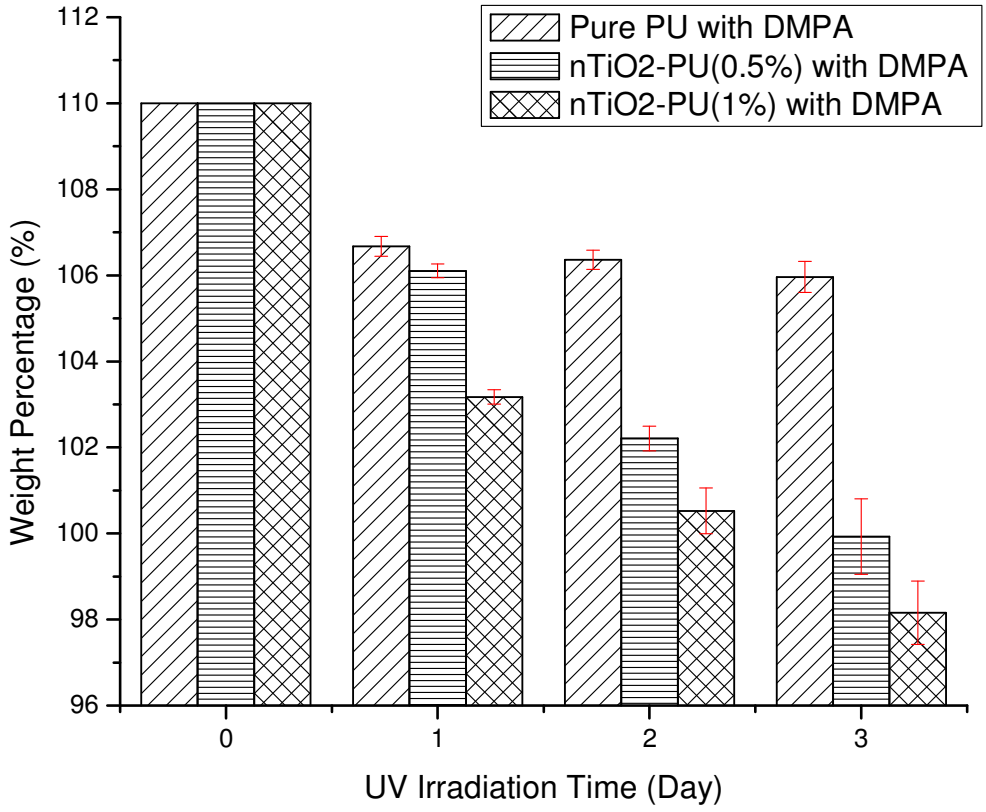

Figure 4.27 Weight changes (by percentage) of pure PU, 0.5% nano-TiO_2-PU and 1% nano-TiO_2-PU with DMPA during UV treatment. Error bars show the ± standard deviation of the test results.

4.4.9 Comparison between model 'dirt' compounds

As mentioned before, two different kinds of 'dirt' were used in the self-cleaning study, with a comparison between them as follows.

During each experiment, 10% additional stearic acid and DMPA were added onto the polymer coating samples, giving 110% weight percentage at the start of each test. Figure 4.27 shows the weight change of pure PU sample with excess DMPA and stearic acid as 'dirt' during the UV irradiation.

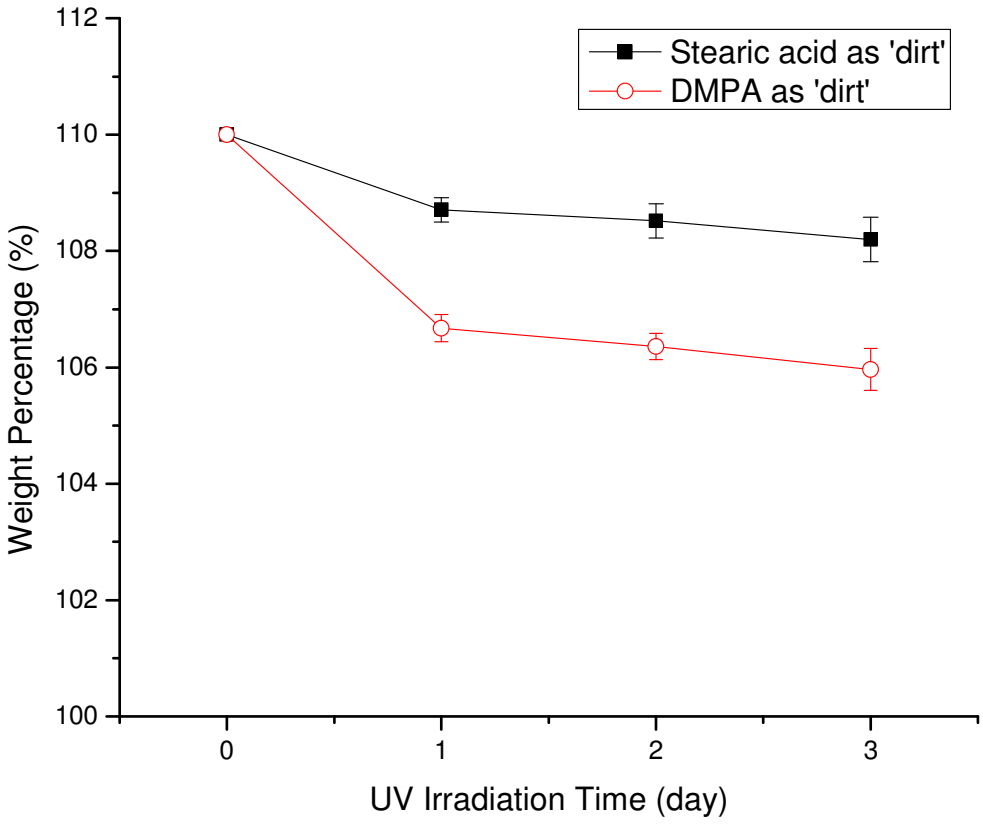

Figure 4.28 Weight change (by percentage) of pure PU sample with excess 10% stearic acid and DMPA as 'dirt' during UV treatment. Error bars show the ± standard deviation of the test results.

It is clear that both model compounds have some weight loss during the UV treatment after one day; the weight loss became insignificant later. However, the weight loss of DMPA used was higher than that of stearic acid. Similar results were found in Figure 4.28, which shows the weight change of 1% nano-TiO_2-PU sample with excess DMPA and stearic acid as 'dirt' during the UV irradiation.

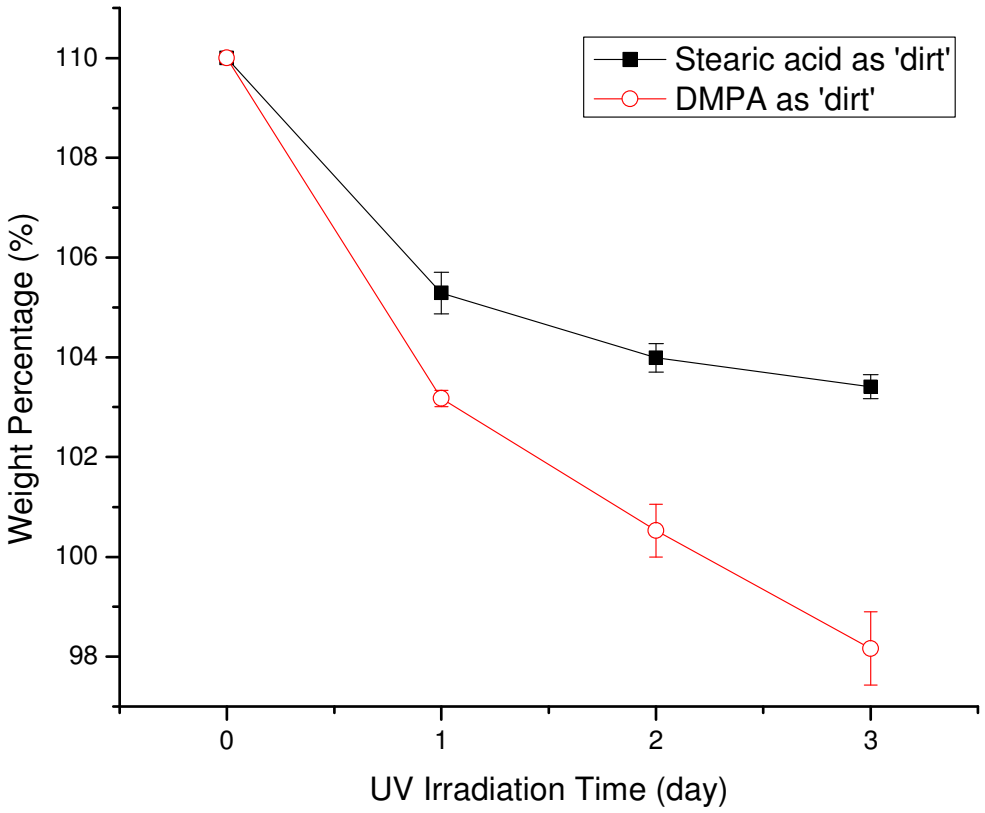

Figure 4.29 Weight change (by percentage) of 1% nano-TiO_2-PU sample with excess 10% stearic acid and DMPA as 'dirt' during UV treatment. Error bars show the ± standard deviation of the test results.

This is attributed to stearic acid having a higher molecular weight and more complex chemical composition than DMPA. Stearic acid is a compound with 18 carbon atoms, while DMPA is a smaller molecule with a simple 5 carbon composition, and is more oxidized. Therefore, the degradation of stearic acid would take more energy/time than that of DMPA. While in this case with the same amount of energy, the degradation process of stearic acid would take longer time than that of DMPA.

4.4.10 Thermal Stability

TGA was performed to measure the thermal stability of the PU coatings. Decomposition temperature is defined by 50% decomposition of the material (i.e. 50% wt loss).[102] Figure

4.29 shows the TGA output in the form of percent weight loss as a function of temperature. It is observed from Figure 4.29 that the decomposition behavior of both samples are in the form of a two step degradation process, and the decomposition temperature for nano-TiO_2-PU (404.2 ^oC) is higher than pure PU (396.1 ^oC).

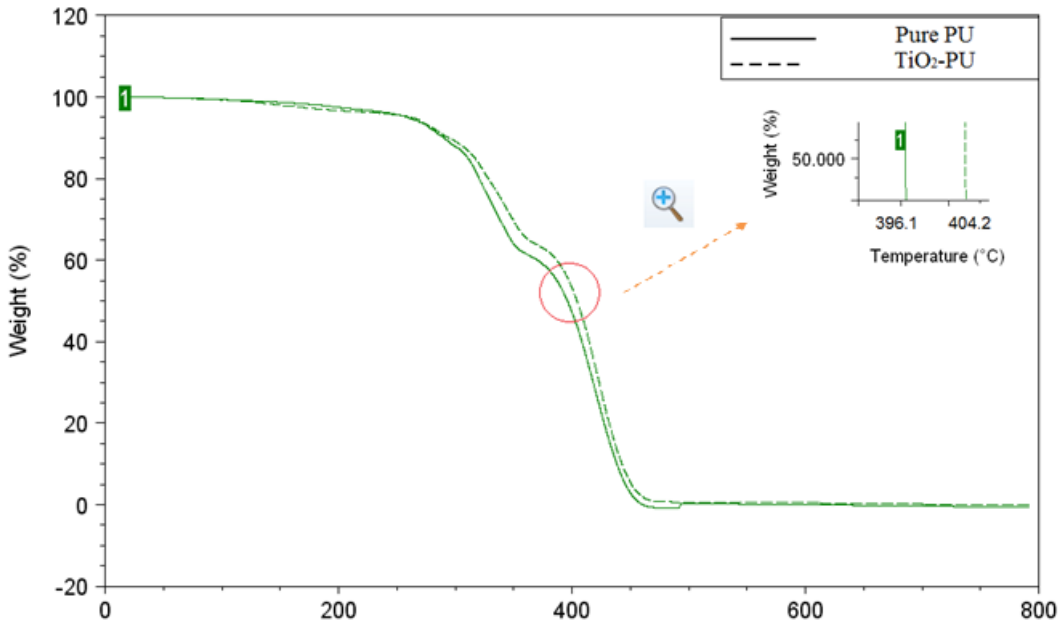

Figure 4.30 TGA output for pure PU and nano-TiO_2-PU (1%) samples.

The decomposition of the PU samples shifted to a higher temperature with coordination of nano-TiO_2, indicating that coordination of nano-TiO_2 offers a stabilizing effect against decomposition. This protection from thermal degradation is enhanced by keeping the PU chains and the molecular structure intact, which results in an increasing decomposition temperature.[102] Similar enhancement of thermal stability has been reported,[102] the decomposition temperature of PU increased from 347^oC to 365^oC due to 1%TiO_2 incorporation.

4.4.11 Mechanical Property of commercial PU samples

In addition to examining the tensile properties of the synthesized polyurethane nanocomposites, commercially available polyurethanes were also tested according to ASTM D882-10.

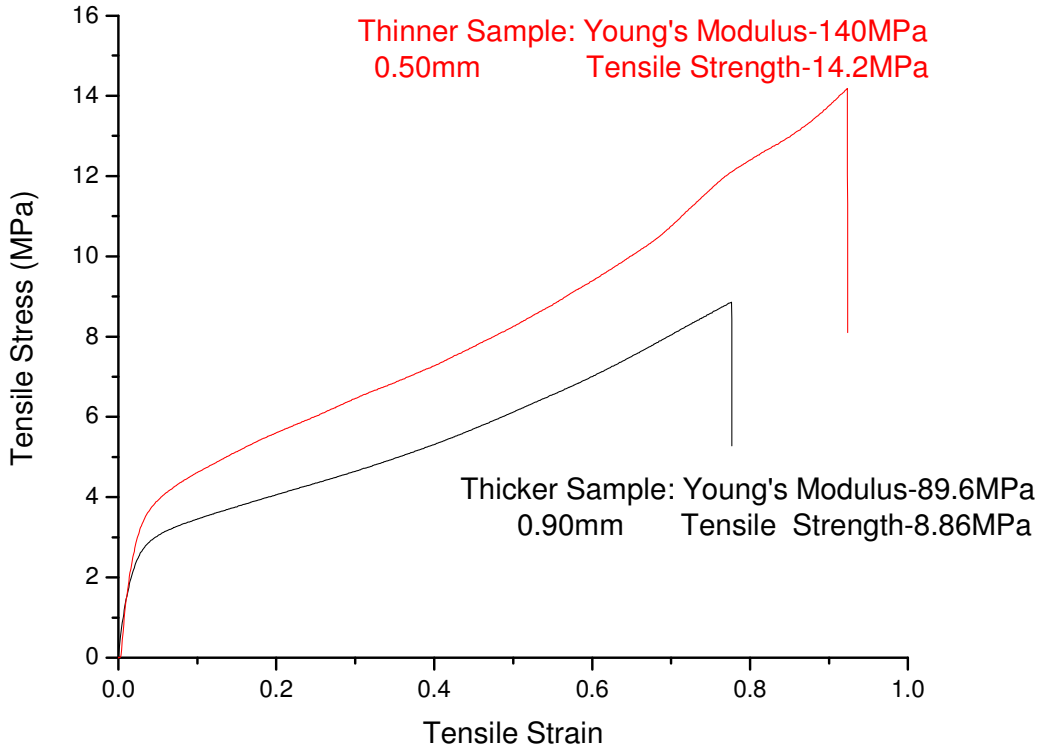

Figure 4.31 Tensile stress-strain plots of commercial PU samples with different thickness(thicker samples: around 0.90mm, thinner samples: around 0.50mm). Sample(gauge length: 100mm, width: 5-10mm, thickness: around 0.50mm or 0.90mm) was tested at a constant crosshead speed of 50mm/min.

Figure 4.30 shows the tensile test results for the pure PU sample with different thicknesses, which were obtained by adjusting the weight of PU samples in the mold. With the same dimensions in the mold, the sample with more weight would result in a higher thickness. Young's modulus was calculated from the slope of the initial linear part of the stress-strain curve, while the maximum stress at failure was taken as the tensile strength.

It is observed from Figure 4.30 that the thinner sample (0.50mm) has a higher Young's modulus value (140 MPa) and higher tensile strength value (14.2 MPa) than that of the thicker sample (0.90mm) (89.6 MPa for Young's modulus and 8.86 MPa for tensile

strength). The reason for the thinner sample having better mechanical properties is attributed to being easier to dry and solidify. The thicker the sample is; the resulting sample became softer. A summary of the tensile test results of pure PU samples with different thickness is given at Table 4.5.

Table 4.5 Summary of tensile test results of commercial PU samples with different thickness(thicker samples: around 0.90mm, thinner samples: around 0.50mm). Sample(gauge length: 100mm, width: 5-10mm, thickness: around 0.50mm or 0.90mm) was tested at a constant crosshead speed of 50mm/min.

Sample Name	Sample No.	Tensile Modulus (MPa)	Tensile Strength (MPa)
Thinner Sample (0.50mm)	1	93.7	8.91
	2	94.6	7.86
	3*	89.6	8.86
	Avg. ± S.D.	92.6 ± 2.67	8.54 ± 0.59
Thicker Sample (0.90mm)	1	140	16.1
	2	138	10.1
	3*	140	14.2
	Avg. ± S.D.	139 ± 1.2	13.5 ± 3.07

It can be observed that the stress-strain curves are showing two linear regions indicating the material is strong and tough. In the first linear region, high tensile stress change within small tensile strain change indicates strong materials.[52,54] In the second linear region, tensile stress continues to increase for a big tensile strain change indicates tough materials.[52,54] This is attributed to the segmented structure of polyurethane (Figure 3.18), i.e. the composition and arrangement of the hard and soft segments have a great impact on the resulting physical and mechanical properties of the PU.[13,61,62] The hard segment provides superior tensile strength and hardness; while the soft segment gives the polyurethane elasticity and flexibility. With both segments, the polyurethane product can achieve very good elasticity while maintaining reasonably high tensile strength.[13,14]

Recent and ongoing research on polymer/inorganic nanocomposites has demonstrated that there is significant enhancement in the mechanical property values over the pure polymer without compromising other properties. Saha et al.[102] reported a 15% increase in tensile modulus (from 137.3 MPa to 157.4 MPa) and a 5% increase in tensile strength (from 4.0 MPa to 4.2 MPa) with only 1% TiO_2 infusion.

The mechanical properties of commercial PU mixed with different concentrations of TiO_2 were also studied. Samples are prepared in experimental section 4.2.7, where no coordination between nano-TiO_2 and PU, using anatase nano-powder as nano-TiO_2. Figure 4.31 shows the tensile tension test results of pure PU, 1% nano-TiO_2/PU and 2% nano-TiO_2/PU samples. The Young's modulus is calculated from the slope of the initial linear part of the stress-strain curve, while the maximum stress at failure is taken as the tensile strength.

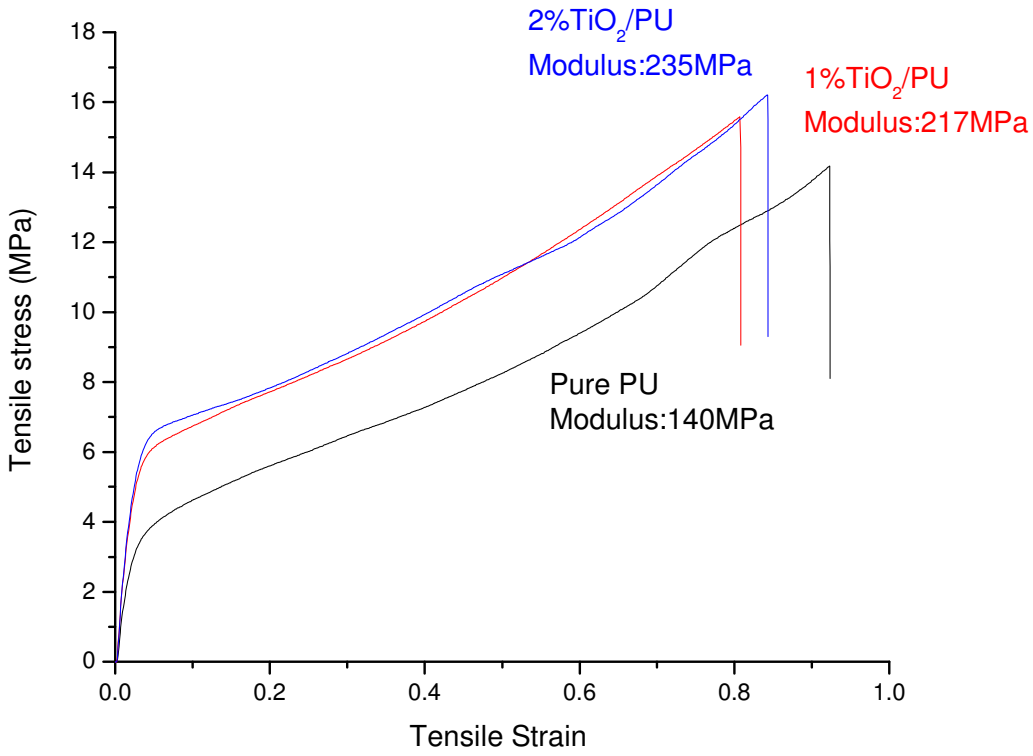

Figure 4.32 Tensile stress-strain curves of commercial PU samples with different TiO_2 concentration(0%, 1% and 2%). Sample(gauge length: 100mm, width: 5-10mm, thickness: around 0.50mm) was tested at a constant crosshead speed of 50mm/min.

It is clear that the tensile strength and modulus are significantly higher for the nano-TiO_2-PU sample than for the pure PU sample. Also, there is an increase though very slightly in

both the tensile strength and modulus with increasing concentration of TiO_2. A summary of the tensile test results of pure PU, 1%nano-TiO_2/PU and 2%nano-TiO_2/PU samples at the same thickness is given in Table 4.6.

Table 4.6 Summary of tensile test results of commercial PU samples with different TiO_2 concentration(0%, 1% and 2%). Sample(gauge length: 100mm, width: 5-10mm, thickness: around 0.50mm) was tested at a constant crosshead speed of 50mm/min.

Sample Name	Sample Number	Young's Modulus (MPa)		Tensile Strength (MPa)	
		Data	Avg. ± S.D.	Data	Avg. ± S.D.
Pure PU	1	140	139.33 ±1.15	16.1	13.47 ± 3.47
	2	138		10.1	
	3	140		14.2	
1% nano-TiO_2/PU	1	216	218.00 ± 2.65	13.9	14.57 ± 0.91
	2	217		15.6	
	3	221		14.2	
2% nano-TiO_2/PU	1	226	232.33 ± 5.51	14.7	15.30 ± 0.79
	2	236		15.0	
	3	235		16.2	

Addition of only 1wt% and 2wt% TiO_2 into the PU film increases its Young's modulus about 56.5% and 66.7%, respectively. As for the tensile strength of both samples, an increase of 8.2% and 13.6% for 1wt% and 2wt% addition was observed. However, as shown in Table 4.6, even though the average tensile strength values showed an increase, the actual test values are not as consistent as the Young's modulus values. This means the enhancement of tensile strength is probable, but not definite.

4.5 Conclusion

Two commonly used approaches for PU synthesis were investigated in this chapter. By comparing the FTIR spectra, urethane formation for products from both methods are confirmed; and also no difference were observed indicating the same chemical composition for both products. The molecular weight of the resulting polymer was found to be 15,581Da by GPC, with corresponding signal peaks of refractive index, low/high angle light scattering to prove the existence of polymer. Tensile test results showed higher Young's modulus (4.44 MPa to 3.98 MPa) and tensile strength (16.47 MPa to 10.21 MPa) for pre-polymer method PU compared to one-shot method PU.

Coordination between DMPA and nano-TiO_2 were confirmed by TGA and further identified as monodentate mode by FTIR. nano-TiO_2-PU was synthesized by a 'grafting from' technique using pre-polymer method. The surface of nano-TiO_2-PU became more hydrophilic (contact angle decreased to 58.1^o from 90.5^o) when exposed to UV treatment; whereas pure PU surface did not show such change. As the time of UV treatment extend, no further decrease in contact angle was observed meaning this nano-TiO_2-PU surface cannot reach super-hydrophilic.

Self-cleaning was demonstrated using stearic acid and DMPA as models for 'dirt'. Results pointed out that higher concentration of TiO_2 in polymer nanocomposites exhibited better self-cleaning property; while pure PU did not exhibit self-cleaning property. Comparison between stearic acid and DMPA revealed simpler molecules are easier towards degradation.

Also, enhancements in the thermal stability (decomposition temperature increased to 404.2^oC from 396.1^oC) and mechanical properties (Young's modulus increased by 56.5%) were observed with the addition of only 1wt% TiO_2.

Chapter 5

5 Synthesis and Characterization of TiO_2 Polyester nanocomposites

Polyesters are another class of polymer investigated in this thesis produced by step-growth polymerization with hydroxyl groups as one the functional groups required for polymerization.

In this chapter, linear aliphatic polyester was synthesized via direct-polycondensation. FTIR, GPC, DSC were used to characterize the synthesized polyester product. Due to challenges when forming films using the synthesized polyester, nano-TiO_2 was mixed physically with commercial polyester, polycaprolactone (PCL) and polyethylene terephthalate (PET), via solvent or blending. The self-cleaning properties of the nano-TiO_2/PCL mixtures were explored using stearic acid as a model compound for'dirt'. While for nano-TiO_2/PET, both the mechanical properties and self-cleaning properties were studied.

5.1 Introduction

Self-cleaning coatings using nanostructured titania (nano-TiO_2) have been of significant interest both academically and industrially.[1,82,83] Currently, TiO_2 photocatalysis is actively used in environmental decontamination[84,85] because of the photodegradation of organic compounds. Although most photocatalytic self-cleaning coatings research has focused on self-cleaning glass, self-cleaning polymers for paints and coatings are of significant industrial and scientific importance.[1] However, little work has been performed on the chemistry for the integration of nano-TiO_2 into polymers for self-cleaning coatings, in which the nanoparticles are chemically linked to the polymer chains.

Polyesters are used worldwide and have a wide variety of applications, including synthetic fibers, films, beverage bottles, and molded plastic parts.[16] Linear aliphatic polyesters were first synthesized by Carothers and coworkers at DuPont,[64] which are nowadays among the most used biodegradable polymers in medical applications.

Recently, biodegradable polyesters as a substitute to plastic products have become of tremendous interest due to emerging environmental concerns.[103]

Both polycaprolactone (PCL) and poly(ethylene terephthalate) (PET) were investigated in this study. PCL was chosen as the aliphatic polyester because of its low cost and wide applications, such as thin-walled tree seedling containers[65], implantable drug delivery devices[67,104], and shopping bags[68]. Because of its biocompatibility, low T_g and high permeability[69], PCL is one of the most commonly used materials in biodegradable drug delivery systems.[65] Various drug-delivery devices made of PCL can be easily degraded by hydrolysis in physiological conditions (such as in the human body).[70,71]

PET was chosen as the aromatic polyester as it has a high melting point and good hydrolytic stability, as originally synthesized by Whinfield and Dickson.[64] With an annual worldwide production of around 60 million tons, PET is the one of the most used polyester worldwide. The main applications of PET are fibers for textiles, films and bottles because of its excellent properties as tensile impact strength, chemical resistance, processability, clarity and thermal stability.[16,73] There are currently two main approaches to PET synthesis, polycondensation and ring-opening polymerization.[16] Polycondensation is the traditional synthesis process, which involves the synthesis of bis-(2-hydroxyethyl) terephthalate (BHET) in the first step and melt polycondensation of BHET in the second step. Ring-opening polymerization is a novel synthesis process, which is ring-opening polymerization of cyclic oligoesters.

5.2 Experimental

5.2.1 Materials

All chemicals were either purchased from Sigma-Aldrich (Mississauga, ON) or Caledon Labs (Georgetown,ON). Titanium dioxide (anatase nanopowder, < 25nm) was calcined at 400^{o}C before use. 1,4-Butanediol, 99%, phthalic anhydride(PA), ACS reagent, ≥99%, 2,2-Dimethyl-1,3-propanediol (DMPD), 99%, dibutyltindilaurate (DBTDL), 95% were used as prepared by Sigma-Aldrich. PCL was in pellet shape with molecular weight of 70,000-90,000 Da. PET was also in pellet shape with 30% glass particles as reinforcer.

Both polymer were also used as prepared by Sigma-Aldrich. Adipic acid, reagent, ≥99%, tetrahydrofuran (THF), HPCL grade, ≥99.9% were used as prepared by Caledon Labs.

5.2.2 Experimental Setup

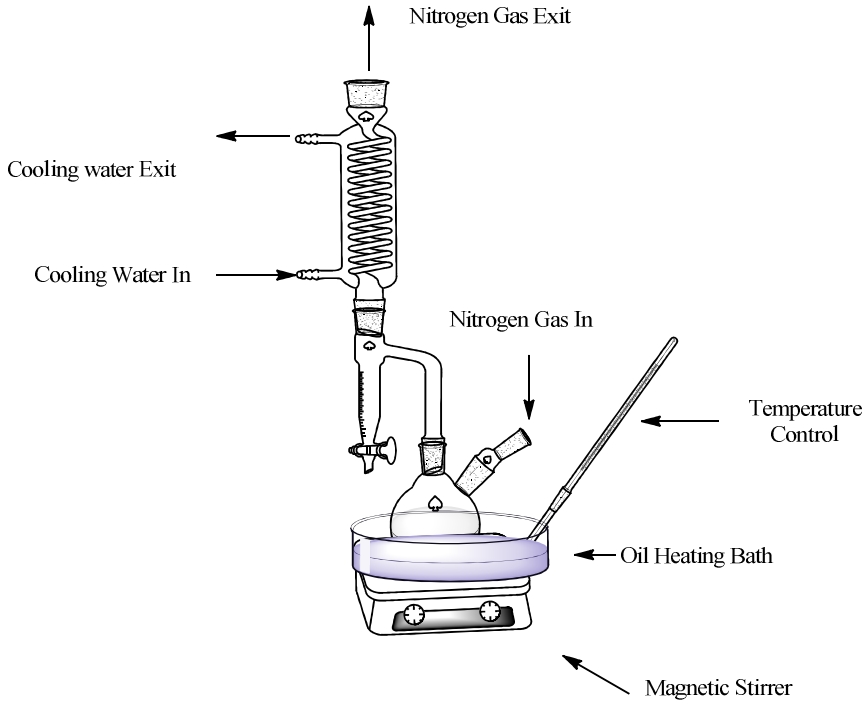

Figure 5.1 Polyester Synthesis Setup.

The synthesis experimental setup, as illustrated in Figure 5.1, consists of an oil bath for reaction temperature control and a two-neck round-bottomed flask equipped with a mechanical stirrer, a nitrogen inlet and a condenser for: a) mixing reactants and catalyst during polymerization, b) providing a purge stream of nitrogen gas to bring byproduct (water vapor) out, c) cooling water vapors into liquid to be collected. The distilling trap is used to collect the byproduct, water, for estimation of monomer conversion.

A VWR® ceramic top hot plate stirrer with temperature control was used to provide mechanical stirring and heating. All glassware were dried in an oven at 80 ºC and cooled in a desiccator overnight to avoid moisture.

5.2.3 Synthesis of linear polyester

Pthalic anhydride, adipic acid, 2,2-dimethyl-1,3-propanediol and 1,4-butanediol with a molar ratio of 1:4.95:1.36:6.98 were charged into the flask and heated to around 120°C using a slow stream of nitrogen gas and constantly mixed by magnetic stirring. After all monomers were molten, 0.05wt% of DBTDL based on the total weight of monomers was added as the catalyst. The reaction was then heated and kept at 165°C for about 4h.[105] Vacuum was used in order to remove formed condensate byproducts and the reaction was stopped when no further water was collected in the distilling trap.

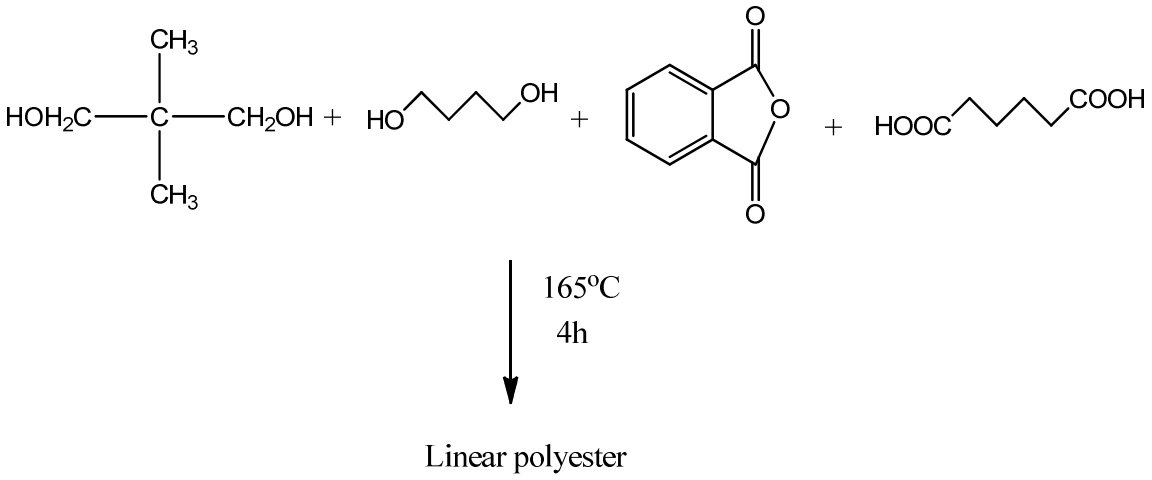

Figure 5.2 Scheme for linear polyester synthesis.

5.2.4 nano-TiO_2/PCL sample preparation

Because of its good solubility in THF, nano-TiO_2-PCLwas prepared via a solution approach. The sample was generally prepared by three steps: first, nano-TiO_2 was dispersed with THF solvent with the aid of ultrasonication; then, PCL of the corresponding weight in the same THF solvent was dissolved to form a homogenous solution. Finally, the homogenous solution was poured onto a Teflon plate to form sample films for subsequent analysis and testing.

5.2.5 nano-TiO_2/PET sample preparation

Since PET is not as easily dissolved in solvent as PCL, nano-TiO_2-PET was prepared by mechanical blending. nano-TiO_2-PET samples were usually prepared by two steps: blending and molding.

First, nano-TiO_2 powder was simply mixed with PET granules mechanically. The mixture was then put into an extruder at 280 ^oC for further blending. After blending, the solids were melted in an injector at 290 ^oC, and then injected into a mold (40 ^oC) to form a rectangular shape samples for subsequent property testing.

5.3 Characterization

5.3.1 Fourier Transform Infrared Spectroscopy

FTIR analysis was performed using an ATR-FTIR spectroscope (Nicolet 6700 FT-IR Spectrometer, Thermo Scientific, USA) in the range of 500-4000 cm^{-1} with 32 scans for each sample to measure and identify the variations of the functional groups and characteristic peaks.

5.3.2 Differential scanning calorimetry

Differential scanning calorimetry (DSC) was performed using a differential scanning calorimeter (SDT Q600, TA Instruments, USA) with the spectra analyzed using the instrument software (Universal Analysis 2000, TA Instruments, USA). Experiments were carried out under nitrogen gas atmosphere. Samples weighing 10-15 mg were kept in an alumina sample pan and heated from room temperature to 250ºC at a heating rate of 10ºC/min. The real time heat flow as function of temperature was recorded during the experiment using Universal Analysis 2000 data acquisition system.

5.3.3 Gel Permeation Chromatography

Gel Permeation Chromatography (GPC) was used to determine the relative molecular weights of polyester as well as its polydispersity. 30 mg of polyester sample was first dissolved in 10 mL THF solvent. The solution was then filtered by syringe filter featuring 0.2 μm pore size. 100 μL of filtered solution was taken from the vial each time for the gel

column (GPCmax VE-2001,Viscotek, USA) with a flow rate of 1mL/min at room temperature. Signals are collected by a detector (TDA 302 triple detector array, Viscotek, USA) during a 45 minute run. Polystyrene standards with known molecular weight were used to calibrate the system.

5.3.4 Contact Angle Characterization

Hydrophilic and hydrophobic behavior was evaluated by measuring the contact angle of a water droplet on the films under ambient conditions using the sessile drop method. The contact angle measurement was performed using a standard contact angle goniometer (Model 200, Ramé-Hart Instrument Co., USA). The coating surface was placed and leveled on the test cell between the light source and microscope. Then 10μLwater was deposited onto the coating surface through a syringe. After the liquid drop reaches its equilibrium state, its digital image can be recorded and the contour fitted by software (DROPimage Standard v2.4,ramé-hart instrument co., USA).

5.3.5 Self-cleaning Property Test

Photocatalytic activity that leads to the self-cleaning property of the nano-TiO_2/PCL coatings was examined by monitoring the degradation of 'dirt' on the polymer surface. Weight losses of samples were recorded during the degradation process. Stearic acid was chosen as the model compound for 'dirt' to test the coatings self-cleaning ability.

For nano-TiO_2/PCL samples, the test process started with dissolving 2g nano-TiO_2/PCL with 0.2g excess 'dirt' compound (10%wt) into THF solvent. The solution was then poured into round Teflon dishes (d=70mm) to form thin films of the nanocomposites. The films were then irradiated perpendicular to the light source at a constant distance of 20cm with a high intensity UV lamp (Blak-Ray B100-AP,UVP, USA). The weights of samples were recorded during the irradiation.

For nano-TiO_2/PET samples, stearic acid solution was deposited on the surface of already weighted nano-TiO_2/PET sample. After the solvent evaporate, samples were then irradiated perpendicular to the light source at a constant distance of 5cm with a high

intensity UV lamp (Blak-Ray B100-AP,UVP, USA). The weights of samples were recorded during the irradiation.

5.3.6 Mechanical Property Test

Tensile tests were performed to determine the mechanical properties according to the ASTM D638-10 using molded nano-TiO_2/PET samples. Samples were prepared into rectangular shapes with 50 mm length and 5mm width using mini-injector. Specimens were loaded between grips (5943 Single Column Tabletop Systems, Instron®, USA) with 25 mm gauge length and tested at a rate of 3.75 mm/min.

5.4 Results and Discussion

Linear polyester was synthesized using the setup in Figure 5.1 and chemicals in Figure 5.2. As shown in Figure 5.3, the linear polyester product is a yellowish powder-like polymeric texture.

Figure 5.3 Digital picture of synthesized linear polyester from experimental section 5.2.3. Raw materials: Pthalic anhydride, adipic acid, 2,2-dimethyl-1,3-propanediol and 1,4-butanediol. Reaction took place at 165^{o}C under nitrogen flow protection.

5.4.1 FTIR of synthesized linear polyester

The final products of polyesters were characterized by FTIR analysis in absorbance mode. The FTIR spectrum of the synthesized linear polyester (from Figure 5.3) is shown in Figure 5.4, where no peaks from 4000-3000cm^{-1} were detected. This absence of hydroxyl

groups indicates the complete conversion of alcohol monomers,[88,89] proving the esterification reaction had taken place. Moreover, peaks at 1700cm^{-1} and 1320-1000cm^{-1} are characteristic ester absorption peaks, indicating the ester product.

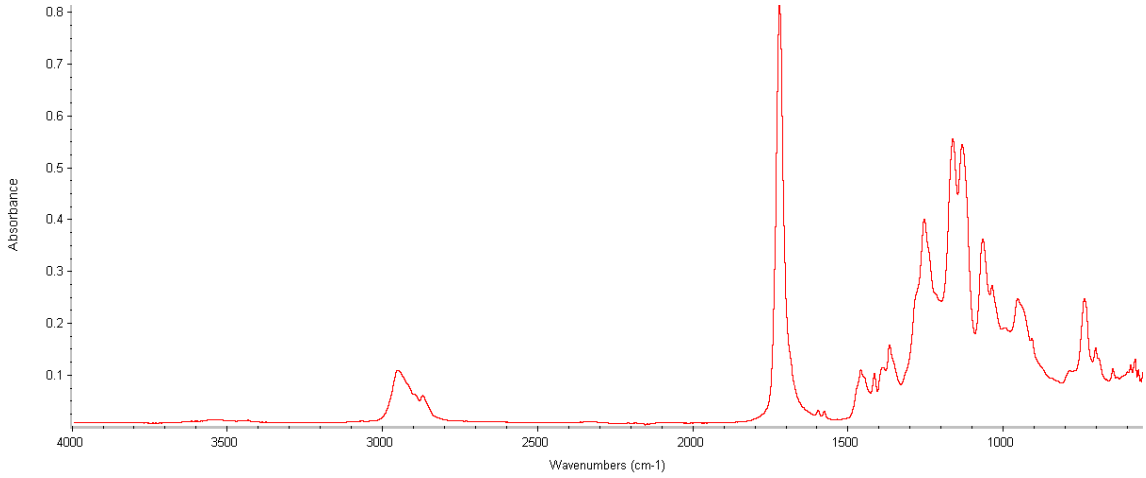

Figure 5.4 FTIR spectrum of synthesized linear polyester from experimental section 5.2.3. Raw materials: Pthalic anhydride, adipic acid, 2,2-dimethyl-1,3-propanediol and 1,4-butanediol. Reaction took place at 165^{o}C under nitrogen flow protection.

5.4.2 Melting point of synthesized linear polyester

The melting point of the synthesized linear polyester was investigated using DSC. Figure 5.5 shows the heat flow change versus temperature during the heating process. In this curve, an endothermic peak at 45^{o}C is observed, indicating the melting point of the linear polyester product. Also, only one single endothermic peak indicated that this sample is one single chemical rather than several chemicals mixtures (raw materials).

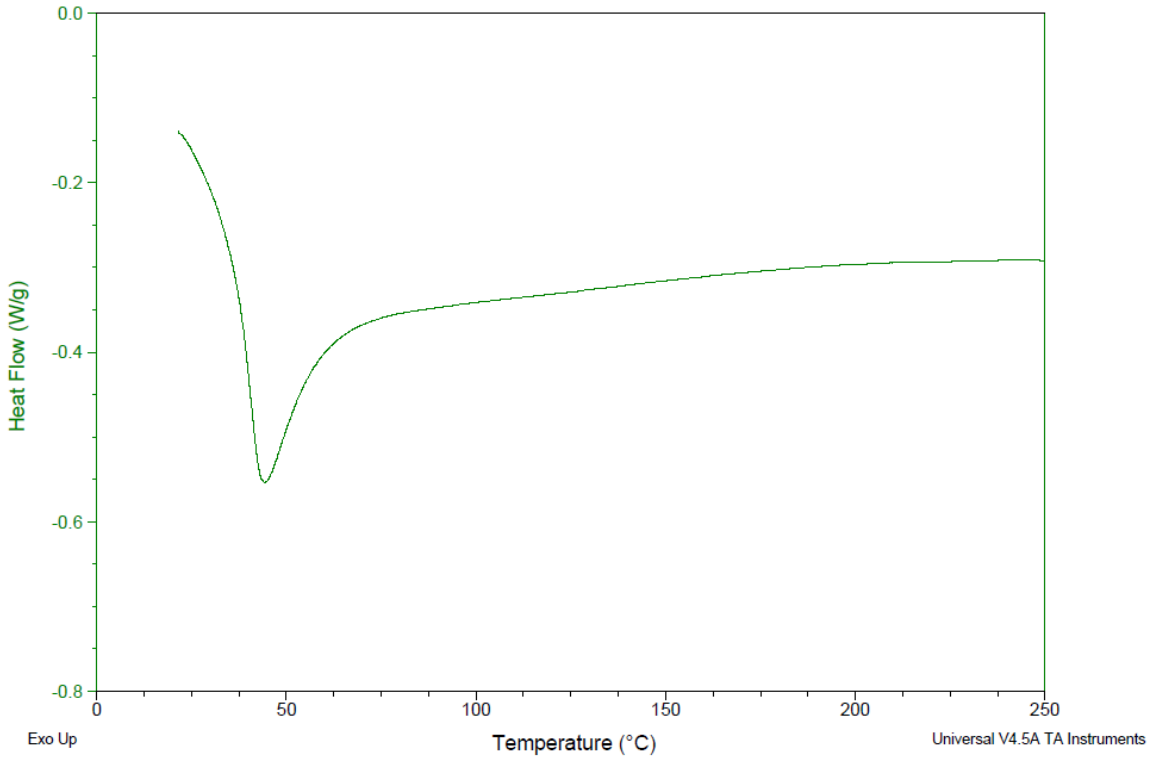

Figure 5.5 DSC analysis curve of synthesized linear polyester from experimental section 5.2.3. Raw materials: Pthalic anhydride, adipic acid, 2,2-dimethyl-1,3-propanediol and 1,4-butanediol. Reaction took place at 165^{o}C under nitrogen flow protection.

Moreover, the melting point ranges of raw materials (pthalic anhydride, adipic acid, 2,2-dimethyl-1,3-propanediol and 1,4-butanediol) were found to be 131-134^{o}C, 151-153^{o}C, 124-130^{o}C , 16^{o}C respectively according to manufacturer's MSDS. None of this temperature had corresponding endothermic peak in this curve, indicating the absence of raw materials, therefore proving the polymerization had taken place.

5.4.3 Molecular weight of synthesized polyester and commercial PCL

GPC analysis was performed to investigate the molecular weight of the resulting polymer by comparing with polystyrene standards. Figure 5.6 shows the GPC chromatograms for commercial PCL. In this chromatogram, it is observed that three peaks (Red for RI signal, black and green for low/high angle light scattering) on retention volume 23-27 mL

overlap with each other, indicating the presence of macromolecular molecule, or in another word polymer. By comparing to PS standard, the molecular weight of the commercial PCL is 43,528±1,545 Da (calculated from GPC software) after 2 runs.

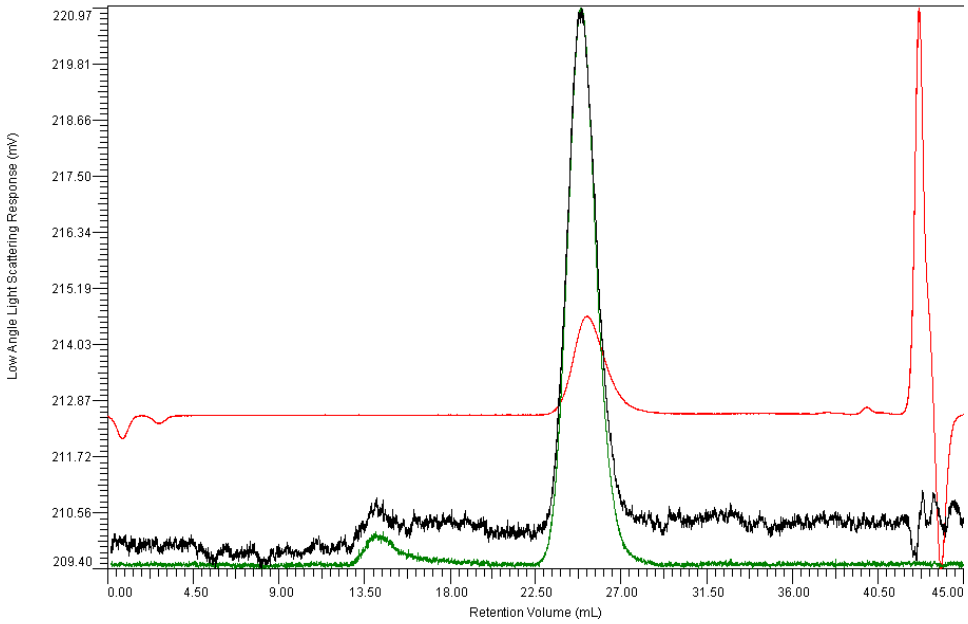

Figure 5.6 GPC chromagraph of commercial PCL (M_w= 43,528).

Figure 5.7 shows the GPC chromagraph of synthesized linear polyester. In this polyester chromatogram, three peaks (Red for RI signal, black and green for low/high angle light scattering) at a retention volume of 23-27 mL overlap with each other, indicating the presence of polymer.

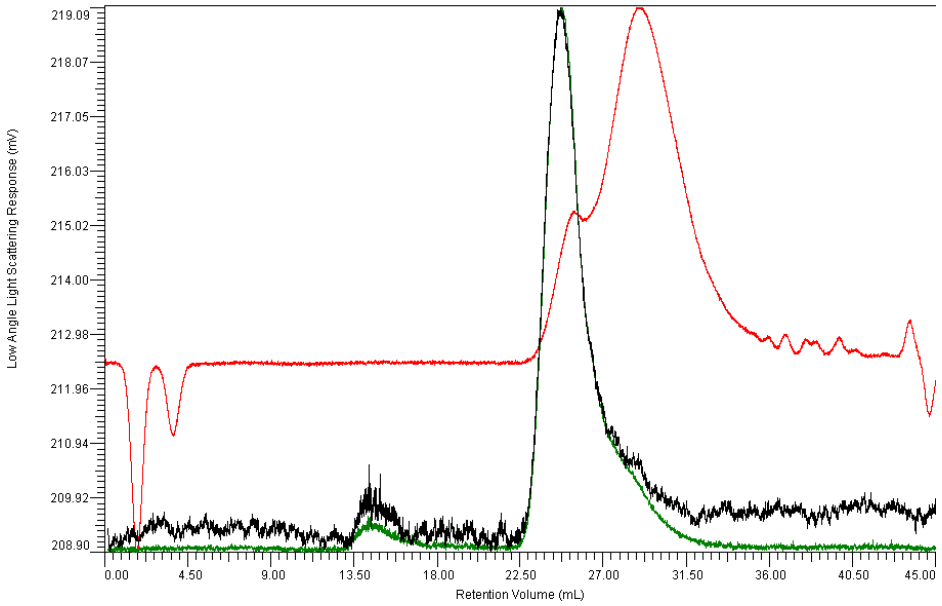

Figure 5.7 GPC chromagraphs of synthesized linear polyester (M_w= 42,154) from experimental section 5.2.3. Raw materials: Pthalic anhydride, adipic acid, 2,2-dimethyl-1,3-propanediol and 1,4-butanediol. Reaction took place at 165^{o}C under nitrogen flow protection.

Moreover, at a retention volume 27-32mL, the appearance of red peaks without corresponding black and green peaks indicates this is an organic molecule, which suggests the presence of low molecular oligomers. By comparing to PS standard, polyester samples have molecular weight of 42,154±623Da (calculated from GPC software) after 3 runs.

5.4.4 Surface Hydrophilicity of PCL and nano-TiO_2/PCL

As previously discussed, the self-cleaning effect is related to the surface hydrophilicity which can be characterized by measuring the contact angle, i.e. the angle formed between the surfaces of a liquid drop deposited on the surface of a solid.[17,20]

The sessile drop method was chosen as the measurement method for contact angle analysis because of its accuracy and simplicity. In order to form flat test surfaces for contact angle measurements, polymer coatings were coated on microscope slides using spin-coating at 2000 rpm for 2 minutes for PCL related samples. Figure 5.8 shows the

images of contact angle for pure PCL and nano-TiO_2-PCL samples before UV irradiation. Before UV irradiation, both the pure PU (82.4^o) and Ti-PU (78.9^o) have similar contact angles near 80^o. Therefore, both surfaces were hydrophilic without UV irradiation. A detailed summary of the contact angle results is given in Table 5.1.

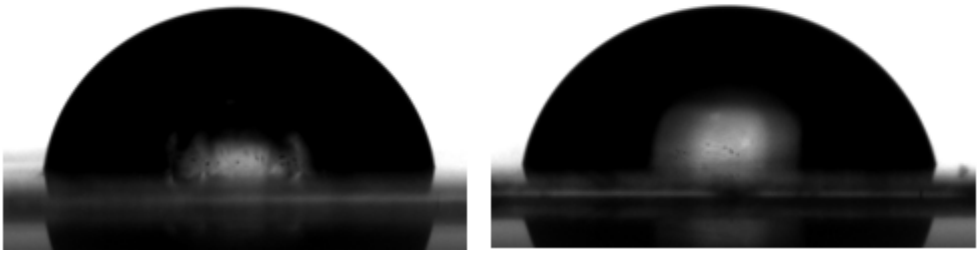

(a) **(b)**

Figure 5.8 Contact Angle pictures of (a) Pure PCL and (b) nano-TiO_2-PCL surfaces.

Table 5.1 Contact angle results of Pure PCL and nano-TiO_2/PCL

Name / No.	Contact Angle (°)	
	Pure PCL	nano-TiO_2/PCL
1	81.6	77.9
2	83.2	80.0
3*	82.4	78.9
Avg.± S.D.	82.40 ±0.80	78.93 ± 1.05

* These two test results were chosen to stand for each sample in Figure 5.8.

Table 5.2 shows the contact angle change of nano-TiO_2/PCL during UV exposure. nano-TiO_2 concentration is 1% in the nano-TiO_2/PCL sample. These results show that after UV irradiation, the contact angle of nano-TiO_2/PCL surface decreased from 78.93^o to 58.33^o, i.e. the surface became more hydrophilic after UV irradiation. This increase in hydrophilicity can be explained by the nature of the UV irradiation process. Upon UV irradiation, TiO_2 photo-generated holes can produce OH radicals which can result in an increase of OH groups thus increasing the surface energy. With an increase of surface energy on the polymer surface, the contact angle would decrease, forming a more hydrophilic surface.[11]

Table 5.2 Summary of contact angles of nano-TiO_2/PCL before and after 4h UV treatment

Condition / No.	Contact Angle (°)	
	Before UV	After UV
1	77.9	59.8
2	80.0	57.8
3*	78.9	57.4
Avg.± S.D.	78.93 ± 1.05	58.33 ± 1.29

Also, as the time of UV treatment extended, the contact angle did not show any further decrease, which is similar to the results found with nano-TiO_2-PU in the last chapter.

5.4.5 nano-TiO_2/PCL photo-catalysis using stearic acid as 'dirt'

As mentioned in the previous chapter, stearic acid is the standard model compound for 'dirt', being used in self-cleaning studies. Here, stearic acid degradation was monitored by weight changes when the polyester nanocomposite samples were exposed to UV treatment. Stearic acid was added in the first step of nano-TiO_2/PCL preparation step using a TiO_2 concentration of 1% in the nano-TiO_2/PCL sample.

Figure 5.9 shows the weight percentage change of the TiO_2/PCL sample when treated with UV irradiation for various lengths of time. The weight percentage begins with 110% because of the 10% additional stearic acid added.

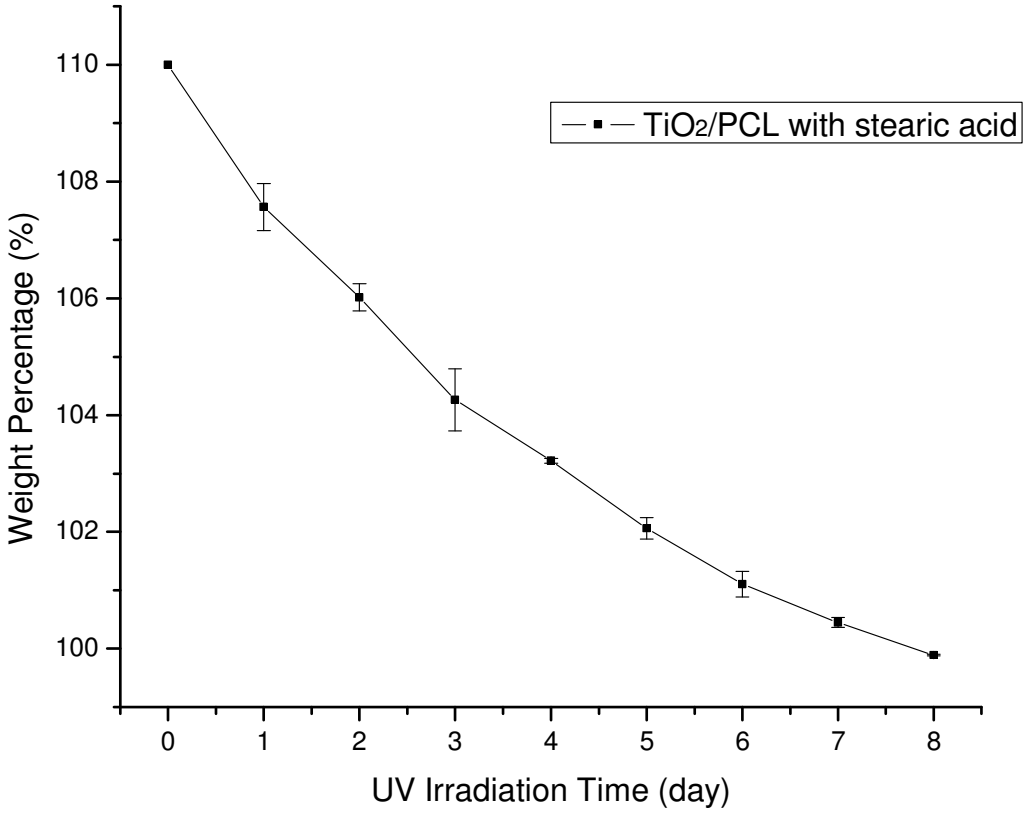

Figure 5.9 Weight change (by percentage) of 1% TiO_2/PCL mixture sample with additional 10% stearic acid during UV treatment. Error bars show the ± standard deviation of the test results.

After 8 days of UV treatment, the weight of sample dropped to 100%, indicating the degradation of stearic acid as being complete. This weight loss decreased slowly as the stearic acid concentration decreased during the decomposition process. In addition, when the length of UV exposure time was extended after stearic acid degradation, we find that the weight was still dropping. This means the TiO_2-PCL was degrading itself when exposed to UV light.

Comparing between the pure PCL sample and the TiO_2-PCL sample as shown in Figure 5.10, it is shown that stearic acid is decomposing even without the presence of TiO_2. Here, the weight value is almost constant after 48 hours, indicating that UV light has a

limited effect on decomposing stearic acid. Similar results were observed in the last chapter for polyurethane self-cleaning tests.

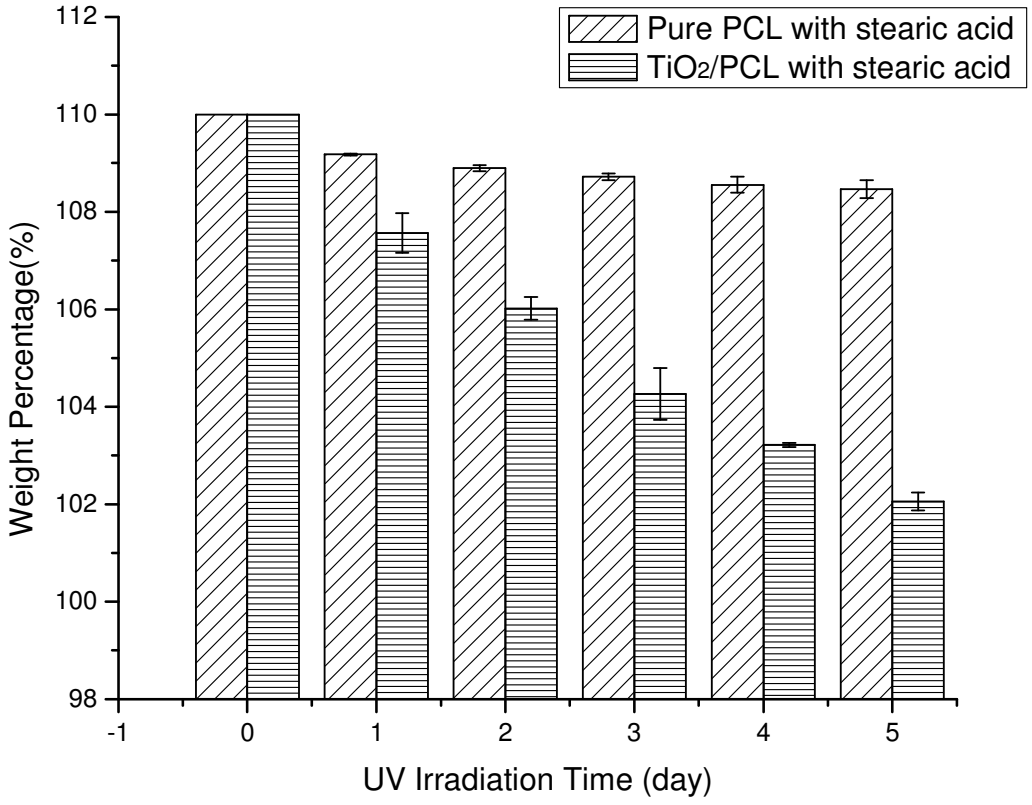

Figure 5.10 Weight changes (by percentage) of Pure PCL sample and TiO_2/PCL mixture sample with additional 10% stearic acid during UV treatment. Error bars show the ± standard deviation of the test results.

Also, it is clear that the weight loss of the TiO_2-PCL sample is much higher than that of the pure PCL sample during the same UV exposure time. This proves that TiO_2 plays a very important role in stearic acid decomposition, i.e. it provides it with self-cleaning properties.

5.4.6 Evidence of stearic acid degradation

Two control experiments were performed to corroborate the self-cleaning properties of TiO_2-PCL. The first control experiment compared the weight change between the pure PCL samples w/without stearic acid. The results (Figure 5.11) clearly show that the stearic acid, not PCL, is degrading.

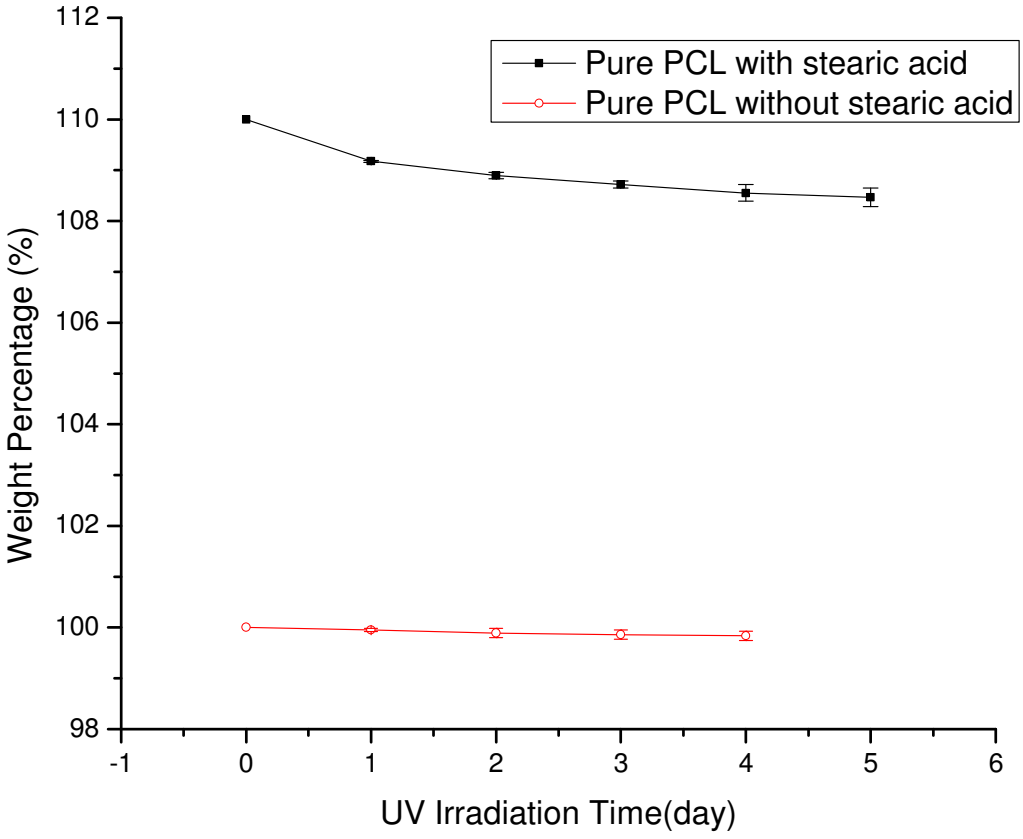

Figure 5.11 Weight changes (by percentage) of pure PCL samples (with and without additional 10% stearic acid) during UV treatment. Error bars show the ± standard deviation of the test results.

In the graph, the weight of the pure PCL sample without stearic acid did not change significantly during the experimental time-frame, indicating pure PCL did not decompose under UV irradiation. The weight change of the pure PCL sample with stearic acid

dropped slightly, indicating that stearic acid went through partial decomposition under UV irradiation.

Another control experiment compared the weight changes between the TiO_2/PCL samples with and without stearic acid, as shown in Figure 5.12. The results clearly show the self-cleaning property of TiO_2/PCL. Because of the additional 10% stearic acid added, the TiO_2/PCL with stearic acid sample begins at 110% while the TiO_2/PCL without stearic acid sample begins at 100%.

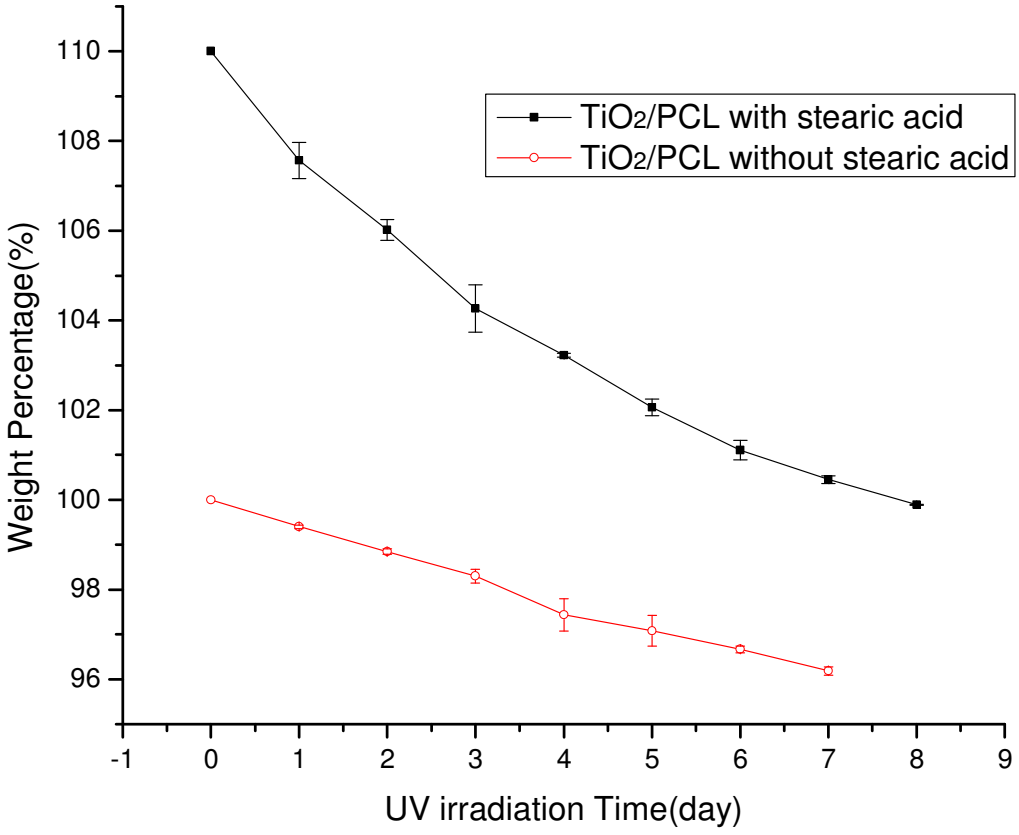

Figure 5.12 Weight changes (by percentage) of TiO_2/PCL samples (with and without additional 10% stearic acid) during UV treatment. Error bars show the ± standard deviation of the test results.

It is shown in the graph that the weight of the TiO_2/PCL sample without stearic acid decreased during the UV irradiation, meaning TiO_2/PCL is decomposing under UV irradiation. There are several reasons leading to this weight loss. First, PCL is not very chemically stable compared to the other types of polyester, as it can be easily degraded.[104] This easy degradation makes PCL popular for studying biomedical polymers. Also, TiO_2 under UV irradiation has a very strong ability to decompose organic molecules. Meanwhile, the weight loss of the TiO_2/PCL sample with stearic acid is much higher than that of the one without stearic acid. This indicates that stearic acid also underwent the decomposition process, which supports the fact that TiO_2/PCL has a self-cleaning ability.

5.4.7 The effect of TiO_2 concentration on nano-TiO_2/PCL self-cleaning property

In addition to previous self-cleaning property experiments, the effect of different TiO_2 concentrations (1%, 2% and 5%) on the self-cleaning properties was also investigated.

Figure 5.13 shows the results of self-cleaning property tests of nano-TiO_2/PCL with different nano-TiO_2 concentrations (using anatase nano-TiO_2). It is clear that the nano-TiO_2/PCL samples have significantly more weight loss than the pure PCL samples. For the pure PCL sample, only 1% weight loss was achieved after 1 day of UV irradiation, and there is still only 1.5% weight loss after 4 days UV irradiation. On the other hand, for nano-TiO_2/PCL samples, the weights were continuing dropping (from approximately 3% after 1 day to approximately 7% after 4 days) as the UV irradiation time extend.

Moreover, it is noticed that the weight loss of the samples is higher for the samples containing higher nano-TiO_2 concentrations. However, this comparison is not very obvious, since the error bars of each samples overlap with each other, indicating the trend of higher weight loss for higher nano-TiO_2 concentration is not definite. The variability increases with increasing wt. % TiO_2. Theoretically, with higher concentrations of nano-TiO_2, the self-cleaning property of the nano-TiO_2/PCL nanocomposites would be better, i.e. higher weight losses are expected as shown in the last chapter for nano-TiO_2-PU. The reason for this result is attributed to poor nano-TiO_2 dispersion in the nano-TiO_2/PCL

nanocomposites. It is commonly known that nanoparticles are usually not well dispersed in organic matrices. Therefore, even with higher nano-TiO_2 concentrations, the amount of effective nano-TiO_2 contributing to photocatalysis might not be higher, which leads to similar self-cleaning properties.

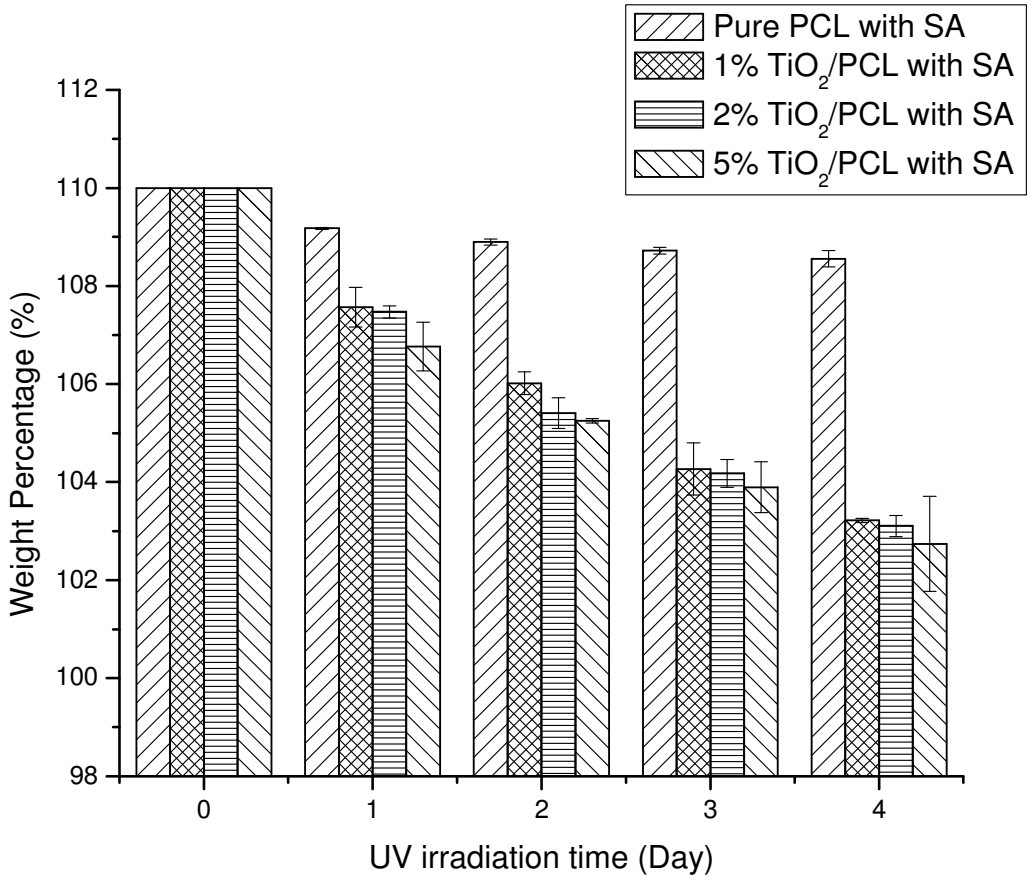

Figure 5.13 Weight changes (by percentage) of pure PCL, 1% nano-TiO_2/PCL, 2% nano-TiO_2/PCL and 5% nano-TiO_2/PCL with 10% stearic acid during UV treatment. Error bars show the ± standard deviation of the test results.

5.4.8 Mechanical Properties of nano-TiO_2/PET

Tensile tests were performed to investigate nano-TiO_2's effect on mechanical properties of PET. All samples were prepared in dumbbell shaped specimens prepared by injection molding. Images of the PET sample before testing and failed PET sample after testing are shown in Figure 5.14.

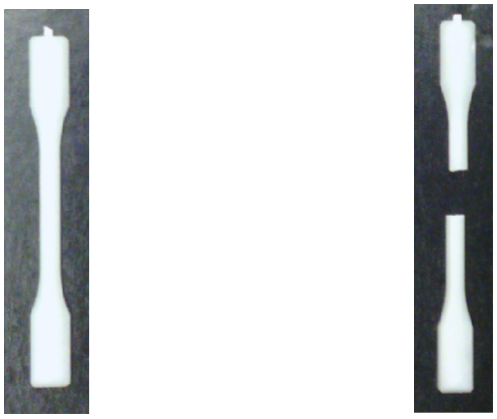

Figure 5.14 Images of PET sample before tensile test (left) and failed PET sample after tensile test (right). The rectangular region in the middle of the sample is the test region. Samples (Gauge length: 25mm, width: 5mm, thickness: 1mm) was tested at a constant crosshead speed of 3.75mm/min.

Figure 5.15 shows the tensile stress-strain plots of pure PET and TiO_2/PET samples. The tensile modulus of both samples are almost the same (2530 MPa for pure PET sample and 2580 MPa for TiO_2/PET sample), which means that TiO_2 did not have any significant effect on the PET's modulus. This is attributed to the nanoparticles not being chemically attached to the polymer backbone as was performed with the polyurethane samples.

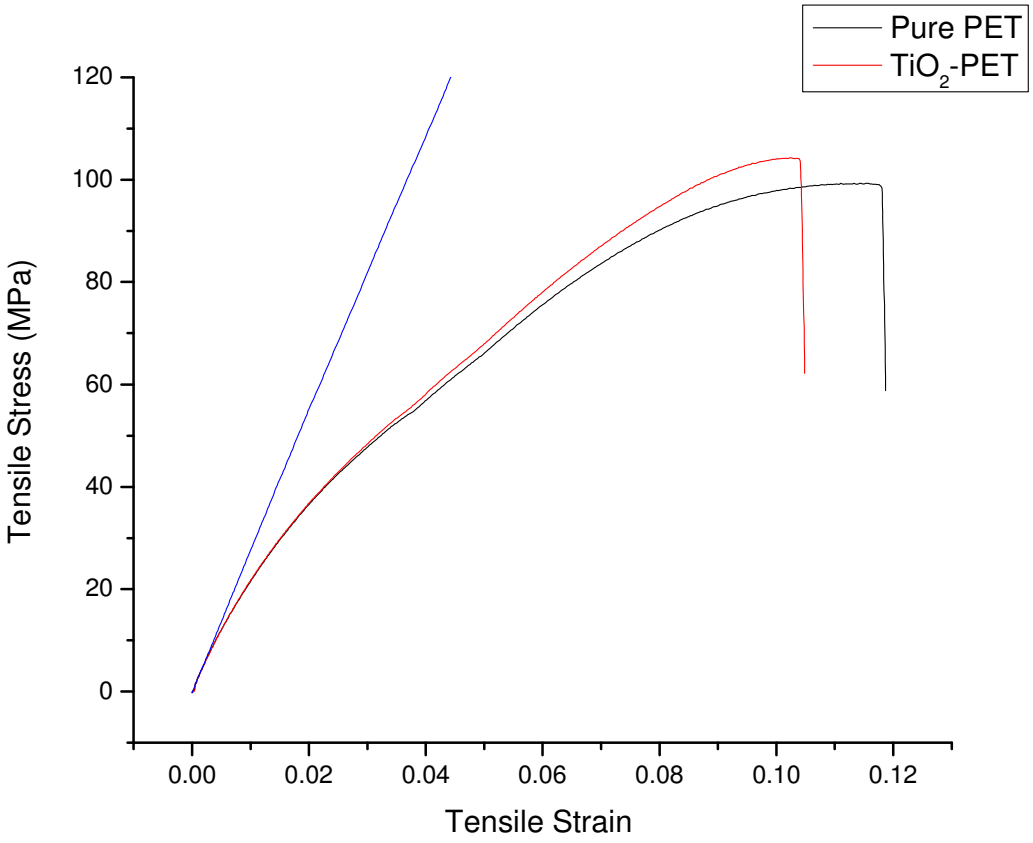

Figure 5.15 Tensile stress-strain plots of pure PET and TiO_2/PET samples. Samples (Gauge length: 25mm, width: 5mm, thickness: 1mm) was tested at a constant crosshead speed of 3.75mm/min.

However, a small increase in the tensile strength was observed, from 99.3 MPa (pure PET) to 104 MPa (TiO_2/PET). This indicates that TiO_2 has slightly increased the tensile strength of PET. Also, the elongation at break of the TiO_2/PET sample is slightly smaller than that of the pure PET sample, which corroborates the result of increased tensile strength. The elongation at break of polymer would normally decrease when the tensile strength of polymer was increased.[90-92] Table 5.3 gives the summary of the tensile test results showing that the average test results are consistent to the results in the graph.

Table 5.3 Summary of the PET tensile test results. Samples (Gauge length: 25mm, width: 5mm, thickness: 1mm) was tested at a constant crosshead speed of 3.75mm/min.

Sample Name	Sample No.	Tensile Modulus (MPa)	Tensile Strength (MPa)	Elongation at Break(%)
Pure PET	1*	2530	99.3	11.76
	2	2420	99.4	10.44
	3	2620	98.1	10.04
	Avg.±S.D.	2523±100	98.9±0.7	10.75±0.9
TiO_2/PET	1	2460	103	9.20
	2	2590	106	8.92
	3*	2580	104	10.40
	Avg. ±S.D.	2543±72	104±1.5	9.51±0.78

5.4.9 Self-cleaning Property of nano-TiO_2/PET

For the self-cleaning test, stearic acid was dissolved in THF solution and then deposited onto the PET sample surface. The white powder on the sample shown in Figure 5.16 is stearic acid.

Figure 5.16 Image of nano-TiO_2/PET with deposited stearic acid on the surface.

The weight changes of TiO_2/PET samples with stearic acid were recorded in this experiment as shown in Figure 5.17. The graph begins with 100% of stearic acid as the weight of TiO_2/PET was deducted.

It is observed that the weight of stearic acid drops after UV irradiation, indicating the decomposition of stearic acid. However, after 1 day, the weight almost remains stable as

the UV irradiation time was increased. This trend is similar to the trends for pure PU and pure PCL self-cleaning test as described previously. The initial weight loss is due to the stearic acid degraded from UV high energy.

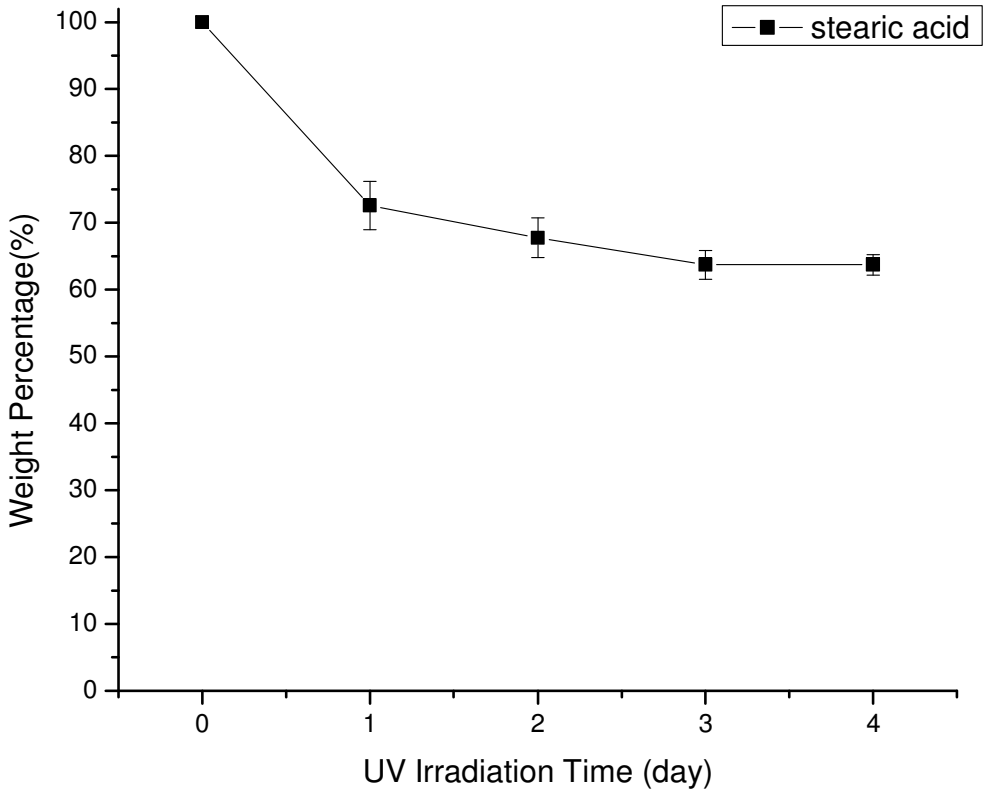

Figure 5.17 Weight percent change of stearic acid on the nano-TiO_2/PET surface. Error bars show the ± standard deviation of the test results.

The reason for the absence of self-cleaning properties of TiO_2/PET sample is that the samples were too thick. TiO_2 only has photo-catalytic properties when exposed to UV irradiation directly.[10,106] However, in these samples, TiO_2 was mostly mixed inside the sample. Therefore, for thicker samples, there is very little TiO_2 on the sample surface which results in the observed poor self-cleaning properties.

5.5 Conclusion

Linear aliphatic polyesters were synthesized in this chapter. FTIR spectroscopy of the resulting polymer confirmed its ester group formation. The molecular weight of the polyester products was found to around 42,000 Da by GPC

Due to the difficulty of film formation, commercially available polyester (PCL and PET) was used to investigate the self-cleaning and mechanical properties of nano-TiO_2/polyester nanocomposites. For nano-TiO_2/PCL, a similar decrease in contact angle was observed as found with nano-TiO_2-PU. The contact angle of nano-TiO_2/PCL surface decreased to 58.3^o from 78.9^o after UV treatment for 4h. No further decrease was found as the time of UV treatment was extended.

Using stearic acid as a model compound for 'dirt', the self-cleaning test results of nano-TiO_2/PCL are similar to those of nano-TiO_2-PU samples in the previous chapter, showing good self-cleaning properties. However, for the nano-TiO_2/PET samples, no self-cleaning property was found attributed to a lack TiO_2 on the sample surface.

For tensile tests, no increase in Young's modulus was found with addition of TiO_2 because of the 30% glass reinforcer in the purchased PET pellets. However, an increase in tensile strength (from 98.9 MPa to 104 MPa) was observed with addition of 1wt% TiO_2 even with the existence of 30% glass. A corresponding decrease in elongation is observed along with an increase of tensile strength.

Chapter 6

6 Conclusions

This thesis has investigated self-cleaning polyurethane and polyester coatings. Because of their numerous advantages and extensive potential applications, the future of self-cleaning coatings is very promising. The purpose of this study was to synthesize and characterize the TiO_2 based polymer coatings, while testing them for self-cleaning and mechanical properties. The main conclusions can be summarized as follows:

1. Two methods for polyurethane synthesis were investigated and compared using different characterization methods. It was found that the pre-polymer method produced segmented PU with alternatively arranged chains, while the “one-shot” method produced segmented PUs with randomly arranged chains. FTIR results showed that both types of synthesized polymer shared the same chemical composition; whereas the mechanical property testing results showed that the products from the pre-polymer method gave superior mechanical properties, indicating a more organized chain structure.

2. nano-TiO_2 coordinated polyurethane, (nano-TiO_2-PU) was successfully synthesized using the pre-polymer method. With UV irradiation, nano-TiO_2-PU shows hydrophilicity and photocatalytic activity in comparison to pure PU. The thermal stability of nano-TiO_2-PU also increased compared to pure PU.

3. Two different model compounds for ‘dirt’ were used to investigate the photocatalysis of nano-TiO_2-PU. Compared to stearic acid, DMPA was much more easily decomposed under UV irradiation attributed to its smaller molecular weight and higher degree of oxidation.

4. Linear aliphatic polyester with average molecular weight of around 42,000 was synthesized, however, the nTiO2 has not yet linked on the polyester.

5. Due to the difficulty of film formation for synthesized polyester, PCL and PET were purchased to investigate the self-cleaning properties of TiO_2 based polyester. nano-TiO_2/PCL was prepared through a simple physical mixture via THF solvent. With UV

irradiation, nano-TiO_2-PCL also shows hydrophilicity and photocatalysis activity as nano-TiO_2-PU. nano-TiO_2/PET was prepared through mechanical blending since PET was not easily dissolved in solvent. Samples were prepared via an injection molder for mechanical tensile tests. The tensile strength was slightly increased with the addition of nano-TiO_2. However, nano-TiO_2/PET samples did not show significant photocatalysis activity when exposed to UV irradiation, attributed to the nano-TiO_2/PET samples having a relatively large thickness of 1 mm.

It is recommended that further research be undertaken in the following areas:

1.Super-hydrophilicity: Even though the synthesized polymers have been shown to be able to achieve hydrophilicty under UV irradiation, they are far from super-hydrophilic which are self-cleaning. For segmented PU synthesis, some other soft segments, for example, polyethylene oxide glycol, may be used to improve the product wettability.

2. Photocatalysis of nano-TiO_2/PET sample: In this study, the photocatalysis activity was not achieved because of the sample thickness. Future studies should focus on thin film samples of nano-TiO_2/PET.

3. Extending the absorption light range of TiO_2 into thevisible region: UV light is not always available during daily use. By extending the absorption range into the visible region, the efficacy of the coating would be significantly improved.

4. Polyester synthesis and its functionalization: Future polyester synthesis can focus on optimizing the monomer ratio to get polyesters with better mechanical properties. Also, DMPA has a similar chemical structure as DMPD (2,2-Dimethyl-1,3-propanediol), therefore, it may be used as a monomer in polyester synthesis to replace DMPD. In addition, PTHF may be a good addition for polyester synthesis to improve the film formation property of the resulting polyester. With a hydroxyl group on each end of the molecule, PTHF can be a useful soft segment for polyester synthesis.

References

1 Charpentier, P. A. *et al.* Nano-TiO2/polyurethane composites for antibacterial and self-cleaning coatings. *Nanotechnology* **23**, 425606 (2012).

2 Burgess, K. D. *Self-cleaning titania-polyurethane composites*. (School of Graduate and Postdoctoral Studies, University of Western Ontario, 2007).

3 Mills, A. & Wang, J. Simultaneous monitoring of the destruction of stearic acid and generation of carbon dioxide by self-cleaning semiconductor photocatalytic films. *Journal of Photochemistry and Photobiology A: Chemistry* **182**, 181-186 (2006).

4 Paz, Y., Luo, Z., Rabenberg, L. & Heller, A. Photooxidative self-cleaning transparent titanium dioxide films on glass. *Journal of Materials Research* **10**, 2842-2848 (1995).

5 Lin, W. *Polyurethane self-cleaning coating*. (School of Graduate and Postdoctoral Studies, University of Western Ontario, 2011).

6 *How self-cleaning glass works*, <http://www.pilkington.com/products/bp/bybenefit/selfcleaning/activ/how-it-works/default.htm> (

7 Parkin, I. P. & Palgrave, R. G. Self-cleaning coatings. *J.Mater.Chem.* **15**, 1689-1695 (2005).

8 Ganesh, V. A., Raut, H. K., Nair, A. S. & Ramakrishna, S. A review on self-cleaning coatings. *J.Mater.Chem.* **21**, 16304-16322 (2011).

9 Rios, P. F., Dodiuk, H. & Kenig, S. Self-cleaning coatings. *Surface Engineering* **25**, 89-92 (2009).

10 Fujishima, A., Rao, T. N. & Tryk, D. A. Titanium dioxide photocatalysis. *Journal of Photochemistry and Photobiology C: Photochemistry Reviews* **1**, 1-21 (2000).

11 Irie, H. & Hashimoto, K. Photocatalytic active surfaces and photo-induced high hydrophilicity/high hydrophobicity. *Environmental Photochemistry Part II*, 425-450 (2005).

12 Bayer, O. Das Di-Isocyanat-Polyadditionsverfahren (Polyurethane). *Angewandte Chemie* **59**, 257-272, doi:10.1002/ange.19470590901 (1947).

13 Szycher, M. *Szycher's handbook of polyurethanes*. (CRC Press, 1999).

14 Oertel, G. Polyurethane handbook. *Reinf.Plast.* **30**, 51 (1986).

15 Król, P. Synthesis methods, chemical structures and phase structures of linear polyurethanes. Properties and applications of linear polyurethanes in polyurethane elastomers, copolymers and ionomers. *Progress in materials science* **52**, 915-1015 (2007).

16 Pang, K., Kotek, R. & Tonelli, A. Review of conventional and novel polymerization processes for polyesters. *Progress in polymer science* **31**, 1009-1037 (2006).

17 Barnes, G. *Interfacial science :an introduction*. Vol. 2; 2 (Oxford University Press; Oxford University Press).

18 Kwok, D. Y. & Neumann, A. W. Contact angle measurement and contact angle interpretation. *Advances in Colloid and Interface Science* **81**, 167-249 (1999).

19 Hiemenz, P. C. & Rajagopalan, R. *Principles of colloid and surface chemistry*. Vol. 3 , rev a expa (Marcel Dekker, 1997).

20 Park, S.-J. & Seo, M.-K. *Interface science and composites*. Vol. 18 (Academic Press/Elsevier, 2011).

21 Barthlott, W. & Neinhuis, C. Purity of the sacred lotus, or escape from contamination in biological surfaces. *Planta* **202**, 1-8, doi:10.1007/s004250050096 (1997).

22 Nakajima, A., Hashimoto, K. & Watanabe, T. Recent studies on super-hydrophobic films. *Monatshefte für Chemie/Chemical Monthly* **132**, 31-41 (2001).

23 Feng, L. *et al.* Super-Hydrophobic Surfaces: From Natural to Artificial. *Advanced Materials* **14**, 1857-1860 (2002).

24 Watanabe, T. *et al.* Photocatalytic activity and photoinduced hydrophilicity of titanium dioxide coated glass. *Thin Solid Films* **351**, 260-263 (1999).

25 Yates Jr, J. T. Photochemistry on TiO2: Mechanisms behind the surface chemistry. *Surface Science* **603**, 1605-1612 (2009).

26 Takeuchi, M., Sakamoto, K., Martra, G., Coluccia, S. & Anpo, M. Mechanism of photoinduced superhydrophilicity on the TiO2 photocatalyst surface. *The Journal of Physical Chemistry B* **109**, 15422-15428 (2005).

27 Wang, R. *et al.* Light-induced amphiphilic surfaces. *Nature* **388**, 431-432 (1997).

28 Wang, R. *et al.* Photogeneration of highly amphiphilic TiO2 surfaces. *Advanced Materials* **10**, 135-138 (1998).

29 Sakai, N., Wang, R., Fujishima, A., Watanabe, T. & Hashimoto, K. Effect of ultrasonic treatment on highly hydrophilic TiO2 surfaces. *Langmuir* **14**, 5918-5920 (1998).

30 Wang, R., Sakai, N., Fujishima, A., Watanabe, T. & Hashimoto, K. Studies of surface wettability conversion on TiO2 single-crystal surfaces. *The Journal of Physical Chemistry B* **103**, 2188-2194 (1999).

31 Sakai, N., Fujishima, A., Watanabe, T. & Hashimoto, K. Enhancement of the photoinduced hydrophilic conversion rate of TiO2 film electrode surfaces by anodic polarization. *The Journal of Physical Chemistry B* **105**, 3023-3026 (2001).

32 Carp, O., Huisman, C. L. & Reller, A. Photoinduced reactivity of titanium dioxide. *Progress in Solid State Chemistry* **32**, 33-177 (2004).

33 Hagfeldt, A. & Graetzel, M. Light-induced redox reactions in nanocrystalline systems. *Chemical Reviews;(United States)* **95** (1995).

34 Brunella, M. F. *et al.* Photocatalytic behavior of different titanium dioxide layers. *Thin Solid Films* **515**, 6309-6313 (2007).

35 Greenwood, N. N. & Earnshaw, A. *Chemistry of the elements*. Vol. 2 (Butterworth-Heinemann, 1997).

36 Shangdi, M. & Ching, W. Y. Electronic and Optical Properties of Three Phases of TiO2. *J Phys Rev B* **51**, 13-023 (1995).

37 Mogyorosi, K., Dekany, I. & Fendler, J. H. Preparation and characterization of clay mineral intercalated titanium dioxide nanoparticles. *Langmuir* **19**, 2938-2946 (2003).

38 Bavykin, D. V., Walsh, F. C. & Royal Society of, C. *Titanate and titania nanotubes :synthesis, properties and applcations*. Vol. 12 (Royal Society of Chemistry, 2010).

39 Mills, A. & Lee, S. K. A web-based overview of semiconductor photochemistry-based current commercial applications. *Journal of Photochemistry and Photobiology A: Chemistry* **152**, 233-247 (2002).

40 Malati, M. A. & Wong, W. K. Doping TiO2 for solar energy applications. *Surface Technology* **22**, 305-322 (1984).

41 Chen, J., Yao, M. & Wang, X. Investigation of transition metal ion doping behaviors on TiO2 nanoparticles. *Journal of Nanoparticle Research* **10**, 163-171, doi:10.1007/s11051-007-9237-3 (2008).

42 Serpone, N. & Pelizzetti, E. *Photocatalysis :fundamentals and applications*. (Wiley, 1989).

43 Kutal, C. & Serpone, N. *Photosensitive metal-organic systems*. (ACS Publications, 1993).

44 Herrmann, J. M. Heterogeneous photocatalysis: fundamentals and applications to the removal of various types of aqueous pollutants. *Catalysis Today* **53**, 115-129 (1999).

45 Ramamurthy, V. & Schanze, K. S. *Semiconductor photochemistry and photophysics*. Vol. 10 (Marcel Dekker, 2003).

46 Hoffman, A. J., Carraway, E. R. & Hoffmann, M. R. Photocatalytic production of H2O2 and organic peroxides on quantum-sized semiconductor colloids. *Environmental science & technology* **28**, 776-785 (1994).

47 Carraway, E. R., Hoffman, A. J. & Hoffmann, M. R. Photocatalytic oxidation of organic acids on quantum-sized semiconductor colloids. *Environmental science & technology* **28**, 786-793 (1994).

48 Matthews, R. W. Hydroxylation reactions induced by near-ultraviolet photolysis of aqueous titanium dioxide suspensions. *J.Chem.Soc., Faraday Trans.1* **80**, 457-471 (1984).

49 Ross, A. B. *et al.* NDRL-NIST Solution Kinetics Database:-Ver. 3.0, Notre Dame Radiation Laboratory, Notre Dame, IN and National Institute of Standards and Technology, Gaithersburg, MD, 1998. *J.Phys.Chem.Ref.Data* **17** (1988).

50 Ahluwalia, V. K. & Mishra, A. *Polymer science :a text book*. (CRC/Taylor & Francis ;, 2008).

51 Ravve, A. *Principles of polymer chemistry*. Vol. 2 (Kluwer Academic/Plenum Publishers, 2000).

52 Fried, J. R. *Polymer science and technology*. Vol. 2 (Prentice Hall PTR, 2003).

53 Odian, G. G. *Principles of polymerization*. Vol. 4th (Wiley-Interscience, 2004).

54 Bahadur, P. & Sastry, N. V. *Principles of polymer science*. Vol. 2 (Alpha Science International, 2005).

55 Carraher, C. E. *Introduction to polymer chemistry*. Vol. 2 (CRC Press, 2010).

56 Carraher, C. E. & Seymour, R. B. *SeymourCarraher's polymer chemistry*. Vol. 7th (CRC Press, 2008).

57 Chattopadhyay, D. K. & Raju, K. Structural engineering of polyurethane coatings for high performance applications. *Progress in polymer science* **32**, 352-418 (2007).

58 Wirpsza, Z., Kemp, T. J. & Skup, A. *Polyurethanes: chemistry, technology and applications*. Vol. 575 (Ellis Horwood London, 1993).

59 Elabd, Y. A., Sloan, J. M. & Barbari, T. A. Diffusion of acetonitrile in conformational isomers of an H12MDI polyurethane. *Polymer* **41**, 2203-2212 (2000).

60 Dearth, R. S., Mertes, H. & Jacobs, P. J. An overview of the structure/property relationship of coatings based on 4, 4′ -dicyclohexylmethane diisocyanate (H12MDI). *Progress in organic coatings* **29**, 73-79 (1996).

61 Hourston, D. J., Williams, G., Satguru, R., Padget, J. D. & Pears, D. Structure–property study of polyurethane anionomers based on various polyols and diisocyanates. *Journal of Applied Polymer Science* **66**, 2035-2044, doi:10.1002/(sici)1097-4628(19971205)66:10<2035::aid-app21>3.0.co;2-1 (1997).

62 Polus, I. Synthesis of polyurethane coating components with IPDI and TMDI. *European Journal of Wood and Wood Products* **61**, 238-240, doi:10.1007/s00107-003-0390-9 (2003).

63 Schneider, N. S., Illinger, J. L. & Karasz, F. E. The interaction of water with polyurethanes containing block copolymer soft segments. *Journal of Applied Polymer Science* **47**, 1419-1425 (1993).

64 Mark, H. F. & Kroschwitz, J. I. *Encyclopedia of polymer science and engineering*. Vol. 2 (Wiley, 1985).

65 Albertsson, A. C. & Varma, I. Aliphatic polyesters: synthesis, properties and applications. *Degradable Aliphatic Polyesters*, 1-40 (2002).

66 Ikada, Y. & Tsuji, H. Biodegradable polyesters for medical and ecological applications. *Macromolecular rapid communications* **21**, 117-132 (2000).

67 Engelberg, I. & Kohn, J. Physico-mechanical properties of degradable polymers used in medical applications: a comparative study. *Biomaterials* **12**, 292-304 (1991).

68 Darwis, D., Mitomo, H., Enjoji, T., Yoshii, F. & Makuuchi, K. Enzymatic degradation of radiation crosslinked poly (ε − caprolactone). *Polymer Degradation and Stability* **62**, 259-265 (1998).

69 van Dorp, A. G. M., Verhoeven, M. C. H., Koerten, H. K., van Blitterswijk, C. A. & Ponec, M. Bilayered biodegradable poly (ethylene glycol)/poly (butylene terephthalate) copolymer (Polyactive™) as substrate for human fibroblasts and keratinocytes. *Journal of Biomedical Materials Research* **47**, 292-300 (1999).

70 Woodruff, M. A. & Hutmacher, D. W. The return of a forgotten polymer—Polycaprolactone in the 21st century. *Progress in Polymer Science* **35**, 1217-1256 (2010).

71 Leja, K. & Lewandowicz, G. Polymer biodegradation and biodegradable polymers—a review. *Polish J.Environ.Stud* **19**, 255-266 (2010).

72 Brunelle, D. J. *et al.* Semicrystalline polymers via ring-opening polymerization: preparation and polymerization of alkylene phthalate cyclic oligomers. *Macromolecules* **31**, 4782-4790 (1998).

73 Fink, J. K., Thomas, S. & P. M, V. *Handbook of engineering and specialty thermoplastics*. (Wiley ;, 2010).

74 Samant, K. D. & Ng, K. M. Synthesis of prepolymerization stage in polycondensation processes. *AICHE Journal* **45**, 1808-1829 (1999).

75 Braun, D., Cherdron, H. & Kern, W. *Techniques of polymer syntheses and characterization*. (Wiley-Interscience, 1972).

76 Tomita, K. & Ida, H. Studies on the formation of poly (ethylene terephthalate): 2. Rate of transesterification of dimethyl terephthalate with ethylene glycol. *Polymer* **14**, 55-60 (1973).

77 Yang, K. S., An, K. H., Choi, C. N., Jin, S. R. & Kim, C. Y. Solubility and esterification kinetics of terephthalic acid in ethylene glycol III. The effects of functional groups. *Journal of Applied Polymer Science* **60**, 1033-1039 (1996).

78 Nagahata, R. *et al.* Solid-phase thermal polymerization of macrocyclic ethylene terephthalate dimer using various transesterification catalysts. *Journal of Polymer Science Part A: Polymer Chemistry* **38**, 3360-3368 (2000).

79 Youk, J. H., Boulares, A., Kambour, R. P. & MacKnight, W. J. Polymerization of ethylene terephthalate cyclic oligomers with a cyclic dibutyltin initiator. *Macromolecules* **33**, 3600-3605 (2000).

80 Youk, J. H., Kambour, R. P. & MacKnight, W. J. Polymerization of ethylene terephthalate cyclic oligomers with antimony trioxide. *Macromolecules* **33**, 3594-3599 (2000).

81 Burch, R. R., Lustig, S. R. & Spinu, M. Synthesis of cyclic oligoesters and their rapid polymerization to high molecular weight. *Macromolecules* **33**, 5053-5064 (2000).

82 Zhang, X., Su, H., Zhao, Y. & Tan, T. Antimicrobial activities of hydrophilic polyurethane/titanium dioxide complex film under visible light irradiation. *Journal of Photochemistry and Photobiology A: Chemistry* **199**, 123-129 (2008).

83 Yagci, M. B., Bolca, S., Heuts, J. P. A. & Ming, W. Self-stratifying antimicrobial polyurethane coatings. *Progress in Organic Coatings* **72**, 305-314 (2011).

84 Zhang, L., Kanki, T., Sano, N. & Toyoda, A. Development of TiO2 photocatalyst reaction for water purification. *Separation and purification technology* **31**, 105-110 (2003).

85 Zhao, J. & Yang, X. Photocatalytic oxidation for indoor air purification: a literature review. *Building and Environment* **38**, 645-654 (2003).

86 Rotzinger, F. P., Kesselman-Truttmann, J. M., Hug, S. J., Shklover, V. & Grätzel, M. Structure and vibrational spectrum of formate and acetate adsorbed from aqueous solution onto the TiO2 rutile (110) surface. *The Journal of Physical Chemistry B* **108**, 5004-5017 (2004).

87 Yilgor, I., Yilgor, E., Guler, I. G., Ward, T. C. & Wilkes, G. L. FTIR investigation of the influence of diisocyanate symmetry on the morphology development in model segmented polyurethanes. *Special issue in honour of James McGrath* **47**, 4105-4114, doi:10.1016/j.polymer.2006.02.027 (2006).

88 Smith, B. C. *Fundamentals of Fourier transform infrared spectroscopy*. Vol. 2 (CRC Press, 2011).

89 Stuart, B. *Infrared spectroscopy :fundamentals and applications*. (J. Wiley, 2004).

90 Bower, D. I. *An introduction to polymer physics*. (Cambridge University Press, 2002).

91 Elias, H.-G. *An introduction to polymer science*. Vol. 1 (Vch, 1997).

92 Nielsen, L. E. *Mechanical properties of polymers*. (Reinhold Pub. Corp.).

93 Rurack, K. & MartÃ-nez-MÃ¡Ã±ez, R. n. *The supramolecular chemistry of organic-inorganic hybrid materials*. (Wiley, 2010).

94 Mark, J. E., Lee, C. Y. C., Biancini, P. A. & American Chemical, S. *Hybrid organic-inorganic composites*. Vol. 585 (American Chemical Society, 1995).

95 Horikoshi, S., Serpone, N., Hisamatsu, Y. & Hidaka, H. Photocatalyzed degradation of polymers in aqueous semiconductor suspensions. 3. photooxidation of a solid polymer: TiO2-blended poly (vinyl chloride) film. *Environmental science & technology* **32**, 4010-4016 (1998).

96 Manelis, G. B. *Thermal decomposition and combustion of explosives and propellants*. (Taylor & Francis, 2003).

97 Li, L. *et al.* Photosensitive polyimide (PSPI) materials containing inorganic nano particles (I) PSPI/TiO2 hybrid materials by sol-gel process. *Materials Chemistry and Physics* **74**, 210-213 (2002).

98 Hu, Q. & Marand, E. In situ formation of nanosized TiO2 domains within poly (amide–imide) by a sol–gel process. *Polymer* **40**, 4833-4843 (1999).

99 Guan, K. Relationship between photocatalytic activity, hydrophilicity and self-cleaning effect of TiO2/SiO2 films. *Surface and Coatings Technology* **191**, 155-160 (2005).

100 Mellott, N. P., Durucan, C., Pantano, C. G. & Guglielmi, M. Commercial and laboratory prepared titanium dioxide thin films for self-cleaning glasses: photocatalytic performance and chemical durability. *Thin Solid Films* **502**, 112-120 (2006).

101 Liaw, D. J., Lin, S. P. & Liaw, B. Y. Photolysis of bisphenol-based polyurethanes in solution. *Journal of Polymer Science Part A: Polymer Chemistry* **37**, 1331-1339 (1999).

102 Saha, M. C., Kabir, M. E. & Jeelani, S. Enhancement in thermal and mechanical properties of polyurethane foam infused with nanoparticles. *Materials Science and Engineering: A* **479**, 213-222 (2008).

103 Vert, M., Schwarch, G. & Coudane, J. Present and future of PLA polymers. *Journal of Macromolecular Science, Part A: Pure and Applied Chemistry* **32**, 787-796 (1995).

104 Ali, S. A. M., Zhong, S. P., Doherty, P. J. & Williams, D. F. Mechanisms of polymer degradation in implantable devices: I. Poly (caprolactone). *Biomaterials* **14**, 648-656 (1993).

105 Chen, Y., Zhou, S., Gu, G. & Wu, L. Microstructure and properties of polyester-based polyurethane/titania hybrid films prepared by sol–gel process. *Polymer* **47**, 1640-1648 (2006).

106 Kaneko, M. & Okura, I. *Photocatalysis :science and technology*. (Kodansha ;, 2002).

Curriculum Vitae

Name:	Yixing Tang
Post-secondary Education and Degrees:	East China University of Science and Technology Shanghai, China 2006-2012 B.E. The University of Western Ontario London, Ontario, Canada 2010-2012M.E.Sc.
Related Work Experience	Teaching Assistant The University of Western Ontario 2011-2012 Research Assistant The University of Western Ontario 2010-2012